CODEN:LUTEDX/(TEIE-5386)/1-150/(2017)

Industrial Electrical Engineering and Automation

Current ripple simulation of the electric system in an electric bus

Christian Lugnberg
David Wenander

Division of Industrial Electrical Engineering and Automation
Faculty of Engineering, Lund University

Abstract

With effect of global warming and climate change the electrification of vehicles enables a more sustainable and environmentally friendly alternative to conventional vehicles as it reduces toxic emissions and overall energy consumption. Different extents of electrification is today used. Hybrid and electric vehicles are two examples. Tools to simplify the design of electric vehicles are of value to predict the traction voltage system behaviour. One of these behaviours are current and voltage ripple. By making predictions of the life time of components in the traction voltage system, improvement of the system's overall electrical performance and reduction of development costs.

A component level decomposition of the traction voltage system of two different buses was performed. Component specific information for each bus was gathered at Volvo, at Volvo's suppliers and by measurements. Simplified full-system models of two existing buses were built with associated subsystem in the chosen simulation environment. Verification tests were performed on one bus, the electric hybrid. The simulated system's behaviour and its consistency with reality was evaluated.

A complete library of equivalent circuits of the two existing buses was built. The measurements on the electric hybrid followed custom test cases. Component measurements were also performed on four common mode filters as data was insufficient. Results show that the model is not fully consistent with reality. There is uncertainty with the parametrization of components in the model. The model is sensitive to small modifications of parameter values. Especially filter capacitors and inductors. When given parameter values was replaced with values found in literature some results were more consistent with reality. Further investigation is thus needed to ensure the correctness of the model. Therefore another master thesis is planned to continue the work.

Acknowledgements

This thesis was done at Volvo Group Trucks and Technology in Gothenburg, Sweden between the end of August 2016 and the end of January 2017.

To begin with we would like to thank our supervisor, system engineer, Per Widek at Volvo for always being available for guidance, testing ideas, finding creative ways around problems and also long Skype sessions with intense discussions on the topic.

Further on, we would like to thank the Volvo Group Trucks and Technology, GTT, and Volvo Buses employees for all the help, information and ideas. Special thanks and appreciation goes to test engineer Oskar Lingnert (Volvo GTT) for helping us with tests on the bus and having patience to bare with our inexperience in bus testing. A special thanks also goes to Robert Louvandin and his testing crew (Volvo Buses, Arendal) for contributing with valuable advice while measuring, extra hands when needed and also for lending us measuring equipment.

We would also like to show our appreciation for our supervisor Philip Abrahamsson at the Department of Industrial Electrical Engineering and Automation (IEA) at Lund Institute of Technology who always took time to discuss ideas, to come with relevant inputs and to support us throughout our work. Other people at the department of IEA who have come with inputs on our work and that we would like to thank are Bengt Simonsson, Sebastian Hall, Gabriel Dominguez and Samuel Estenlund.

Last but not least we would also like to give a huge thank you to the Professor of the department of IEA and our examiner Mats Alaküla who has been great to discuss ideas and results with and who also had the connections at Volvo to make this thesis possible.

Contents

1 Introduction

Global warming and climate changes are affecting us worldwide and immediate actions are required to resolve these changes [4]. The transport sector alone accounts for about 63% of oil consumption and 29% of all CO_2 emissions in Europe [5]. To be able to alter this, more enviromental friendly alternatives of transport needs to be implemented [5]. Electric buses are today commercially competitive and Volvo Group has a number of different buses on the market; the 7900 Hybrid, the 7900 Electric Hybrid and the 7900 Electric.

Further advantage with electrification of buses is that it enables a more convenient environment for drivers to work in, passengers to commute in, and people on the streets close to traffic. Electric vehicles are also an effective means to reduce noise, toxic emissions and overall energy consumption. Volvo Buses have successfully had conceptual, electric buses operating in Gothenburg on route 55 for over a year. Volvo Buses is looking to expand the implementation of electric buses in cities and elsewhere. Tools to simplify the construction of electric vehicles, e.g. predict the behaviour of current ripple in their electrical systems, are of great value.

1.1 Problem formulation

When converting voltages using power electronic converters (PEC), current ripple can occur. If the magnitude of the current ripple is not within appropriate limits it can cause problems such as thermal fatigue and in consequence decrease the lifespan of components in an electrical system. Previous measurements in Volvo's electric and electric hybrid buses show that current ripple occurs from the different power electronic converters in the TVS. Documented measurements and tests indicate that the subsystem's input filters DC-capacitors can have a shorter lifespan as a consequence of the current ripple. This is an example where current ripple might cause problems for Volvo buses. The work in this thesis is made to investigate the current ripple, simulate the current ripple and furthermore suggest a solution on how to decrease it. The use is to enable evaluation of the real system's behaviour where many subsystems interact and create current and voltage ripple in the DC-link of the TVS. As mentioned previously, these ripples can cause functional disturbances and lifetime limitation of subsystems connected to the same TVS.

1.2 Purpose and aim

The purpose is to build a generic simulation model of the TVS. With the use of appropriate software, a model of the TVS is to be built. In addition a component library is to be established to be able to build different TVS and subsystems to predict future system behaviour. The library is to consist of several minor model parts that can be used as a Lego brick-solution to put together in different ways to model the TVS of different systems.

The aim for this thesis is to build a simulation model accurate enough to be used as a tool when designing the TVS for an electric or electric hybrid bus. Furthermore measurements are required from two different buses to verify the simulated model. This is necessary to verify and ensure that the simulated model is to be consistent with existing systems and components in reality.

A predictive design model of the TVS could therefore be used to write specifications to suppliers or to design before building test vehicles. Furthermore, redesign is therefore possible before manufacturing. As a consequence this can improve vehicles performance, lifetime and reduce their overall development costs.

Additionally a manual for the simulation model is to be written so that a Volvo engineer without previous experience could use the simulation model easily. An appropriate simulation software is to be selected. Finally a solution and future work for the ripple problem is expected to be suggested.

1.3 Scope and limitations

This thesis is limited to the DC-side of the TVS of the electric and hybrid buses. Charging of the TVS from the grid is not included in the evaluation of the current ripple. The model is to be made as generic as possible to enable great flexibility for different simulations of different TVS and subsystems. Yet the model is to be as simple and intuitive to use as possible. The accuracy of the simulated model is supposed to be within a faulty margin of 10% to 20%. As a consequence simplifications in the TVS can be made to a certain extent.

1.4 Thesis outline

In this chapter a background to the thesis is introduced. *Chapter* 2 - *Methods* shows a résumé of how the work is planned and executed. *Chapter* 3 - *Traction voltage system* gives an overview of a bus's required functions and how they can differ between different kinds of buses. In *chapter* 4 - *Equivalent circuit of the traction voltage system* a simplification of the the different traction voltage systems is made. In *chapter* 5 - *Simulation modelling* a software is chosen and the simplified circuits made in the software are presented. The simulation cases performed are listed in *chapter* 6 - *Simulation*. In *chapter* 7 - *Experimental verification and model discussion* measurements are evaluated and the built models are compared with these measurements. A discussion of the results and how realistic they are is also in *chapter* 7. A conclusion, a recommended solution and a recommendation on how to proceed with future work is finally presented in *chapter* 8 - *Conclusion*.

2 Methods

To begin with the functional requirements of the TVS simulation model are to be specified, including which subsystems connected to the same TVS to include in the model. Also which intentional and parasitic components between the TVS and chassis that will be included and also which frequency range will be represented. Understanding of the TVS is necessary to be able to decomposition it on a component level.

To be able to build a simulation model of the TVS for the different buses a lot of information is required. Therefore a substantial amount of time and effort is initially put down to attain component data. During the first month discussions and correspondence with Volvo employees, Volvo suppliers and Volvo sub-suppliers is made to acquire data. Before building the simulation model the appropriate simulation software is selected for the application. Where there is insufficient data, measurements are carried out for these specific components.

Further on measurements are to be made on two different buses and therefore two different simulated TVS are required. As a result a component library is established for the two different TVS. An electrical safety education and preparing education for the workshop is required to execute the measurements. The measurements are carried out to validate the simulation models.

A manual for the simulation model is written so that a Volvo engineer easily can use the simulation tool. Finally a proposition on how to decrease the current ripple is investigated and suggested.

3 Traction voltage system

3.1 Functional requirements for a bus

3.1.1 Basic functional requirements

A conventional bus have a number of required functions. Firstly, for traction a combustion engine is used. Further on, the bus needs to be able to be lowered during passenger entry and exit (a.k.a. kneeling). In addition door opening and closing and breaking also need to be addressed. To enable this an air system with an air compressor is used. Air tanks are pressurized and utilized in order to break, open and close doors and to kneel the bus. Furthermore, the bus requires a climate system to establish a suitable temperature for the driver and the passengers. Remaining functions and requirements for instance steering servo, lights etc. are normally handled by a low voltage system at $24VDC$ in a Volvo bus.

3.1.2 Functional requirements for electric and electric hybrid buses

An electric or a hybrid bus have different ways of fulfilling previously mentioned functional requirements compared to a conventional bus with a combustion engine. The main difference is that electric machine (EM) is used as a traction motor. This electric machine can either be used for motoring or generation. For instance in a situation when the bus is braking downhill the electrical machine is used as a generator. As a consequence the batteries can be drained and charged continuously during drive and are therefore called energy storage systems (ESS). Previously mentioned required functions are fulfilled in the same way as a conventional bus with a combustion engine. However, an electric bus needs to have an additional electric heater. The minor heat losses in the electric system can usually not be used to heat the air in the climate system as compared to a conventional bus with an combustion engine.

Figure 1: The L7900 electic bus being charged via the pantograph. [6]

There are two ways of charging an electric hybrid and an electric bus. Firstly there is the lower power charger (LPC). The LPC is a slow charger and is meant to be connected over night. The LPC has the primary task to maintain the battery cells. Secondly there is the high power charger (HPC). The HPC is a fast charge supplying 600V DC to the TVS and charges for around 6 minutes. This is done by using the pantograph, see figure 1 and is used between itineraries during day operation. The charging station lowers conductors to the bus roof where two charging rails are located. These charging rails are used as conductors to charge the batteries. The charging switch unit (CSU) has the function of connecting the charging rails to the TVS.

Ultimately an electric or hybrid bus has additional requirements and functions. However, the specified requirements and functions addressed here are the most essential to include for the high voltage systems where the current ripple evaluation will be carried out on.

3.2 Types of traction voltage systems

The key components in a high voltage system in a electric hybrid or electric vehicle is the ESS and the electric motor. Therefore the ESS and the electric motor varies greatly between different Volvo buses. Cable lengths are an additional varying factor between different Volvo electric hybrid and electric buses. However a majority of the components are the same as seen in figure 2 and figure 3. A more thorough explanation of the different subsystems in figure 2 and figure 3 is presented below in *section 3.3 - Subsystem specification.*

3.2.1 Electric hybrid

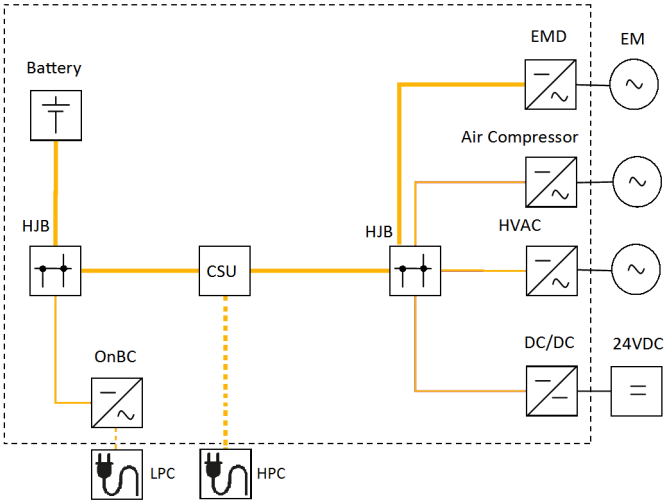

Figure 2: A simplified overview of the 600V DC-system for Volvo's electric hybrid electric bus. Different thickness in the scheme depicts different cable types. Bold orange cables are rated for higher power than thin orange cables. The dotted line represents the limitation of this thesis. The AC-side of the high voltage system will not be evaluated.

3.2.2 Electric

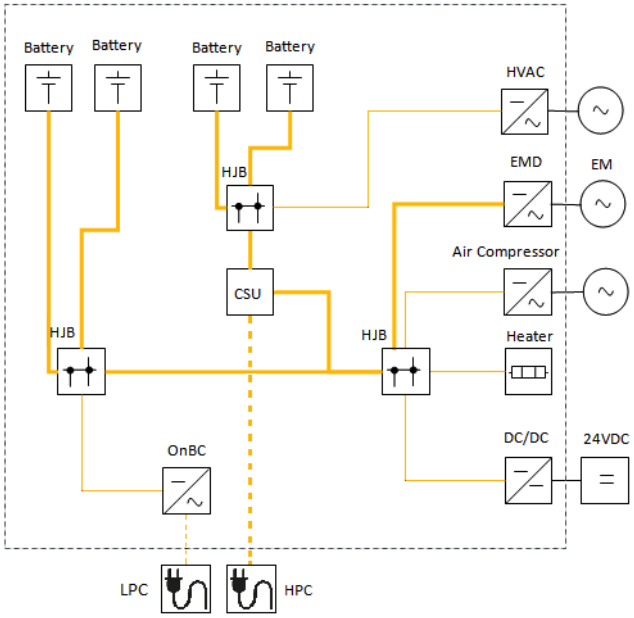

Figure 3: A simplified overview of the 600V DC-system for Volvo's full electric bus. Different thickness in the scheme depicts different cable types. Bold orange cables are rated for higher power than thin orange cables. The dotted line represents the limitation of this thesis. The AC-side of the high voltage system will not be evaluated.

3.3 Subsystem specification

The TVS has different power electronic converters (PEC), they are referenced to as the EMD, DCDC etc. More specific information about them in the upcoming sections.

3.3.1 MDS - Motor drive system

The electric motor drive (EMD) is a power electronic converter supplying the traction motor with voltage and current the DC-side. The electric hybrid bus and the electric bus have two different types of EMD as seen in table 1 and table 2. The traction motor in the both buses is known as the electric machine (EM) and is a permanent magnetized synchronous machine(PMSM).

MDS type B (Electric hybrid)

The base speed varies depending on the applied DC-voltage. Base speed is therefore given at maximum power 180kW at 600V applied voltage.

Converter type	DC/AC 4-quadrant 3-phase
Switching Frequency	$(f_{sw_1}, f_{sw_2}, f_{sw_3})_{EMD_{typeB}}$
Converter load type	PMSM
Converter load power	180kW max, 72kW nominal
Electric Machine base speed	$\omega_{basespeed}$

Table 1: Table showing specification values for the MDS type B.

MDS type C (Electric)

The base speed varies depending on the applied DC-voltage. Base speed is therefore given at maximum power 185kW at 600V applied voltage.

Converter type	DC/AC 4-quadrant 3-phase
Switching Frequency	$(f_{sw_1}, f_{sw_2}, f_{sw_3})_{EMD_{typeC}}$
Converter load type	PMSM
Converter load power	185kW max, 105kW nominal
Electric Machine base speed	$\omega_{basespeed}$

Table 2: Table showing specification values for the MDS type C.

3.3.2 HVAC - Heat Ventilation and Air Conditioning

The HVAC is a part of the air climate system in the bus. A compressor supplied by an induction machine (IM), specific values for the HVAC in table 3. The lowest voltage applied to reach the base speed is used to calculate the converters duty cycle.

Converter type	DC/AC 4-quadrant 3-phase
Switching Frequency	$(f_{sw})_{HVAC}$
Converter load type	IM
Converter load power	11kW max
Electric Machine base speed	$\omega_{basespeed}$
Lowest voltage applied to reach base speed	560V

Table 3: Table showing specification values for the HVAC

3.3.3 Air compressor

The air compressor is driven by an electric machine. It is used by the air system to open and close doors, brake and also to kneel the bus. See table 4 for specific values. The lowest voltage applied to reach the base speed is used to calculate the converters duty cycle.

Converter type	DC/AC 4-quadrant 3-phase
Switching Frequency	$(f_{sw})_{aircomp}$
Converter load type	PMSM
Converter load power	7.5kW max
Electric Machine base speed	$\omega_{basespeed}$
Lowest voltage applied to reach base speed	500V

Table 4: Table showing specification values for the Air compressor

3.3.4 DCDC - Direct Current Converter

Power converter to supply the 24V system used for the steering servo, lights etc. See table 5 for specific values. The lowest voltage applied to reach full performance is used to calculate the converters duty cycle.

Converter type	DC/DC 4-quadrant 1-phase
Switching Frequency	$(f_{sw})_{DCDC}$
Converter load type	24V DC-system
Converter load power	7.5kW max
Lowest voltage applied for full performance	500V

Table 5: Table showing specification values for the DCDC

3.3.5 OnBC - Onboard Charger

The OnBC is a low power charger that is used to charge over longer times and to maintain the batteries. As previously mentioned charging is not included in this thesis and therefore no further data is required.

3.3.6 Heater

The Heater is used to heat the air in the air climate system. The heater is rated at 7kW. The heater is used in the full electric bus as no heat can be utilised and taken from a combustion engine.

3.3.7 Cable

Volvo buses have three types of cable area dimensions in the 600V DC-system 70 mm^2, 50mm^2 and 2x4mm^2. The 70mm^2 is used for the CSU. The 50mm^2 is used for the battery and the EMD. The 2x4mm^2 is used for the remaining parts of the 600V DC-system. The 50mm^2 are shown in figure 2 and figure 3 as yellow cables. The 2x4mm^2 are shown in figure 2 and figure 3 as red cables. The 70mm^2 is not included in any of these schemes.

3.3.8 ESS - Energy Storage System

Battery with coherent subsystem rated at 600V DC.

3.3.9 HJB - Hybrid Junction Box

A box containing fuses and a merge point for cables. Not included in this thesis for evaluation.

3.3.10 CSU - Charging Switch Unit

The charging switch unit (CSU) has the function of connecting the charging rails to the TVS.

3.3.11 Presumed system dynamics

As previously mentioned this thesis main focus is on the DC-side of 600V system, as seen in figure 3 and figure 3. This thesis is limited to when the bus is driving and is in operation. It is not taken into account when it is charging from the grid, HPC or LPC. As a consequence the converters that are of interest are the converters for the HVAC, air compressor, EMD and the DCDC. Additional converters and input filters and also OnBC and heater, will still be connected to the TVS and therefore they will have to be included but without any load. The HJB and the CSU do not have any impact on the TVS in regard to the given faulty margin. In conclusion, the ripple evaluation will be limited to the systems' active converters during drive.

Depending on use, different electric machines in the system have different power ratings. For instance the EM have the highest rated power. The magnitude of the DC current ripple is dependant on what, in this case, the load the EMD is supplying. The electric traction motor is the component with the most power compared to other components in the $600V$ system. Further on, previous Volvo measurements indicate that the EM has a greater current ripple magnitude than the other components. In conclusion, a higher rated power of an electric machine will probably result in a greater magnitude of current ripple.

The input filter on a converter for a certain electric machine is designed to withstand that subsystem's current ripple. However, if different subsystems are connected together in a larger system it is probable that the different subsystems are not designed to withstand each respective produced current ripple. Further on, if the different subsystems have a great difference in power rating it is probable that the lesser power rated subsystems components will, to some extent, deteriorate from thermal exhaustion. This can in result cause functional disturbances and lifetime limitation of subsystems connected to the same larger system.

4 Equivalent circuit of the traction voltage system

4.1 Ambition level for the equivalent circuits

Setting the right scope of how precise the model should be is not obvious. However this is the first step in building a model for the electric system of a bus. Therefore it is important to have the ability to realize a whole system model within the time for a master thesis. Furthermore, the level of the equivalent circuits is to be as generic as possible. The instructed level is to make a rough estimate model with the fault margin aimed to be $\pm 10 - 20$ percent, as mentioned in *section 1.3 - Scope and limitations*. Focus is to build the TVS with all the major subsystems and components included with limited focus on the component details.

4.2 EMD model

The whole TVS consists of several power consumers using power electronic converters as described in *chapter 3 - Traction voltage system*. The EMD is one. To build an equivalent circuit of a DC/AC- or DC/DC-converter to model the EMD, HVAC, air compressor or the DCDC the following sections mention the steps taken to achieve a generic equivalent. As this model is to be of the DC-side of the TVS.
Starting from the basics - *how is DC converted to AC*, *how is current ripple created during conversion* and *what affects the size of the ripple*?

Take the electrical machine as an example of a power consumer. The electrical machine is a three-phase load (and generator) with a three-phase inverter between the DC-side of the TVS and itself and the driven motor. So a simplified model would consist of a three-phase inverter and a RLE-load. The motor drive system (MDS), which is the EMD and the EM could look something like figure 4 below.

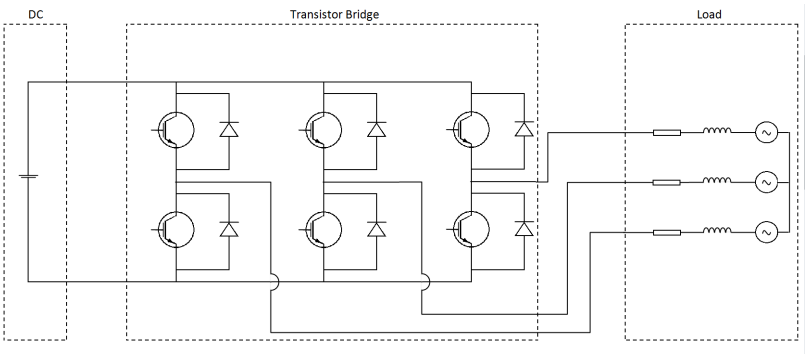

Figure 4: A typical power consumer in the TVS. A three-phase AC-load consuming power from the DC-side of the TVS. DC-link capacitor and remaining input filter excluded.

4.2.1 Current ripple basics

To illustrate how current ripple is created one have the simplest case of a converter, the buck converter or the step-down-converter, see figure 5. It is a one quadrant, 1Q, DCDC converter that steps down the input voltage to the output voltage by controlling how the transistor switch is conducting or not. For example if the input voltage is $10V$ and the transistor switch is conducting 20% of the time i.e. a 20% duty cycle, an output voltage of:

$$10V \cdot 0.2 = 2V$$

is achieved.

As seen in the circuit in figure 5 below a DC source is connected to a transistor switch, a series RLE-load and a free-wheeling diode. The DC source can either be an ideal voltage source, a controlled voltage source, a battery of cells or a single cell [11].

As the load is characterized as inductive it will have a current sluggish behaviour. Therefore when the switch is non-conducting the energy stored in the inductor will need a path to follow which is through the free-wheeling diode and the RLE-load. The following equation can describe the relation between the voltages in the circuit:

$$u = R \cdot i + L \cdot \frac{di}{dt} + e \text{ (eq. 3.1, [2], p.87).}$$

Approximately the resistance is insignificant, thus $R = 0$, this gives

$$di = \frac{u-e}{L} \cdot dt$$

which describes the current derivative. With $u > e$ the derivative is positive when the transistor switch is conducting and negative while non-conducting due to $u = 0 \rightarrow e > u$. This results in a current with the shape of a triangle wave as seen in figure 6.

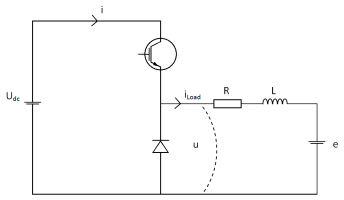

Figure 5: The buck converter circuit.

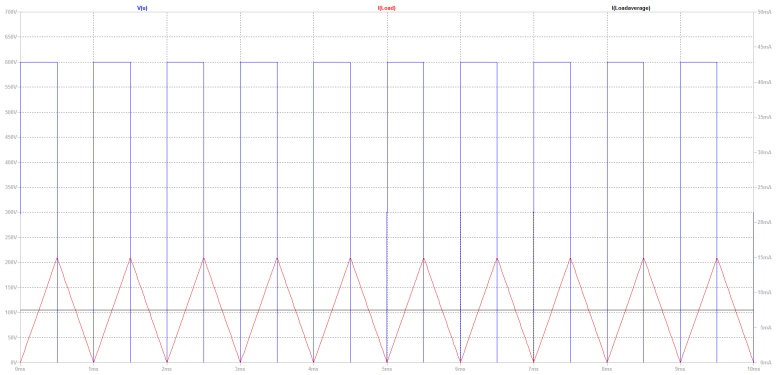

Figure 6: The current behaviour while switching at 50%. Voltage pulses are included to show that the current rises as the voltage over u (while the transistor is conducting) is high and falls as the the voltage is low. The current on the load side becomes rippled due to the produced voltage pulses. See the average current for the average current value of the current ripple. Blue represents the voltage pulses u, red represents load side current i_{load} and black represents the average load current $i_{load_{avg}}$.

4.2.2 Worst case current ripple

To be able to predict the worst case situations for the TVS it is important to understand why and when the current ripple has the greatest magnitude in theory ([2], p.24).

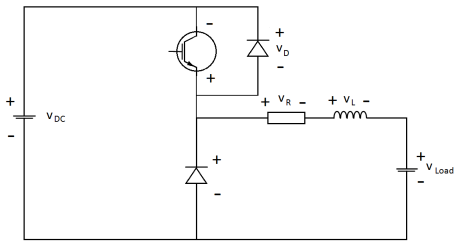

Figure 7: The buck converter circuit with denoted voltage drops over each component. However the voltage drop over the transistor is neglected here. ([2], p.24-25).

As shown in figure 7, the voltage drops occur over each component. The total voltage in the circuit can be seen as:

$$V_{DC} = V_R + V_L + V_D + V_{Load}$$

Where V_R and V_D can be approximated to $0V$ due to the fact that remaining voltage drops have a greater magnitude, see ([2], p.24-25).

As a result this simplifies to:

$$V_{DC} = V_L + V_{Load}$$

The voltage drop over the inductance:

$$V_L = L \cdot \frac{di}{dt}$$

Further on:

$$V_{DC} - V_{Load} = L \cdot \frac{di}{dt},$$

where dt can be written as:

$$dt = D \cdot T_{sw},$$

where T_{sw} is the time period of the switching frequency for the converter.

The duty cycle D is defined as:

$$\Delta i = \frac{V_{DC} - V_{Load}}{L} \cdot dt$$

In summary the current ripple can be written as the following:

$$\Delta i = \frac{V_{DC} - V_{Load}}{L} \cdot \frac{V_{Load}}{V_{DC}} \cdot T_{sw}$$

To evaluate the maximum value of Δi, the expression is differentiated with respect of V_{Load}.

Maximum value of Δi:

$$\Delta i = \frac{V_{DC} - V_{Load}}{L} \cdot \frac{V_{Load}}{V_{DC}} \cdot T_{sw} =$$
$$(\frac{V_{DC} \cdot V_{Load} - V_{Load}^2}{V_{DC}}) \cdot \frac{T_{sw}}{L}$$
$$\frac{\partial \Delta i}{\partial V_{Load}} = (\frac{V_{DC} - 2 \cdot V_{Load}}{V_{DC}}) \cdot \frac{T_{sw}}{L} =$$
$$(\frac{1}{L} - \frac{2 \cdot V_{Load}}{V_{DC} \cdot L}) \cdot T_{sw}$$
$$\frac{\partial \Delta i}{\partial V_{Load}} = 0,0 = (\frac{1}{L} - \frac{2 \cdot V_{Load}}{V_{DC} \cdot L}) \cdot T_{sw}$$
$$\frac{1}{L} = \frac{2 \cdot V_{Load}}{V_{DC} \cdot L} \implies V_{DC} = \frac{V_{Load}}{2}$$

The expression is differentiated with respect of V_{Load} a second time to investigate maximum or minimum point. The result is negative therefore it is a maximum value.

$$\frac{\partial^2 \Delta i}{\partial V_{Load}^2} = -\frac{2}{L \cdot V_{Load}}$$

In conclusion the greatest value of di is at $V_{Load} = \frac{V_{DC}}{2}$ which is the same as a duty cycle of 0.5.

$$\frac{\partial^2 di}{\partial V_{Load}^2} = -\frac{2}{L \cdot V_{Load}}$$

In conclusion the greatest value of di is at $V_{Load} = \frac{V_{DC}}{2}$ which is the same as a duty cycle of 0.5.

4.2.3 Voltage modulation

How the voltage modulation is executed is determining what frequencies the voltage pulses will have. For three-phase voltage modulation there are three well used schemes; *sinusoidal*, *symmetrized* and *bus-clamped* ([2], p.81). By using bus-clamped modulation the voltage pulses will, for three-phase, have the same frequency as the switching frequency. The following section explain how the perceived switching frequency on the DC-side of the TVS relates to the actual switching frequency depending on converter and type of voltage modulation.

To understand differences between different perceived switching frequencies an example can be made with a two quadrant-(2Q) see figure 8, and a four quadrant- (4Q) see figure 9, converter. In this case both has a simple RLE-load. Further down two snapshots from voltage modulation in a 2Q-, respectively a 4Q-converter are shown see figure 10 respectively figure 15.

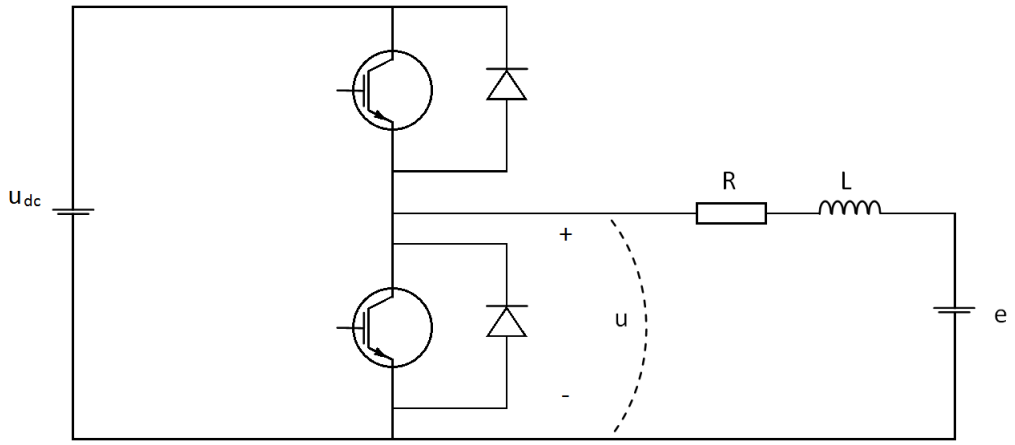

Figure 8: The 2Q-converter.

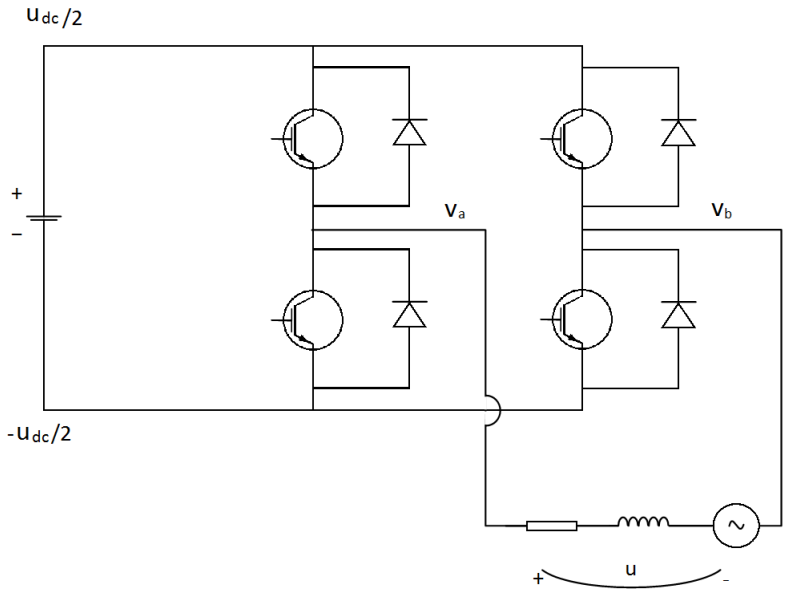

Figure 9: The 4Q-converter.

As seen in figure 8 for when the 2Q the reference value for u, u^* is crossing the triangular voltage modulation carrier wave, $u_{carrier}$ the switch changes state. The transistors can be seen as a switch in figure 8. When the upper transistor is conducting the switch is up and when the lower transistor is conducting the switch is down. So when u^* is larger than $u_{carrier}$ the switch is conducting. The next time the u^* is crossing $u_{carrier}$ the switch changes its state from up to down and a voltage pulse is created. In this case one can clearly see that during one switching period, $T_{sw} = \frac{1}{f_{sw}}$, the 2Q-converter creates one pulse. The perceived switching frequency on the DC-side is thus the same as the actual switching frequency. This is also the case for a 1Q-converter.

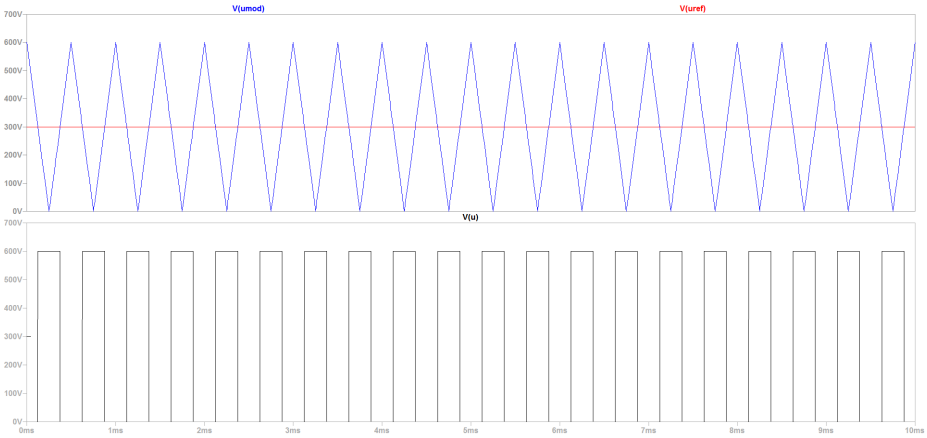

Figure 10: Voltage modulation example for a 2Q-converter. The blue triangular wave V(umod)in this figure is referred to as $u_{carrier}$ in the text. The red represents the reference voltage u^* and the black represents the load side voltage u.

The 4Q converter has at least two reference values instead of one, v_a and v_b. One can say that $v_a = \frac{u^*}{2}$ and $v_b = -\frac{u^*}{2}$. Since there are four transistors in the 4Q there are 4 switch states, as seen in figure 11, figure 12, figure 14 and figure 13. Where switch states in figure 11 and figure 13 are conducting and figure 12 and figure 14 are non-conducting. The transistor conduct through the load when they have opposite position to each other, one on the positive side and the other on the negative side. Further on they are non-conducting through the load when they are either both on the positive side or both on the negative side.

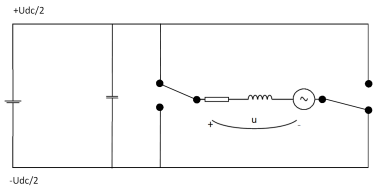

Figure 11: Simplified 4Q converter with simple switches instead of transistors. Switch state with negative total voltage over the load according to the load voltage annotation.

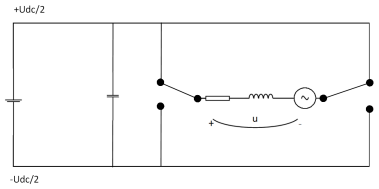

Figure 12: Simplified 4Q converter with simple switches instead of transistors. Switch state with no voltage applied from the converter to the load.

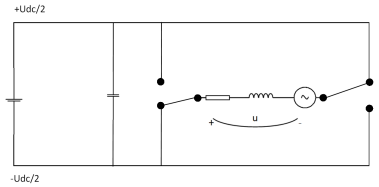

Figure 13: Simplified 4Q converter with simple switches instead of transistors. Switch state with positive total voltage over the load according to the load voltage annotation.

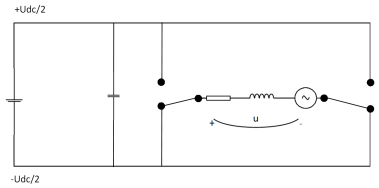

Figure 14: Simplified 4Q converter with simple switches instead of transistors. Switch state with no voltage applied from the converter to the load.

Equivalent to the 2Q the switches switch when a reference value crosses the carrier wave, $u_{carrier}$. In figure 9 starting with both at the bottom line non-conducting. When the reference for v_a crosses $u_{carrier}$ and switches to the top line a path for the current is given and it can pass through the top left transistor, the load and back through the bottom right transistor. When v_b crosses $u_{carrier}$ and both switches are on the top line no path for the current is given. When v_b crosses $u_{carrier}$ for the second time the path is again opened until v_a crosses $u_{carrier}$ for the second time and both switches are on the bottom line. The next switching period T_{sw} the same cycle repeats. During one switching period the 4Q creates two voltage pulses and therefore the perceived frequency is the doubled to the switching frequency. The same is for a 4Q three-phase converter.

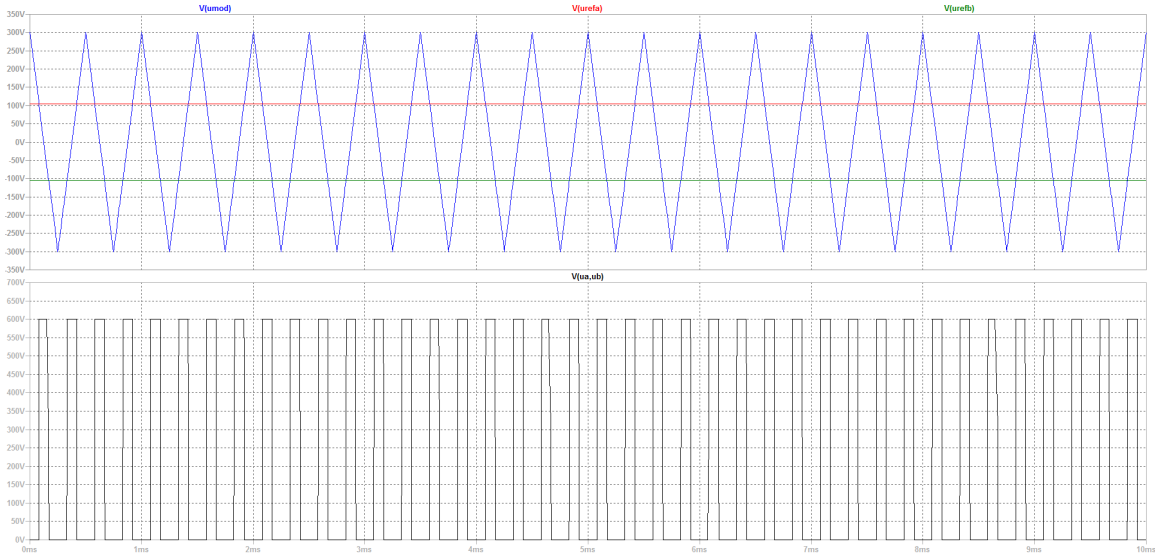

Figure 15: Voltage modulation example for a 4Q-converter. The blue triangular wave V(umod)in this figure is referred to as $u_{carrier}$ in the text. The red and green represents the reference values v_a and v_b and the black represents the oad side voltage u.

4.2.4 4Q-three-phase inverter

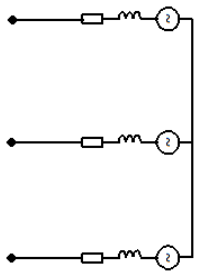

Figure 16: A symmetrical, generic three-phase load.

Why three phase?
To elaborate this a bit it has to do with the torque formation in an electric machine based on the Lorentz forces. Where Lorentz force is the force on a particle in an electromagnetic field [9]. Such a force is created, and produces torque, in the machine with the magnets and an applied current. The need for a smooth torque production where the rotor does not loose its torque formation due to no or uneven current while producing torque is essential for a machine to not jerk during operation. ([1], p.344-345)
So if one can see the need for a three-phase load one can imagine that the three-phase load in figure 16 above is for example an electric machine, more specific a permanent magnetized synchronous machine, PMSM. It consists of a stator and a rotor, windings, permanent magnets etc. In the very simplified model of an electric machine, a PMSM or another type of machine, the resistances represent the machines inner resistance in each phase winding. Equivalent the inductors represent the phase windings inductances. The voltage sources represents the induced voltage in the machine in each phase. This is also called the back-emf, back electromotive force. A very simple representation of something as complex as an electric machine. In combination with a voltage source and a power electronic converter one can model a DC source supplying an electric motor through a PEC, see for instance figure 4.

To model an electric machine the vector planes dq and $\alpha\beta$ are introduced see figure 17, ([1], p. 344, 346). The dq-plane is also called xy and represent a vector-plane rotating in sync and with the same speed as the machine's rotor.

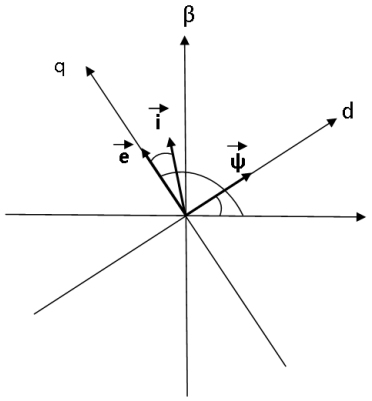

Figure 17: Two imaginary coordinate systems. $\alpha\beta$ which is fixed and dq which rotates with the stator. The d-axis is aligned with with the stator's magnetic flux $\vec{\Psi}$.

To achieve a valid simulation of a motor load the characteristic values of a fictional PMSM was used [8]. The values are listed together with the DC-link voltage and duty cycle in table 6. Also a script to calculate was written in Matlab and can be seen in *Appendix A*.

Property	Parameter	Value	Unit
Resistance	R	0.3	Ohm Ω
Inductance	L	$0.5E-3$	Henry H
Magnetic flux	Ψ	0.8	Weber Wb (Vs)
Maximum power	P_{max}	$52E3$	Watt W
DC-link voltage	U_{dc}	600	Volt V
Duty cycle	D	50	Percent %

Table 6: Properties for the three-phase motor load simulation in LTspice. [8]

To determine the size of the maximum load voltage (line-line) one needs to consider how voltage modulation is done in the converter. In this case symmetrized voltage modulation is used to achieve a larger margin to over modulation compared to for example sinusoidal voltage modulation. This while still give the same load voltage out from the converter.
The liaison between the DC-link voltage and the maximum load voltage is:

$$|\vec{u}|_{max} = \frac{U_{dc}}{\sqrt{2}} \implies |\vec{u}|_{max} = \frac{600}{\sqrt{2}} = 424.2641V$$

For the maximum load current one can with the three-phase power equation

$$P = 3 \cdot U_{LN} \cdot I_{ph,RMS} \cdot \cos\varphi = \sqrt{3} \cdot U_{LL} \cdot I_{ph,RMS} \cdot \cos\varphi, \text{ where } \varphi = 0^\circ$$

(only active power)(eq. 3.8, [1], p.90)

solve for

$$\left|\vec{i}\right|_{max} \text{ with } U_{LL} = |\vec{u}|_{max} \text{ in this case.}$$

$$I_{ph,RMS} = \frac{P_{max}}{\sqrt{3}|\vec{u}|_{max}} \implies \left|\vec{i}\right|_{max} = \sqrt{3} \cdot I_{ph,RMS} \iff$$

$$\left|\vec{i}\right|_{max} = \frac{P_{max}}{|\vec{u}|_{max}} \implies \left|\vec{i}\right|_{max} = \frac{52E3}{424.2641} = 122.5652A$$

Previously in chapter 5.1 and 5.2 the basic principle as well as the worst case of current ripple was presented. The worst case is at a duty cycle of 50%. This gives the absolute load voltage or the back emf, $|\vec{e}|$.

$$D = \frac{|\vec{e}|}{|\vec{u}|_{max}} \iff |\vec{e}| = D \cdot |\vec{u}|_{max} \implies$$

$$|\vec{e}| = 0.5 \cdot 424.2641 = 212.1320V$$

The voltage equation in dq is

$$\vec{u_{dq}} = R \cdot \vec{i_{dq}} + L \cdot \frac{\vec{i_{dq}}}{dt} + j \cdot \omega \cdot L \cdot \vec{i_{dq}} + \vec{e_{dq}} \text{ (eq. 3.6, [1], p.89)} \implies$$

$$\vec{u_{dq}} = R \cdot \vec{i_{dq}} + L \cdot \frac{\vec{i_{dq}}}{dt} + j \cdot \omega \cdot L \cdot \vec{i_{dq}} + \vec{e_{dq}}, \text{ due to stationarity, i.e.}$$

$$L \cdot \frac{\vec{i_{dq}}}{dt} = 0$$

in this case. $\vec{e_{dq}}$ is known and consists of $\vec{\Psi}$ and ω_r which can give the frequency of the rotor which is used in the simulation of the generic three-phase load.

$$\vec{e_{dq}} = \vec{\Psi_{dq}} \cdot \omega_r, \text{ where } \omega_r = \omega_{mech} \implies$$

$$\omega_{mech} = \frac{\vec{e_{dq}}}{\vec{\Psi_{dq}}} \implies$$

$$\frac{212.1320}{0.8} = 265.1650 rad/s$$

with $\omega = 2 \cdot \pi \cdot f$ (eq. 2.87, [1], p.45) one get

$$f_{mech} = \frac{\omega_{mech}}{2 \cdot \pi} \implies f_{mech} = \frac{265.1650}{2 \cdot \pi} = 42.2023 Hz$$

At a point in time, t_x, the coordinate systems $\alpha\beta$ and dq will overlap eachother perfectly. This will happen for every rotation that the rotor makes but at different times. Now suppose $t = t_x$ and at this time the coordinate systems are perfectly aligned. This means that the vectors given in $\alpha\beta$ will be of the same sizes and angles as in dq. The voltage equation can thus be used with the $\alpha\beta$-vectors. The voltage required over the machine to power the load can be calculated with the dq-voltage equation while utilizing the maximum load current at a 50% duty cycle at $t = t_x$.

$$\vec{u_{\alpha\beta}} = R \cdot \vec{i_{\alpha\beta_{max}}} + j \cdot \omega_{mech} \cdot L \cdot \vec{i_{\alpha\beta_{max}}} + \vec{e_{\alpha\beta}} \implies$$
$$\vec{u_{\alpha\beta}} = R \cdot i_{\alpha\beta_{max}} \cdot j + j \cdot \omega_{mech} \cdot L \cdot i_{\alpha\beta_{max}} \cdot j + e_{\alpha\beta} \cdot j \implies$$

$$\vec{u_{\alpha\beta}} = 0.3 \cdot 122.5652 \cdot j + j \cdot 265.1650 \cdot 0.5E - 3 \cdot 122.5652 \cdot j + 212.1320 \cdot j = -16.2500 + j \cdot 248.9016 V$$

Where the total length of the $\vec{u_{\alpha\beta}}$, and the angle, φ, between $\vec{u_{\alpha\beta}}$ and $\vec{e_{\alpha\beta}}$ is

$$\left|\vec{u_{\alpha\beta}}\right| = 249.4315 V \text{ and}$$
$$\varphi = \left|\arctan \frac{Re(\vec{u_{\alpha\beta}})}{Im(\vec{u_{\alpha\beta}})}\right| \cdot \frac{360}{2 \cdot \pi} = 3.7354°$$

To use the results in a three-phase model one needs convert from vector magnitudes to phase magnitudes.

$$\hat{u}_{abc} = \left|\vec{u_{\alpha\beta}}\right| \cdot \sqrt{\frac{2}{3}} = 203.6599 V$$
$$\hat{e}_{abc} = \left|\vec{e_{\alpha\beta}}\right| \cdot \sqrt{\frac{2}{3}} = 173.2051 V$$

4.2.5 Simplified current pulses

To analyse the behaviour of the DC-link current in the model of the inverter and the RLE-load, a simulation tool, LTspice is used. Simulations are carried out to predict the TVS converters current ripple on the dc-link side and how load changes affected the ripple. Depending on TVS status different subsystems will be differently loaded. These simulations were done to establish which load situations caused the greatest magnitude of current ripple. As previously mentioned in *Worst case current ripple* (1.2.2), the largest current ripple occurs when half of the maximum DC-voltage is supplied.

The goal for the inverter model is to evaluate the current ripple from a converter of a subsystem without any filter involvement. The current measured at the DC-voltage source represents the current ripple from the converter straight from the transistor bridge. Therefore an evaluation of the current ripple could be estimated without any converters' input filters effect. As seen in figure 18 the simulation of the inverter produces current pulses to the DC-voltage source. Furthermore the simulation was carried out with ten percent of the DC-voltage supplied to the converter. As a consequence the width of the current pulses represents a duty cycle of 0.1 (10%) which is the same as the duty cycle for the voltage pulses. This result indicated that the converters in the TVS would produce similar current and voltage pulses. As a consequence approximations to simple square shaped current pulses, shown in figure 18, could be made for the simulated current pulses in the inverter model see *Appendix B*.

According to simulations on the fictional motor the maximum current could never exceed $105A$ with $600V$ applied, see figure 18, figure 19 and figure 20. Therefore it appears that the maximum current can never exceed $105A$ regardless of the duty cycle.

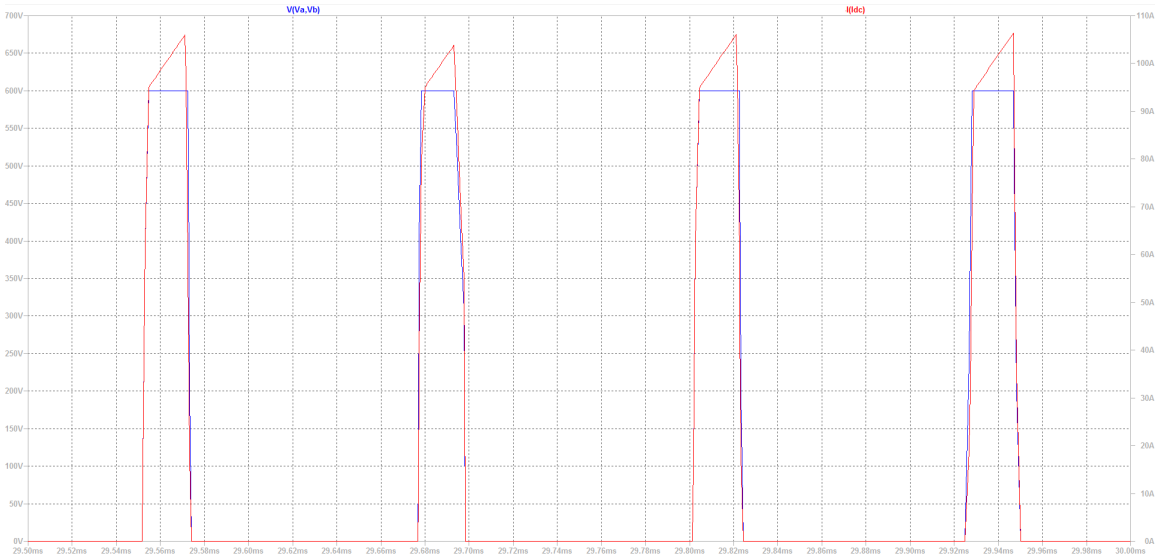

Figure 18: Current square pulses as a result of when ten percent of the DC-voltage is supplied through the inverter (i.e. duty cycle of ten percent). The blue represents load side voltage and the red represents DC-side current.

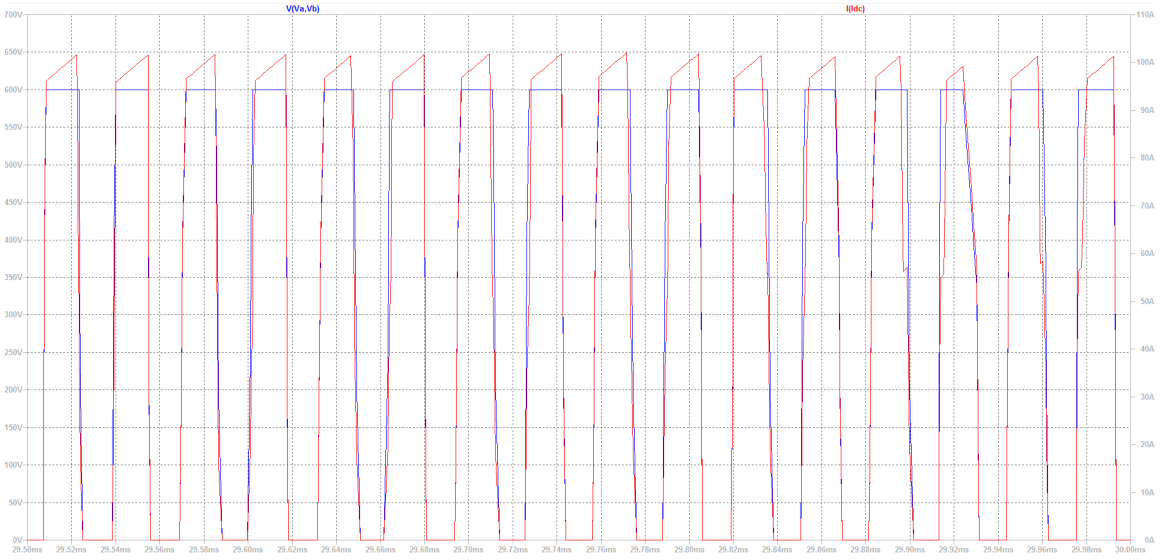

Figure 19: Current square pulses as a result of when 50 percent of the DC-voltage is supplied through the inverter (i.e. duty cycle of 50 percent). The blue represents load side voltage and the red represents DC-side current.

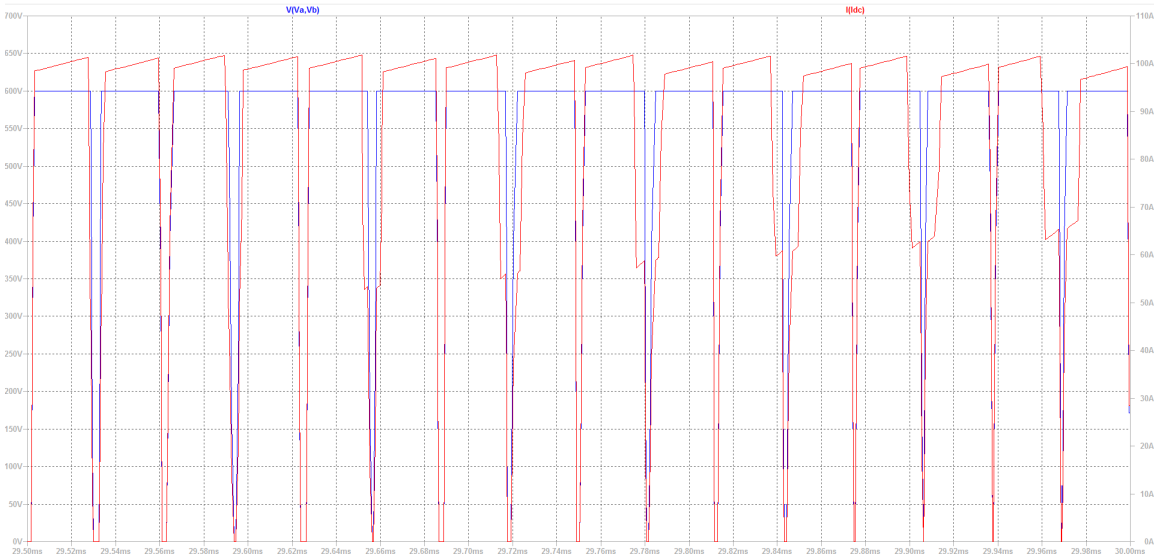

Figure 20: Current square pulses as a result of when 90 percent of the DC-voltage is supplied through the inverter (i.e. duty cycle of 90 percent). The blue represents load side voltage and the red represents DC-side current.

Furthermore the height of the current pulses can be seen as constant, see figure 21.

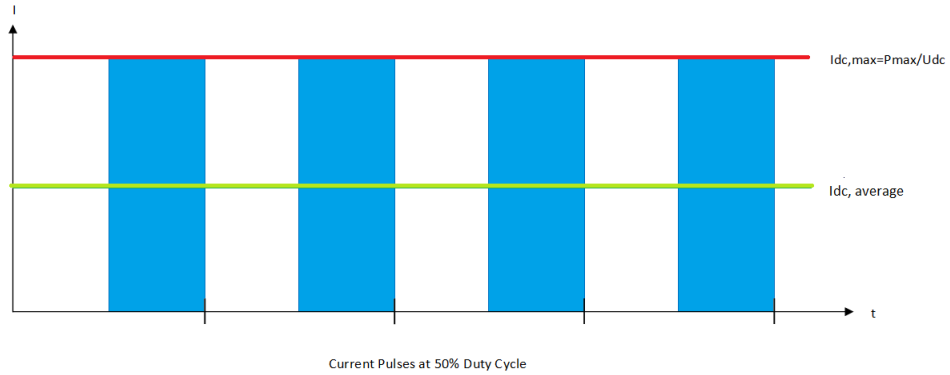

Figure 21: The height of the square pulse is independent of the duty cycle. However, an increase of the duty cycle will result in a wider current pulse and as a consequence an increase of the average current. Here the duty cycle is 50%.

As a consequence the inverter and three-phase load can be simplified to a square pulse. This gives that an equivalent circuit of an EMD can be greatly simplified as a whole. The equivalent circuits for the electric hybrid and the full electric are presented in the two following sections.

4.2.6 EMD electric hybrid model

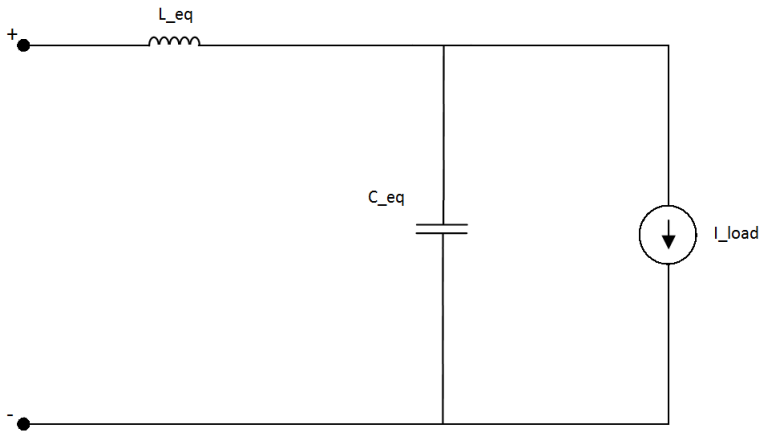

Figure 22: Equivalent circuit of the EMD in the electric hybrid.

The EMD for the electric hybrid, see figure 22. The current pulse generator operates with the frequency pulse frequency equal to twice the switching frequency as was derived in *section 1.2.3 - Voltage modulation* above.

4.2.7 EMD full electric model

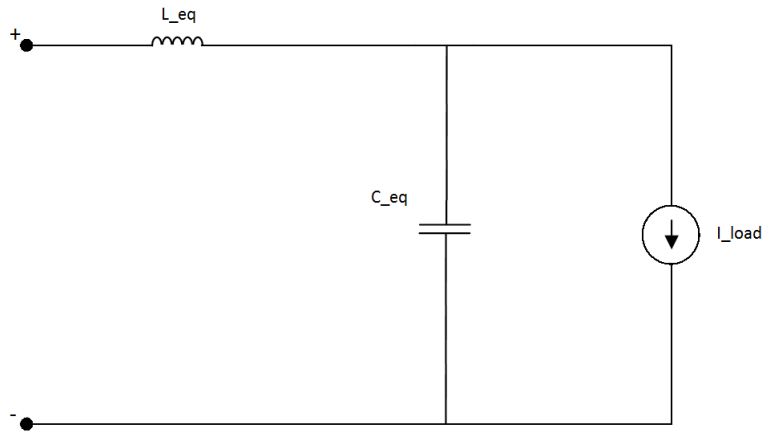

Figure 23: Equivalent circuit of the EMD in the full electric.

The EMD for the full electric hybrid, see figure 23. The current pulse generator operates equivalently as for the electric hybrid. In this model the value of the leakage inductance L is unknown or is to have no influence due its size according to the manufacturer.

4.3 HVAC model

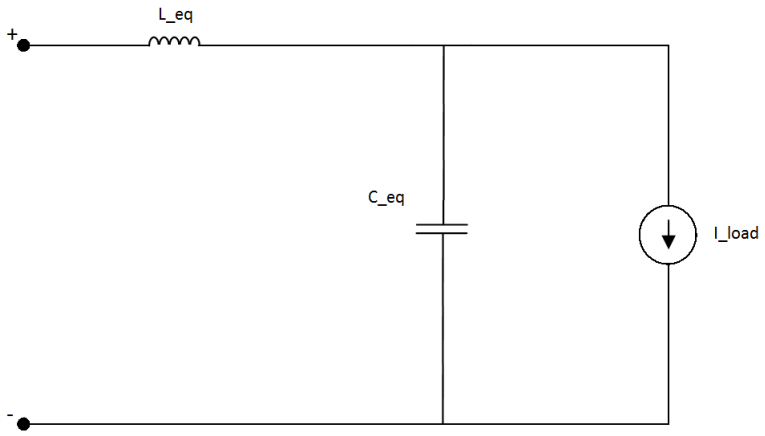

Figure 24: Equivalent circuit of the HVAC in both the electric hybrid and the full electric.

The HVAC, see figure 24, is as the EMD also a DC/AC converter, a three-phase load supplied through a PEC. Hence the same simplification can be made in the equivalent circuit of the HVAC. Worth mentioning is that it has the same perceived frequency as switching frequency. It is not known but most likely it is modulated with bus-clamped voltage modulation as seen in measurements figure 79 and figure 80. This type of modulation is used to reduce switching losses ([2], p.81). The HVAC is an electric machine that operates at base speed and thus has the same output from the inverter, thus its duty cycle is dependent on which DC-link voltage it receives momentarily. The lowest DC-link voltage that can supply full performance, specified by Volvo, to the electric machine through the inverter will ideally (no losses) give a duty cycle of 100 percent. So the duty cycle is therefore dependent on the actual DC-link voltage divided by the lowest DC-link voltage, $560V$ allowed to supply full performance see table 3.

4.4 Aircompressor model

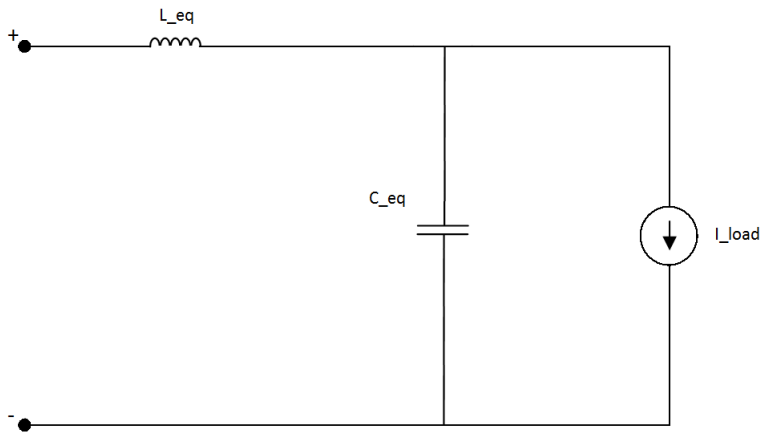

Figure 25: Equivalent circuit of the air compressor in both the electric hybrid and the full electric.

The air compressor, see figure 25, is also a DC/AC converter. The same simplification can be made in the equivalent circuit of the air compressor as well. Worth mentioning is that it, as the HVAC, has the same perceived frequency as switching frequency. It is known that it is modulated with bus-clamped voltage modulation as a means to reduce switching losses ([2], p.81). The air compressor is an electric machine that operates at base speed and thus has the same output from the inverter, thus its duty cycle is dependent on which DC-link voltage it receives at the moment. The lowest DC-link voltage that can supply full performance, specified by Volvo, to the electric machine through the inverter will ideally (no losses) give a duty cycle of 100 percent. So the duty cycle is therefore dependent on the actual DC-link voltage divided by the lowest DC-link voltage, $500V$ allowed to supply full performance see table 4.

4.5 Battery model

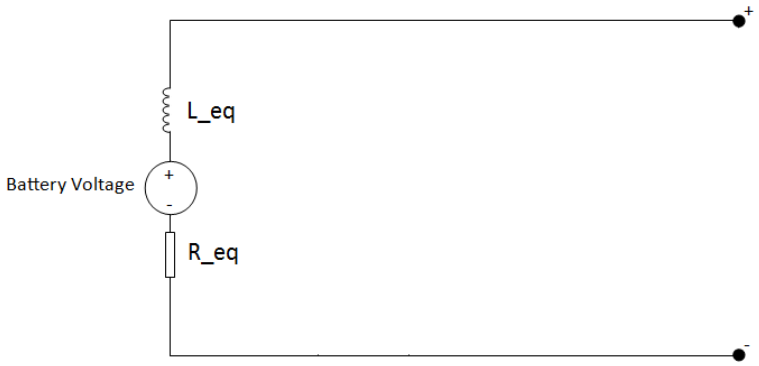

Figure 26: Equivalent circuit of the battery in both the electric hybrid and the full electric.

The battery equivalent, see figure 26, is probably the most simplified. Battery cells and their functions are advanced and difficult to model as a battery in a simple way. To not make the equivalent too complex the ESS' inner inductance and resistance was used in series with a voltage source. The equivalent of a battery is shown above in figure 26.

4.6 DCDC model

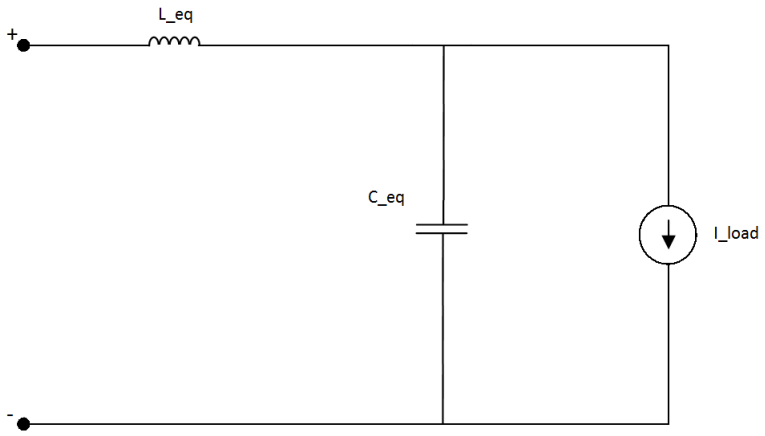

Figure 27: Equivalent circuit of the DCDC in both the electric hybrid and the full electric.

The DCDC, see figure 27, has both a DC/AC-converter (4Q-one-phase) and a AC/DC-rectifier, galvanically isolated through a transformer. Again the simplification can be used for the PEC and the load but for the DCDC the duty cycle is not dependent on a machine's speed since it is not an electric machine. However the duty cycle is approximately the lowest DC-link voltage that can supply full performance charging of the $24V$-system, specified by Volvo. In this case $500V$ divided by the applied DC-voltage. The voltage modulation is symmetrized or sinusoidal and is thus the perceived frequency is the doubled the switching frequency, as seen from measurements in figure 85 and figure 86. The inductors are verified by Volvo in figure 27. However on the circuit board there is an additional common mode choke that is not yet verified.

4.7 OnBC model

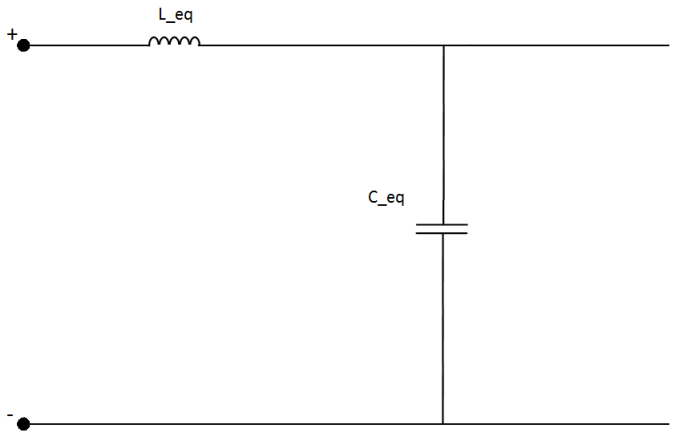

Figure 28: Equivalent circuit of the onboard charger in both the electric hybrid and the full electric.

The onboard charger, see figure 28, is never in operation during tests or simulations in this thesis.

4.8 Heater model

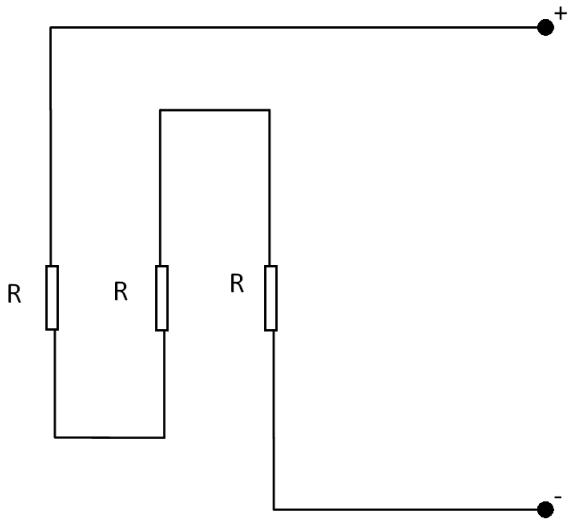

Figure 29: Equivalent circuit of the onboard charger in both the electric hybrid and the electric.

The electric hybrid uses dissipated engine heat to heat air for the climate system in the bus. The heater, see figure 29, is used in the electric as it can not take enough heat energy from its electric motor.

4.9 Cable model

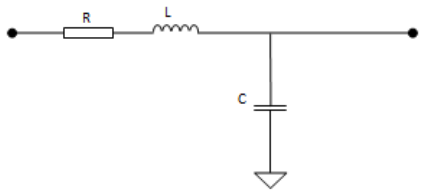

Figure 30: Equivalent circuit of the $50mm^2$ cables in both the electric hybrid and the full electric.

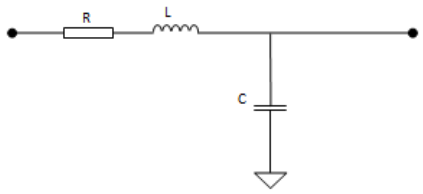

Figure 31: Equivalent circuit of the $2x4mm^2$ cables in both the electric hybrid and the full electric.

The cables are represented with their properties per meter as supplied from the cable manufacturer. The equivalent cable model is used for all dimensions of cables but are given different values on their specific properties. See the cable models of the the $50mm^2$ with specified values in figure 30 and the 2x$4mm^2$ with specified values in figure 31.

5 Simulation modelling

5.1 Software selection

5.1.1 Requirements for the software

On the market there are several software that can be used to build electrical circuits. To find a suitable software for this application a list of requirements is created. The criteria to be fulfilled by the simulation software are the following:

Competency The software is competent enough to manage a whole-system simulation.

Short learning curve The software is intuitive to work with so that a limited time would be spent on guides and manuals.

Simplicity The software is simple so that many colleagues of different positions could work with the software.

Compability The software can be used with Windows OS.

Accessibility The software is accessible in the Volvo IT-portal or online.

5.1.2 Motivation for choise of LTspice

With the information gathered during a previous project done by Haresh Viswanathan (see *Appendix C - Software evaluation*) the choice is LTspice as simulation software. With the following motivation:

- Simple and easy to use without previous experience.
- Accurate enough for the application.
- The schematics editor can be used to create own designs.
- Previously used by colleagues at Volvo in other contexts.
- Free. Available online.

5.2 LTspice component library

The library is built upon the following subsystems that can be connected to larger systems of different kinds. As a consequence different types of TVS and different subsystems can be simulated as preferred.

5.2.1 EMD model

The simulation model circuit of the equivalent circuit of the EMD for the electric hybrid see figure 32.

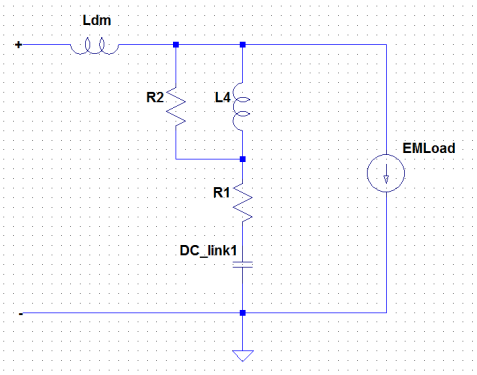

Figure 32: Spice model of the EMD type B.

The simulation model of the equivalent circuit of the EMD for the electric is shown in figure 33.

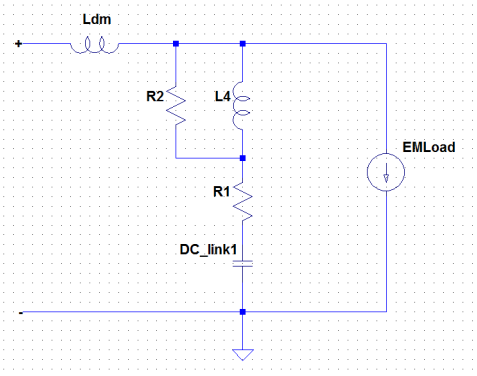

Figure 33: Spice model of the EMD type C.

5.2.2 HVAC model

The simulation model circuit of the equivalent circuit of the HVAC is shown in figure 34.

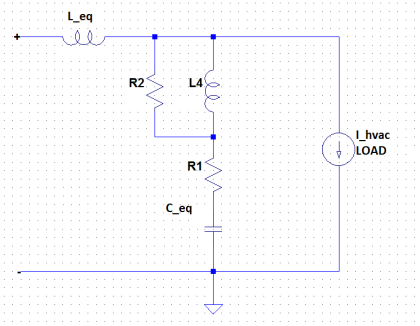

Figure 34: Spice model of the HVAC.

5.2.3 Air compressor model

The simulation model circuit of the equivalent circuit of the air compressor is shown in figure 35.

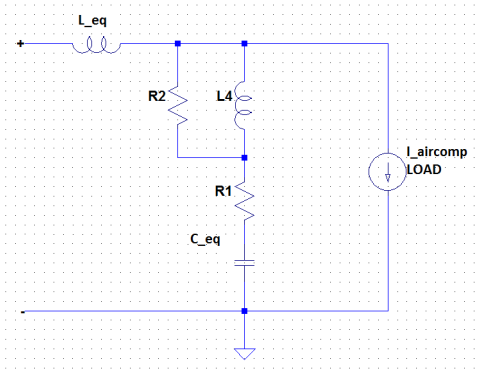

Figure 35: Spice model of the air compressor.

5.2.4 DCDC model

The simulation model circuit of the equivalent circuit of the DCDC is shown in figure 36.

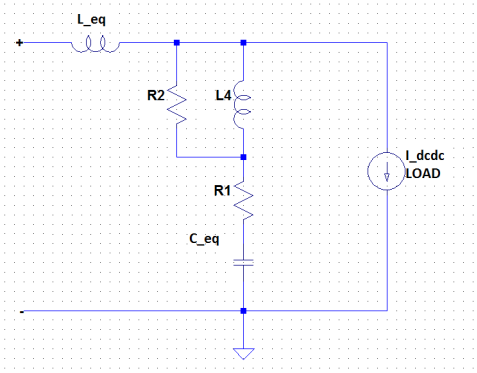

Figure 36: Spice model of the DCDC

5.2.5 OnBC model

The simulation model circuit of the equivalent circuit of the onboard charger is shown in figure 37.

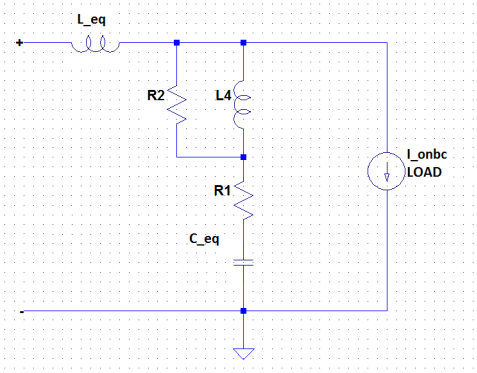

Figure 37: Spice model of the OnBC.

5.2.6 Heater model

The simulation model circuit of the equivalent circuit of the heater is shown in figure 38.

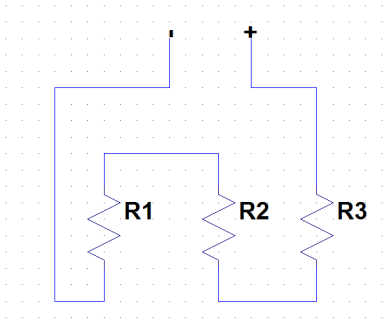

Figure 38: Spice model of the heater.

5.2.7 Cable model

The simulation model circuits of the equivalent circuits of the cables is shown in figure 39 and figure 40.

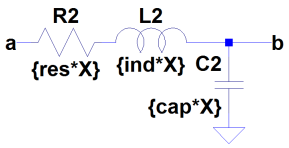

Figure 39: Spice model of the $50mm^2$.

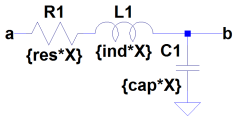

Figure 40: Spice model of the 2x$4mm^2$.

5.2.8 Battery model

The simulation model circuit of the equivalent circuit of the ESS is shown in figure 41.

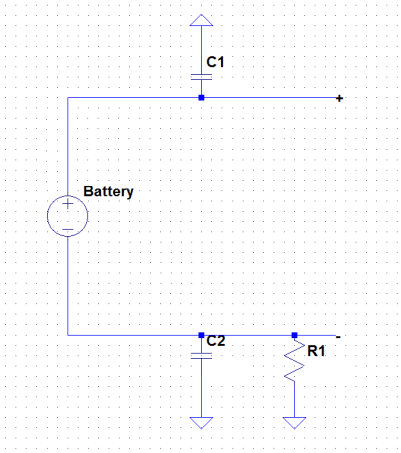

Figure 41: Spice model of the ESS.

5.2.9 Electric hybrid TVS

The simulation model circuit of the equivalent circuit of the whole electric hybrid TVS is shown in figure 42.

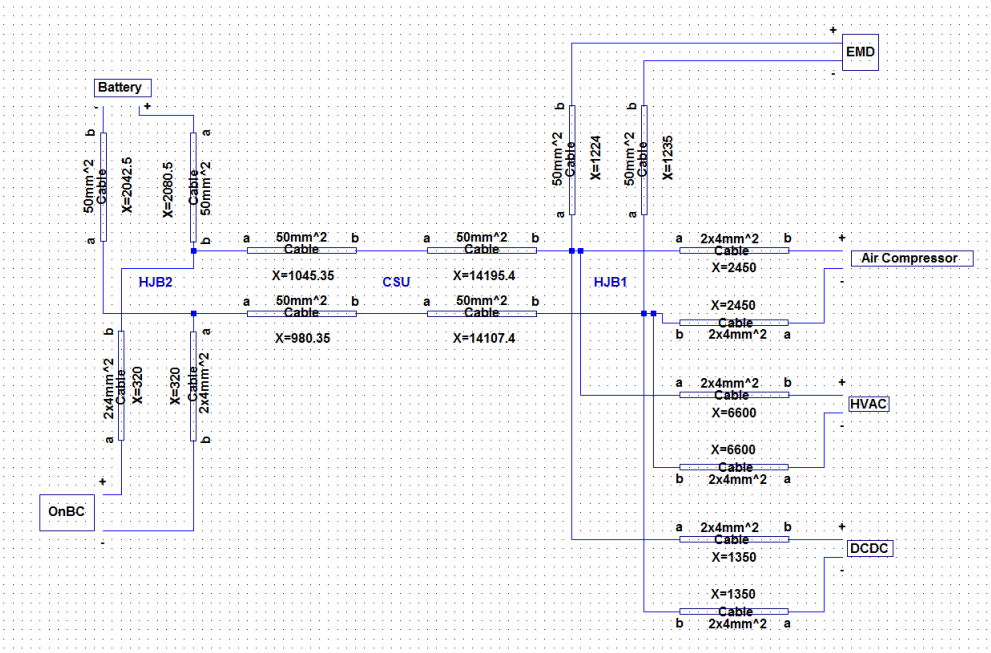

Figure 42: Spice model of the electric hybrid TVS.

5.2.10 Electric TVS

The simulation model circuit of the equivalent circuit of the whole full electric TVS is shown in figure 43.

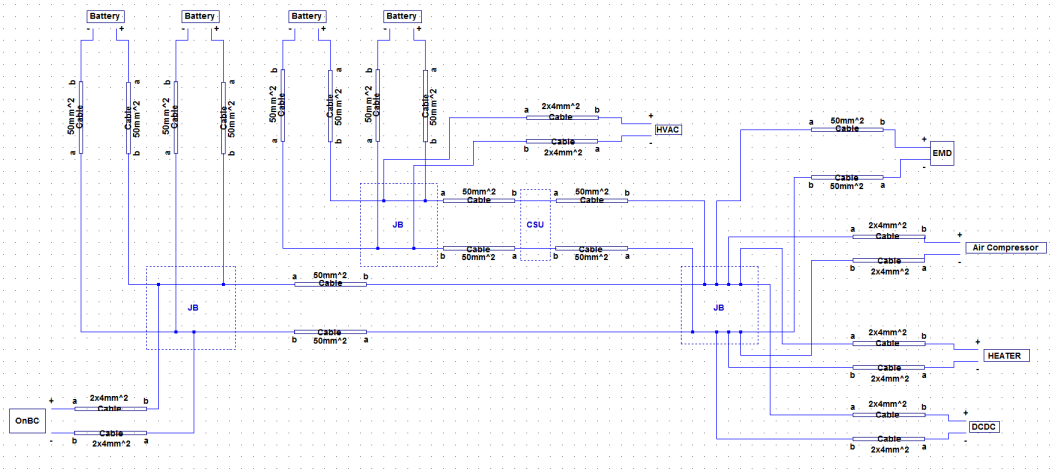

Figure 43: Spice model of the electric TVS.

6 Simulation

Since the traction voltage system consists of many subsystems it is complex. The initial idea was to test each subsystem one by one, to get a greater understanding of how each subsystem's current ripple behaves. Furthermore, the simulations were made to replicate the measurements. This led to the simulation cases below where simulations get the same parameter values in terms of applied load, voltage, switching frequency etc. as given by the test data.

6.1 Simulation cases with parameters given by Volvo

In this section the test cases are performed with the model set with the parameter information given by Volvo and suppliers. These values can be seen in *section 4.2.6* .

6.1.1 EMD and DCDC active

Since there is no measurement of only the EMD running this test case is the EMD and the DCDC active. Both with the applied average voltage of $595V$. The EMD is loaded with the average current of $143A$ at a 50% duty cycle. It has the switching frequency $(f_{sw3})_{EMD_{typeC}}$ and is thus simulated with the perceived switching frequency $2(f_{sw3})_{EMD_{typeC}}$. The DCDC is loaded with the average current of $4.2A$ at a $\frac{500}{595} = 0.84\%$ duty cycle. It is simulated with the perceived switching frequency $2(f_{sw3})_{EMD_{typeC}}$ as it has the switching frequency $(f_{sw3})_{EMD_{typeC}}$. The EMD can switch at different frequencies but as can be seen in the 3D-plots from the measurements in *chapter 7 - Experimental verification and model discussion* the perceived switching frequency of $2(f_{sw3})_{EMD_{typeC}}$ is the one having higher impact on other subsystems. This can be seen in figure 69, figure 70, figure 71, figure 72 and figure 73.

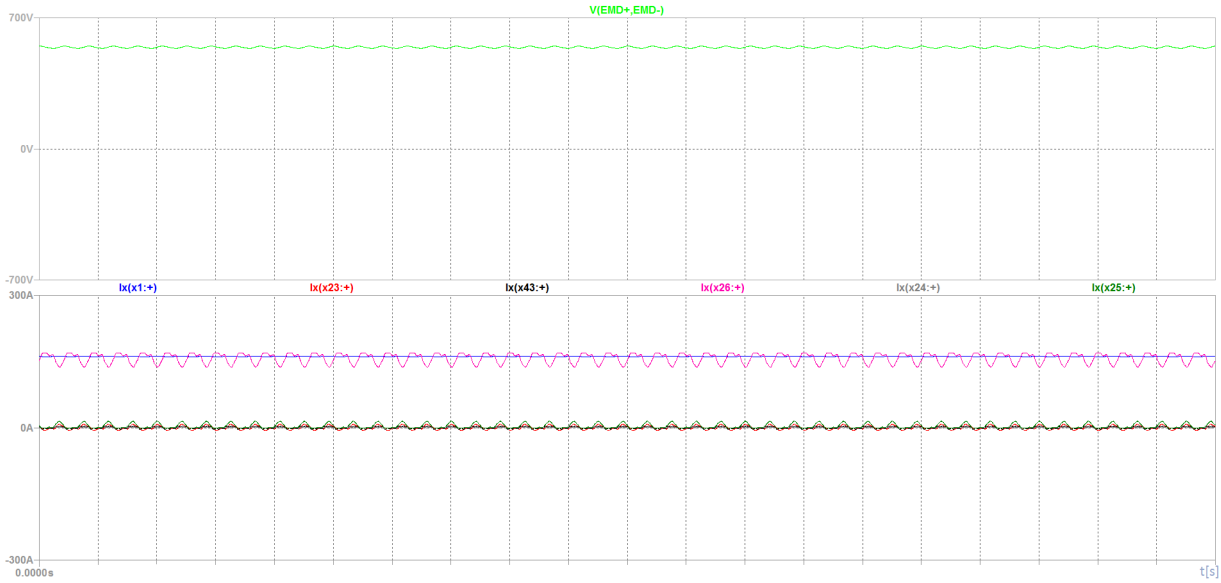

Figure 44: Simulated ripple at EMD base speed and the DCDC loaded with $84A$ on the $24V$-side. The light green represents the DC-voltage, the blue the ESS current, the red the air compressor current, the black the OnBc current, the pink the EMD current, the grey the HVAC current, and the dark green represents the DCDC current.

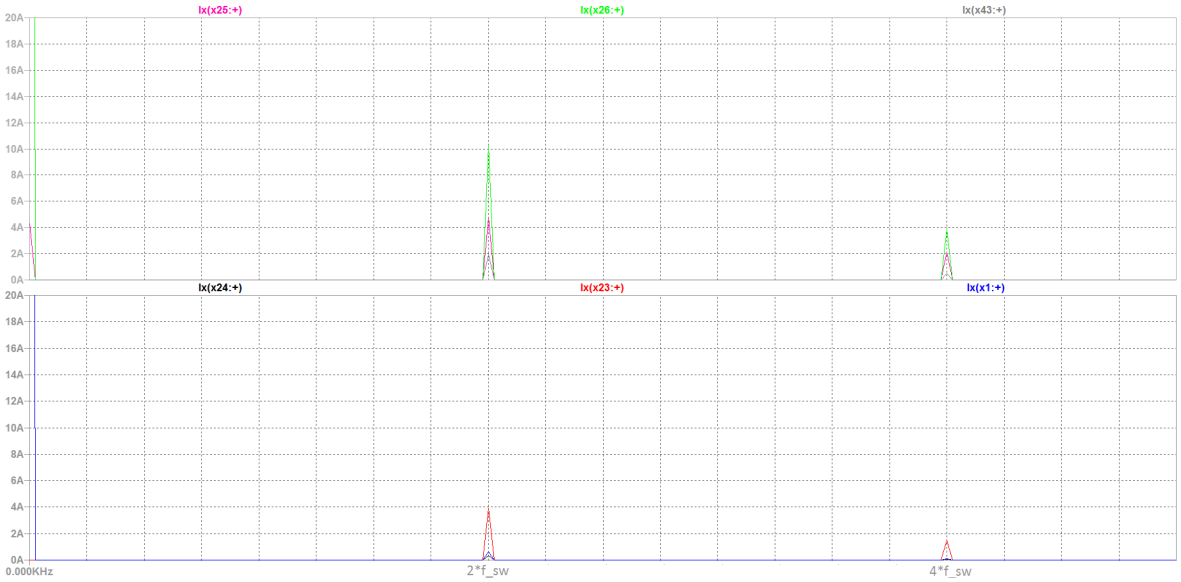

Figure 45: FFT of the subsystem currents when the EMD was simulated at base speed with the DCDC loaded with $84A$ on the $24V$-side. The pink represents the DCDC current, the light green the EMD current, the grey the OnBC current, the black the HVAC current, the red the air compressor current, and the blue represents the ESS current.

In figure 44 it is seen that the EMD (purple) is a far larger power consumer than the DCDC (dark green). The EMD has a repeating tooth-shaped waveform. The DCDC seems to have the same waveform only inverted but it is hard to distinguish. The DCDC average current is $4.3A$, the other subsystems has a zero average current as they are inactive. The FFT analysis was done with focus on $2(f_{sw_3})_{EMD_{typeC}}$ and the current levels can be seen as RMS currents in figure 45 at both $2(f_{sw_3})_{EMD_{typeC}}$ and its multiple $4(f_{sw_3})_{EMD_{typeC}}$. Since the axis are not satisfactory in LTspice all values are clarified in table 7. The timespan in figure 44 is of the same length as the time span of the equivalent plot with measured data in *chapter 7 - Experimental verification and model discussion*.

Subsystem	Parameter	U_{avg} [V]	I_{avg} [A]	$I_{RMS}@2(f_{sw_3})_{EMD_{typeC}}$kHz [A]
ESS	$x1$	-	161.6	0.6
OnBC	$x43$	-	-	1.9
EMD	$x26$	542	157.3	10.3
Air compressor	$x23$	-	-	3.9
HVAC	$x24$	-	-	0.3
DCDC	$x25$	-	4.3	4.7

Table 7: Clarification of values in the ripple- and FFT-plots of the simulated EMD and DCDC.

6.1.2 Only HVAC active

The HVAC is loaded with the average current of $15.68A$ at a $\frac{560}{610} = 0.92\%$ duty cycle. It has the switching frequency $(f_{sw})_{HVAC}$ and is thus simulated with the perceived switching frequency $(f_{sw})_{HVAC}$ as it is believed to be modulated with bus-clamped voltage modulation.

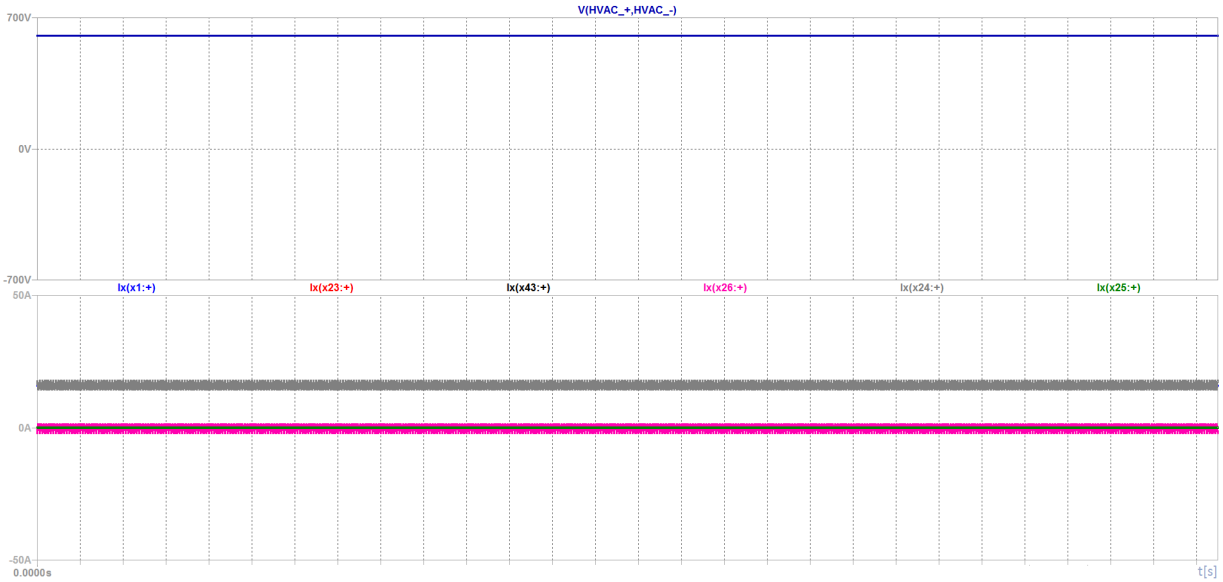

Figure 46: HVAC simulated ripple. The dark blue represents the DC-voltage, the blue the ESS current, the red the air compressor current, the black the OnBc current, the pink the EMD current, the grey the HVAC current, and the dark green represents the DCDC current.

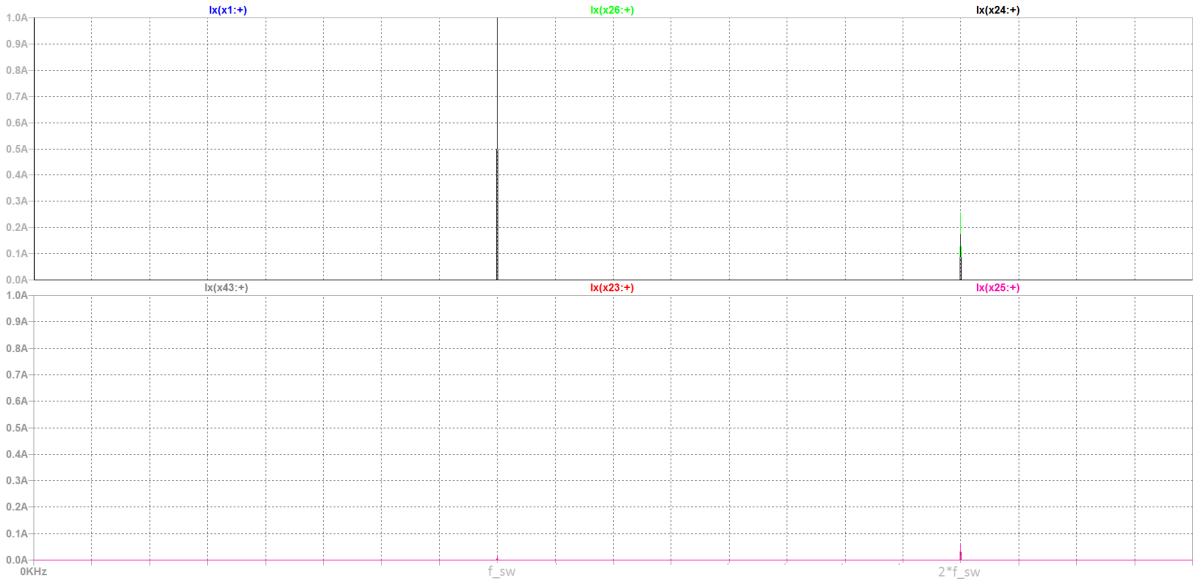

Figure 47: FFT of the subsystem currents when the HVAC was simulated. The pink represents the DCDC current, the light green the EMD current, the grey the OnBC current, the black the HVAC current, the red the air compressor current, and the blue represents the ESS current.

figure 46 shows the average current levels of the HVAC, $15.8A$ and the EMD, $0A$. The ESS current is plotted under the HVAC current and the other currents are plotted under the EMD current. In figure 47 the RMS currents at both $(f_{sw})_{HVAC}$ and the multiple $2(f_{sw})_{HVAC}$ from the FFT analysis can be seen. The FFT was done with focus on $(f_{sw})_{HVAC}$. All values are clarified in table 8. The timespan in figure 46 is of the same length as the time span of the equivalent plot with measured data in *chapter 7 - Experimental verification and model discussion.*

Subsystem	Parameter	U_{avg} [V]	I_{avg} [A]	$I_{RMS}@(f_{sw})_{HVAC}$kHz [A]
ESS	$x1$	-	15.8	1.2E-3
OnBC	$x43$	-	-	5.2E-3
EMD	$x26$	-	-	0
Air compressor	$x23$	-	-	10.4E-3
HVAC	$x24$	604	15.8	1.1
DCDC	$x25$	-	-	12.8E-3

Table 8: Clarification of values in the ripple- and FFT-plots of the simulated HVAC.

6.1.3 Only air compressor active

The air compressor is loaded with the average current of $8.44A$ at a $\frac{500}{616} = 0.81\%$ duty cycle. It has the switching frequency $(f_{sw})_{aircomp}$ and is thus simulated with the perceived switching frequency $(f_{sw})_{aircomp}$ as it is known to be modulated with bus-clamped voltage modulation.

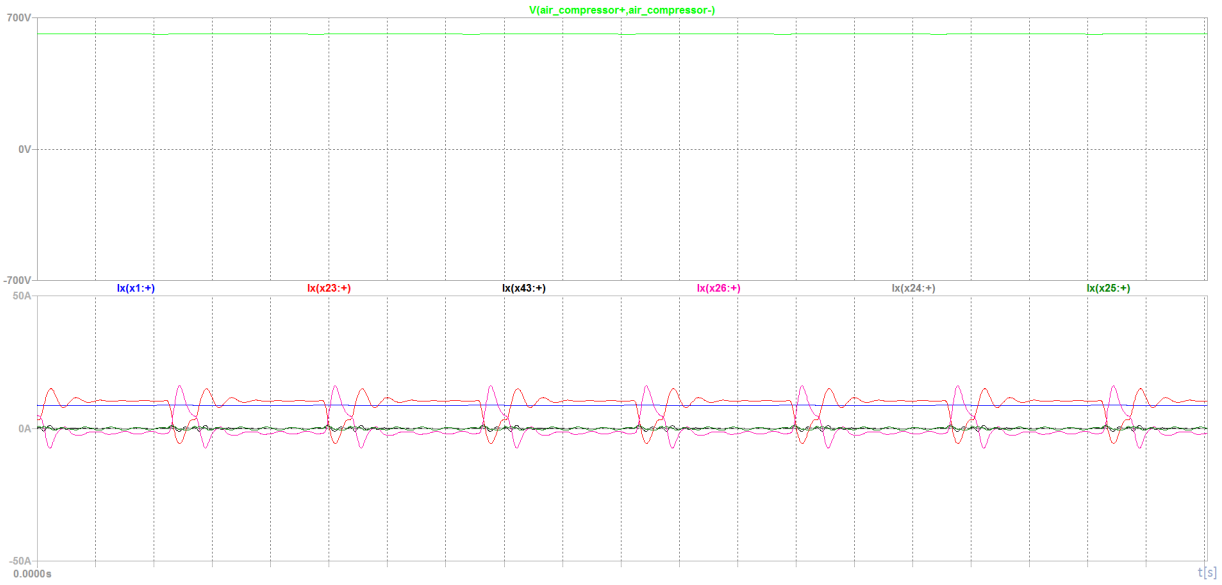

Figure 48: Air compressor simulated current ripple at base speed. The light green represents the DC-voltage, the blue the ESS current, the red the air compressor current, the black the OnBc current, the pink the EMD current, the grey the HVAC current, and the dark green represents the DCDC current.

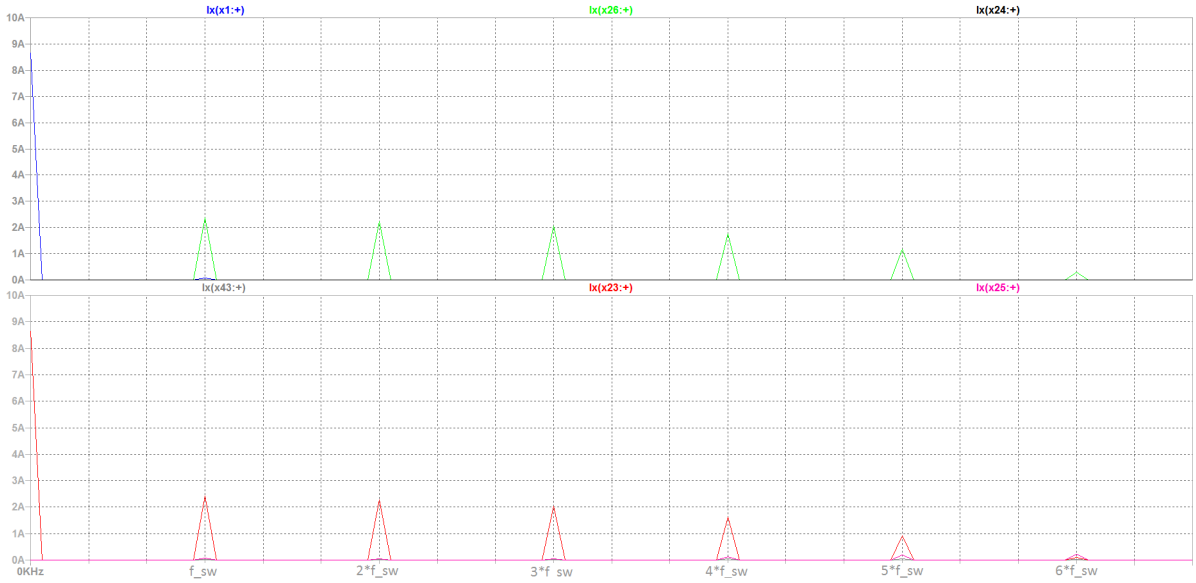

Figure 49: FFT of the subsystem currents when the air compressor was simulated at base speed. The pink represents the DCDC current, the light green the EMD current, the grey the OnBC current, the black the HVAC current, the red the air compressor current, and the blue represents the ESS current

In figure 48 it can be seen that the air compressor current has an oscillating behaviour. It can also be seen that the EMD shows the same behaviour only inverted. The other subsystem currents have an average of $0A$. In figure 49 the RMS currents at $(f_{sw})_{aircomp}$ and the multiples $2(f_{sw})_{aircomp}$, $3(f_{sw})_{aircomp}$, $4(f_{sw})_{aircomp}$, $5(f_{sw})_{aircomp}$ and $6(f_{sw})_{aircomp}$ from the FFT analysis can be seen. The FFT is done with focus on $(f_{sw})_{aircomp}$. All values are clarified in table 9. The timespan in figure 48 is of the same length as the time span of the equivalent plot with measured data in *chapter 7 - Experimental verification and model discussion.*

Subsystem	Parameter	U_{avg} [V]	I_{avg} [A]	$I_{RMS}@(f_{sw})_{aircomp}$kHz [A]
ESS	$x1$	-	8.6	69E-3
OnBC	$x43$	-	-	30E-3
EMD	$x26$	-	-	2.3
Air compressor	$x23$	613	8.7	2.3
HVAC	$x24$	-	-	5E-3
DCDC	$x25$	-	-	70E-3

Table 9: Clarification of values in the ripple- and FFT-plots of the simulated air compressor.

6.1.4 Only DCDC active

The DCDC is loaded with the average current of $8.62A$ at a $\frac{500}{612} = 0.82\%$ duty cycle. It has the switching frequency $(f_{sw})_{DCDC}$ and is thus simulated with the perceived switching frequency $2(f_{sw})_{DCDC}$.

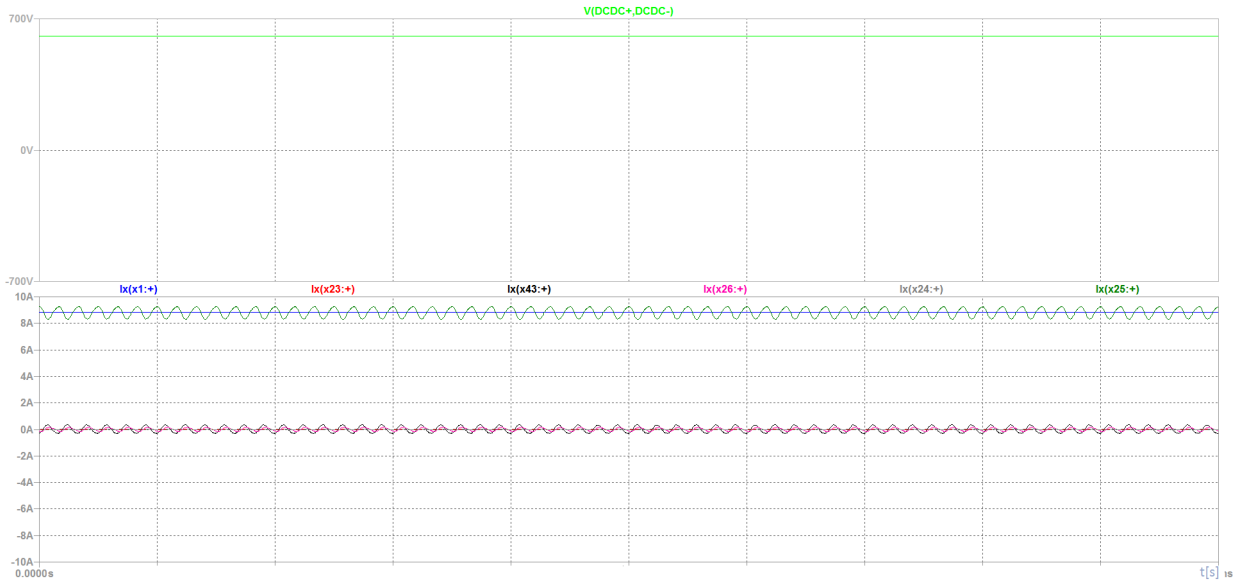

Figure 50: DCDC simulated ripple. The light green represents the DC-voltage, the blue the ESS current, the red the air compressor current, the black the OnBc current, the pink the EMD current, the grey the HVAC current, and the dark green represents the DCDC current.

Figure 51: FFT of the subsystem currents when the DCDC was simulated. The light green represents the DC-voltage, the blue the ESS current, the red the air compressor current, the black the OnBc current, the pink the EMD current, the grey the HVAC current, and the dark green represents the DCDC current.

In figure 50 it can be seen that the DCDC current has a sinusoidal form. It can also be seen that the EMD and the other subsystems show the same behaviour only with the average current around $0A$. In figure 51 the RMS currents at $2(f_{sw})_{DCDC}$ from the FFT analysis can be seen. The FFT was done with focus on $2(f_{sw})_{DCDC}$. All values are clarified in table 10. The timespan in figure 50 is of the same length as the time span of the equivalent plot with measured data in *chapter 7 - Experimental verification and model discussion.*

Subsystem	Parameter	U_{avg} [V]	I_{avg} [A]	I_{RMS}@$2(f_{sw})_{DCDC}$kHz [A]
ESS	$x1$	-	8.8	0
OnBC	$x43$	-	-	0.2
EMD	$x26$	-	-	0.1
Air compressor	$x23$	-	-	17E-3
HVAC	$x24$	-	-	2E-3
DCDC	$x25$	607	8.8	0.3

Table 10: Clarification of values in the ripple- and FFT-plots of the simulated DCDC.

6.2 Simulation cases with experimental parameters

It was decided to experiment with the cable values given as their inductances are $Volvovalue$ per meter for the $50mm^2$-cable at $10kHz$. Cable values were calculated with the wire self inductance calculator from EEWeb [10]. The used cable values are $1\mu H$ per meter for the $50mm^2$-cable and $1.35\mu H$ per meter for the $2x4mm^2$-cable. The same settings for parameter values in terms of applied load, voltage, switching frequency etc. are used as in the section where only Volvo given parameters were used. The only difference compared to *section 6.1 - Simulation cases with parameters given by Volvo* are the cable parameters.

6.2.1 EMD and DCDC active

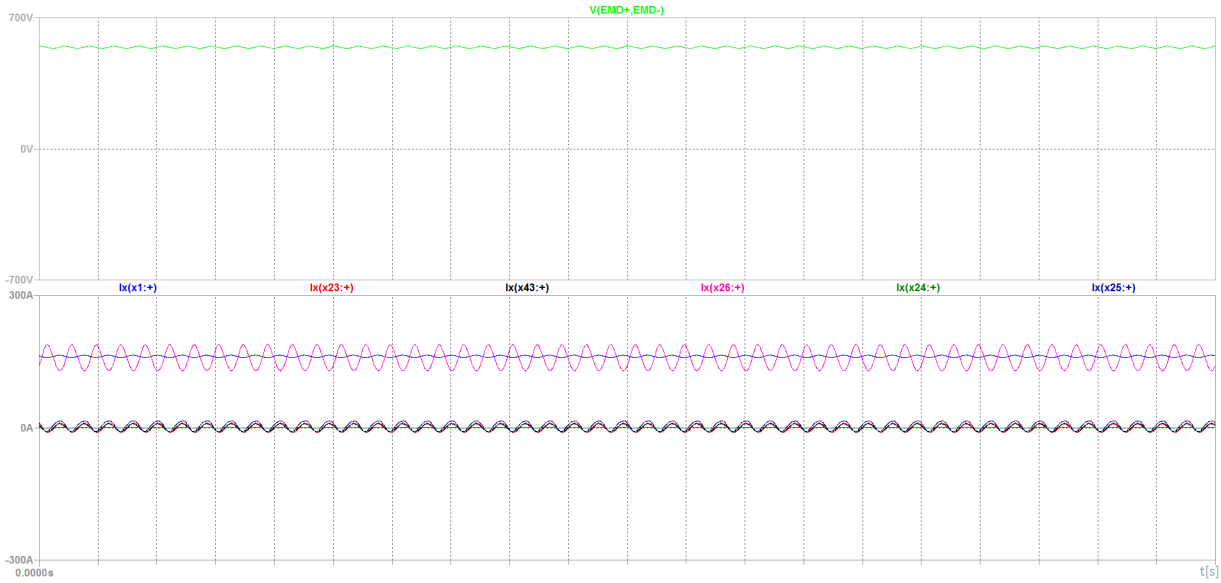

Figure 52: Simulated ripple at EMD base speed and the DCDC loaded with $84A$ on the $24V$-side and also experimental cable values. The light green represents the DC-voltage, the blue the ESS current, the red the air compressor current, the black the OnBc current, the pink the EMD current, the grey the HVAC current, and the dark green represents the DCDC current.

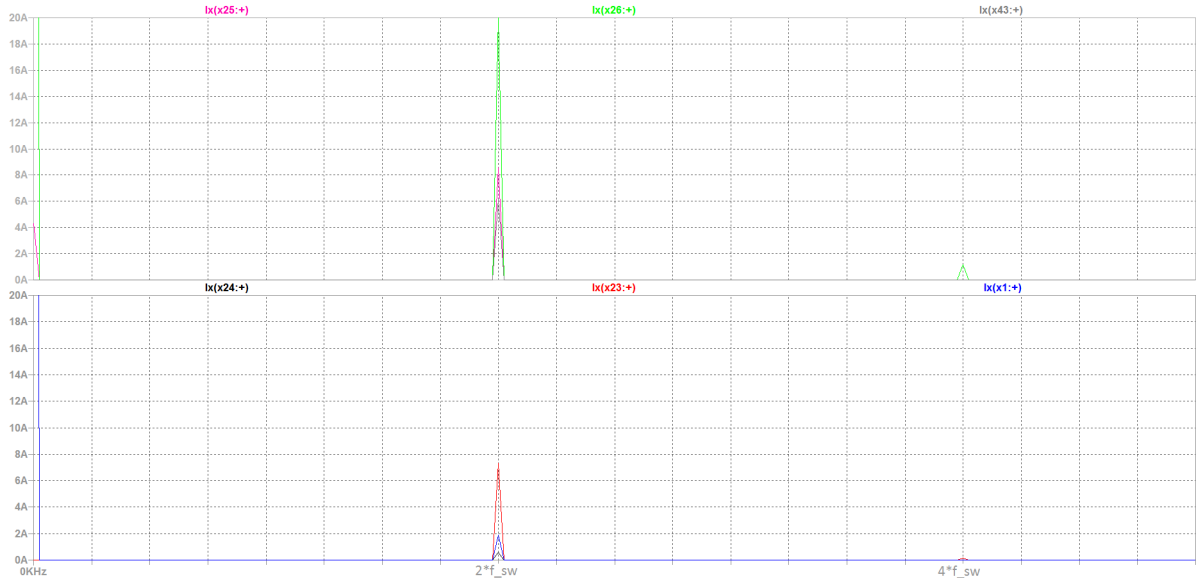

Figure 53: FFT of the subsystem currents when the EMD was simulated at base speed with the DCDC loaded with $84A$ on the $24V$-side and also experimental cable values. The light green represents the DC-voltage, the blue the ESS current, the red the air compressor current, the black the OnBc current, the pink the EMD current, the grey the HVAC current, and the dark green represents the DCDC current.

With the experimental values it is seen in figure 52 that the EMD current waveform is sinusoidal. The other currents also has sinusoidal waveforms. The DCDC average current is $4.3A$, the other subsystems has a zero average current as they are inactive. The FFT analysis was done with focus on $2(f_{sw_3})_{EMD_{typeC}}$ and the current levels can be seen as RMS currents in figure 53 at both $2(f_{sw_3})_{EMD_{typeC}}$ and its multiple $4(f_{sw_3})_{EMD_{typeC}}$. Values are clarified in table 11. The timespan in figure 52 is of the same length as the time span of the equivalent plot with measured data in *chapter 7 - Experimental verification and model discussion.*

Subsystem	Parameter	U_{avg} [V]	I_{avg} [A]	$I_{RMS}@2(f_{sw_3})_{EMD_{typeC}}$kHz [A]
ESS	$x1$	-	161.6	1.8
OnBC	$x43$	-	-	6.2
EMD	$x26$	542	157.3	20.6
Air compressor	$x23$	-	-	7.3
HVAC	$x24$	-	-	0.6
DCDC	$x25$	-	4.3	8.5

Table 11: Clarification of values in the ripple- and FFT-plots of the simulated EMD and DCDC with experimental cable values.

6.2.2 Only HVAC active

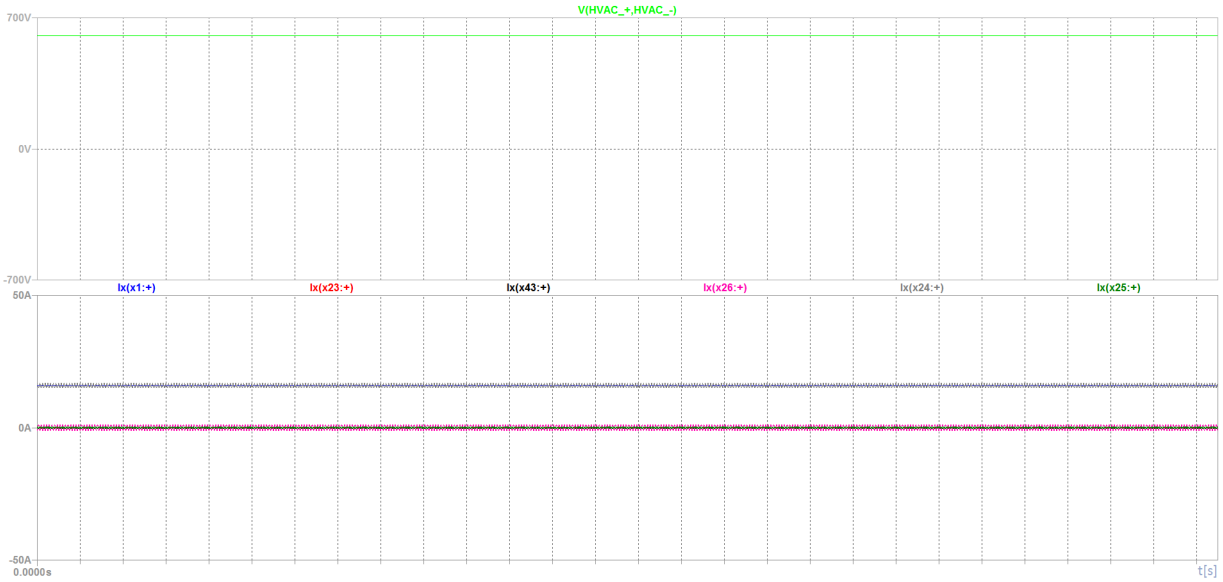

Figure 54: HVAC simulated ripple with experimental cable values. The light green represents the DC-voltage, the blue the ESS current, the red the air compressor current, the black the OnBc current, the pink the EMD current, the grey the HVAC current, and the dark green represents the DCDC current.

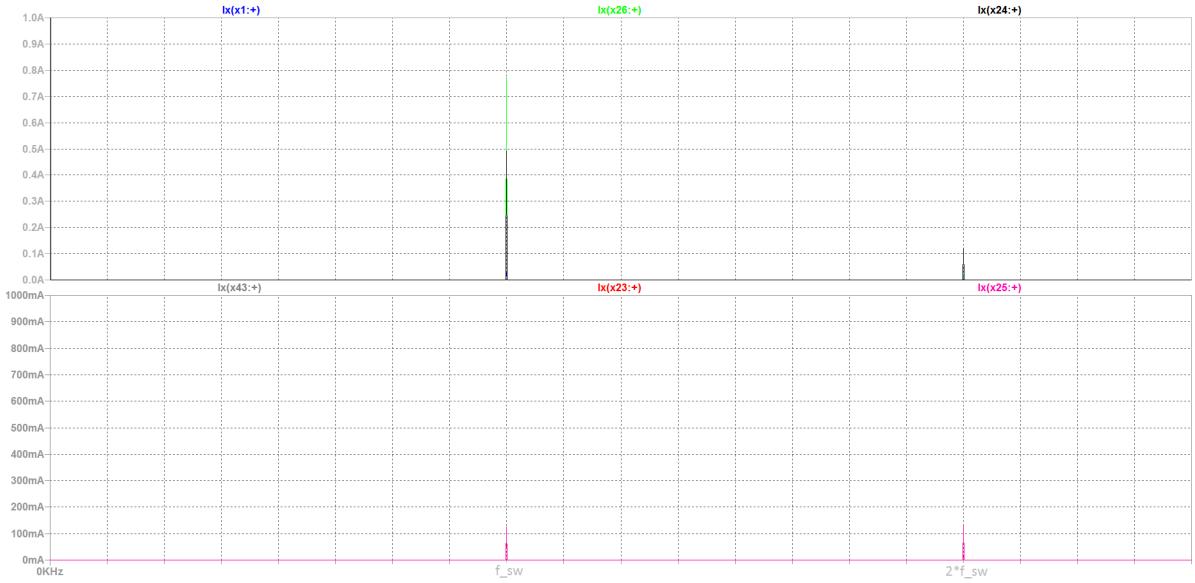

Figure 55: FFT of the subsystem currents when the HVAC was simulated with experimental cable values. The light green represents the DC-voltage, the blue the ESS current, the red the air compressor current, the black the OnBc current, the pink the EMD current, the grey the HVAC current, and the dark green represents the DCDC current.

figure 54 shows the average current levels of the HVAC, $16.3A$ and the EMD, $0A$. The ESS current is plotted under the HVAC current and the other currents are plotted under the EMD current. In figure 55 the RMS currents at both $2(f_{sw})_{HVAC}$ and the multiple $4(f_{sw})_{HVAC}$ from the FFT analysis can be seen. The FFT was done with focus on $2(f_{sw})_{HVAC}$. All values are clarified in table 12. The timespan in figure 54 is of the same length as the time span of the equivalent plot with measured data in *chapter 7 - Experimental verification and model discussion.*

Subsystem	Parameter	U_{avg} [V]	I_{avg} [A]	I_{RMS}@$2(f_{sw})_{HVAC}$kHz [A]
ESS	$x1$	-	15.9	27E-3
OnBC	$x43$	-	-	90E-3
EMD	$x26$	-	-	768E-3
Air compressor	$x23$	-	-	107E-3
HVAC	$x24$	604	16.3	487E-3
DCDC	$x25$	-	-	123E-3

Table 12: Clarification of values in the ripple- and FFT-plots of the simulated HVAC with experimental cable values.

6.2.3 Only air compressor active

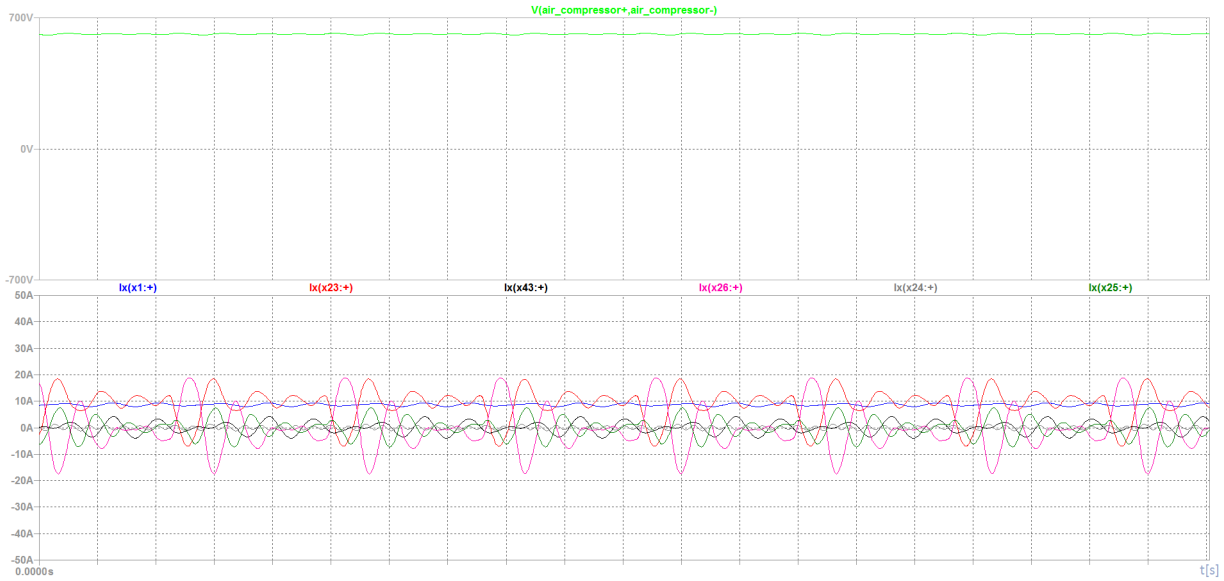

Figure 56: Air compressor simulated ripple with experimental cable values at base speed. The light green represents the DC-voltage, the blue the ESS current, the red the air compressor current, the black the OnBc current, the pink the EMD current, the grey the HVAC current, and the dark green represents the DCDC current.

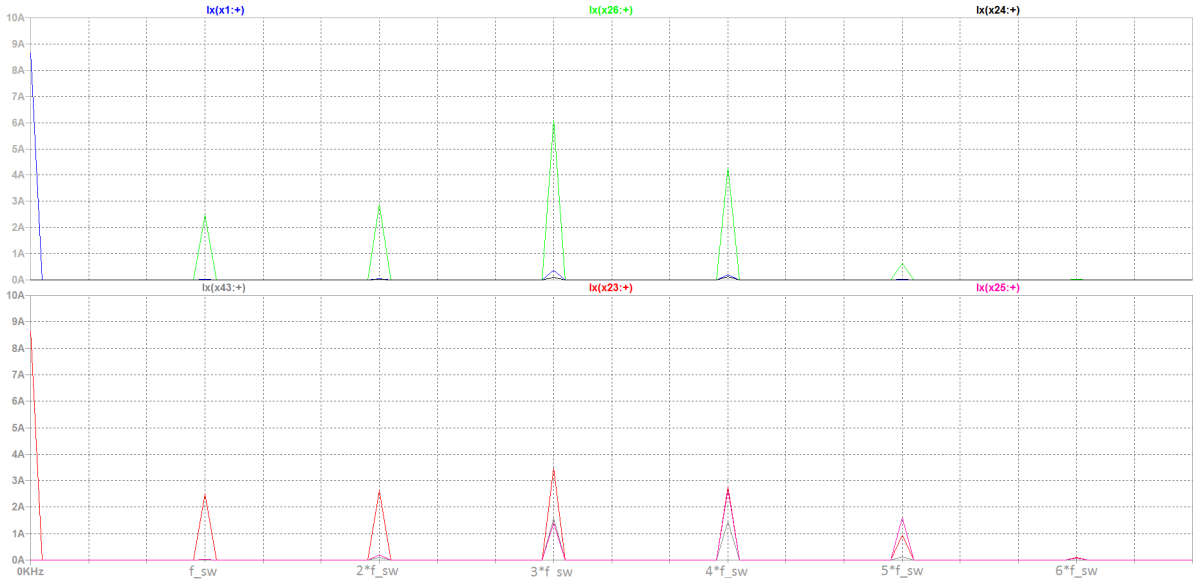

Figure 57: FFT of the subsystem currents when the air compressor was simulated with experimental cable values at base speed. The light green represents the DC-voltage, the blue the ESS current, the red the air compressor current, the black the OnBc current, the pink the EMD current, the grey the HVAC current, and the dark green represents the DCDC current.

In figure 56 it can be seen that the air compressor current has an oscillating behaviour. It can also be seen that the EMD shows the same behaviour only inverted and slightly larger. The other subsystem currents have an average of $0A$. It can also be seen that the DCDC (dark green) gets the same waveform-shape as the air compressor but with lower amplitude and the OnBC (black) gets the same waveform-shape as the EMD compressor but with lower amplitude. In figure 57 the RMS currents at $(f_{sw})_{aircomp}$ and the multiples $2(f_{sw})_{aircomp}$, $3(f_{sw})_{aircomp}$, $4(f_{sw})_{aircomp}$, $5(f_{sw})_{aircomp}$ and $6(f_{sw})_{aircomp}$ from the FFT analysis can be seen. The FFT was done with focus on $(f_{sw})_{aircomp}$. All values are clarified in table 13. The timespan in figure 56 is of the same length as the time span of the equivalent plot with measured data in *chapter 7 - Experimental verification and model discussion*.

Subsystem	Parameter	U_{avg} [V]	I_{avg} [A]	I_{RMS}@$(f_{sw})_{aircomp}$kHz [A]
ESS	$x1$	-	8.6	26E-3
OnBC	$x43$	-	-	12E-3
EMD	$x26$	-	-	2.5
Air compressor	$x23$	613	8.8	2.5
HVAC	$x24$	-	-	3E-3
DCDC	$x25$	-	-	28E-3

Table 13: Clarification of values in the ripple- and FFT-plots of the simulated air compressor with experimental cable values.

6.2.4 Only DCDC active

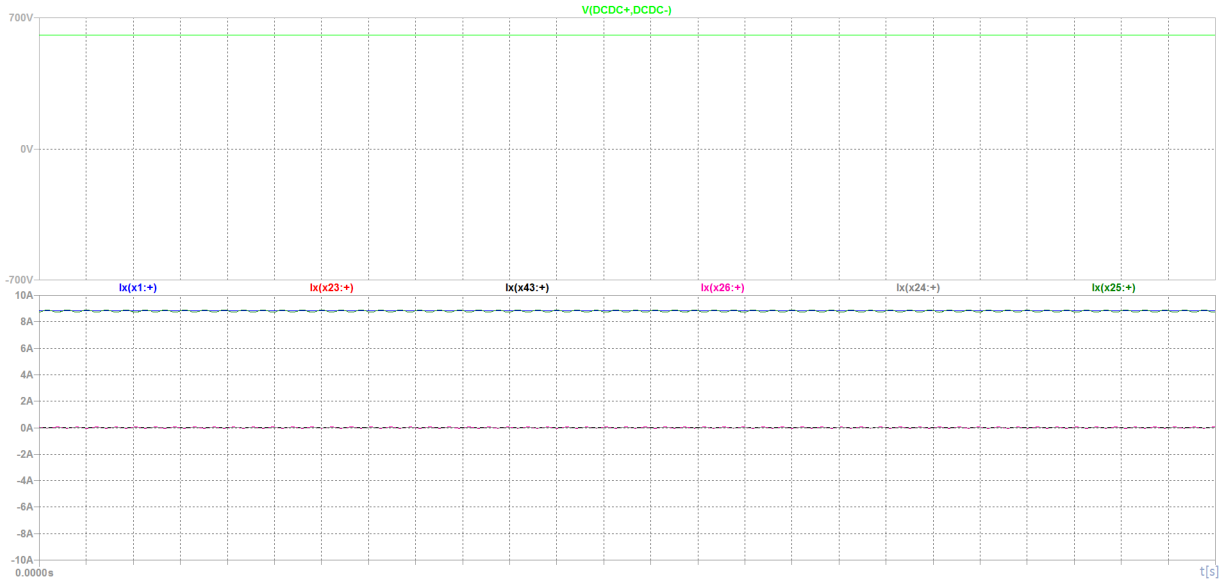

Figure 58: DCDC simulated ripple with experimental cable values. The light green represents the DC-voltage, the blue the ESS current, the red the air compressor current, the black the OnBc current, the pink the EMD current, the grey the HVAC current, and the dark green represents the DCDC current.

Figure 59: FFT of the subsystem currents when the DCDC was simulated with experimental cable values. The light green represents the DC-voltage, the blue the ESS current, the red the air compressor current, the black the OnBc current, the pink the EMD current, the grey the HVAC current, and the dark green represents the DCDC current.

In figure 58 it can be seen that the DCDC current has a sinusoidal form. It can also be seen that the EMD and the other subsystems show the same behaviour only with the average current around $0A$. In figure 59 the RMS currents at $2(f_{sw})_{DCDC}$ from the FFT analysis can be seen. The FFT was done with focus on $2(f_{sw})_{DCDC}$. All values are clarified in table 14. The timespan in figure 58 is of the same length as the time span of the equivalent plot with measured data in *chapter 7 - Experimental verification and model discussion.*

Subsystem	Parameter	U_{avg} [V]	I_{avg} [A]	I_{RMS}@$2(f_{sw})_{DCDC}$kHz [A]
ESS	$x1$	-	8.8	0
OnBC	$x43$	-	-	4E-3
EMD	$x26$	-	-	37E-3
Air compressor	$x23$	-	-	15E-3
HVAC	$x24$	-	-	2E-3
DCDC	$x25$	609	8-8	60E-3

Table 14: Clarification of values in the ripple- and FFT-plots of the simulated DCDC with experimental cable values.

7 Experimental verification and model discussion

7.1 Filter measurements

7.1.1 Measurement setup

Measurements of certain components are necessary when there is insufficient data. As a result measurements were carried out. This was the case with subsystems containing input filters with common mode filters. The common mode filters were measured individually for every subsystems.

Early simulations of the TVS indicated that the CM-filters had a major impact on the current ripple. This corresponds well with theory as CM-filters have inductive qualities and as a consequence will decrease the magnitude of current ripple.

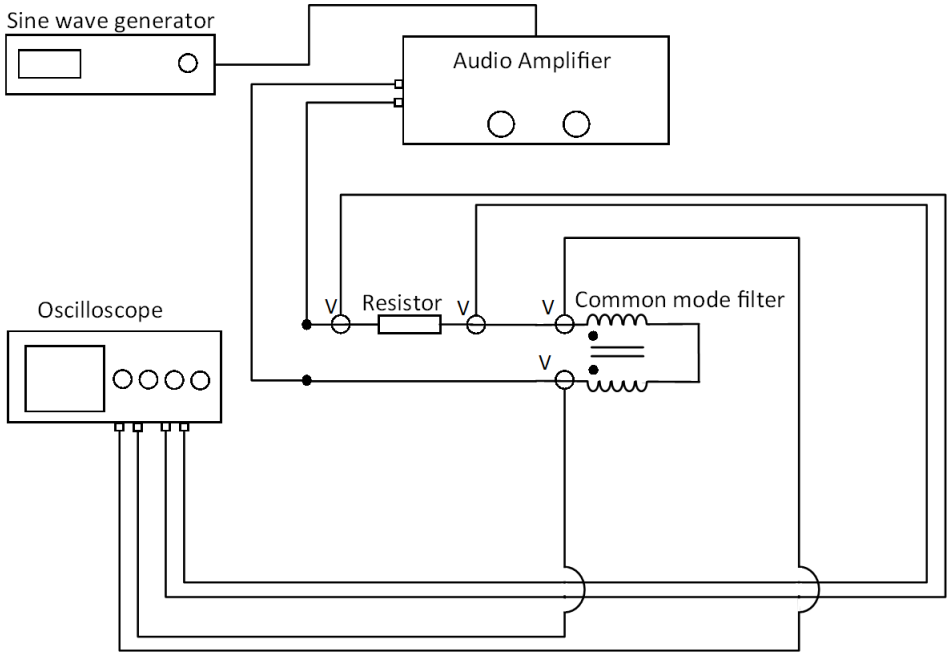

Figure 60: Scheme of the measuring setup

The sine wave generator was connected to the amplifier which in turn was connected to the load, in this case the different CM-filters see figure 68. The CM-filters were, one by one, connected in series with the 1Ω-resistor. The voltage drop measured with differential probes over the 1Ω-resistor worked as a measurement for the current in the common mode filter. The voltage was measured over the CM-filter. An oscilloscope was used to identify the voltage and current amplitudes, the phase shift angles, phase shift times and to verify the output frequencies from the generator. To connect the CM-filters some modifications had to be made where it was difficult to access pins or poles. Some filters were even soldered loose from their circuit boards to not have parasitic components while measuring.
Measurements were made with as high voltage and current as possible to reduce background noise. The highest limit for the current and voltage was reached when the current and voltage was pushed to a level where it started to distort on the oscilloscope display. Initially it was planned to measure both common mode inductance and differential mode inductance. However, when measuring the common mode inductance the currents were not regular sine waves and could not be used. Presumably this was because the inductance became saturated when the filter was set up in CM-mode. However the primary purpose was to find the inductance that affects the ripple and this could still be done with measuring only the differential mode inductance.

The following equipment was used for measuring the CM-filters see figure 61, figure 62, figure 63, figure 64 , figure 65 , figure 66 and figure 67.

TTi TG550 Sine wave generator that allowed setting the frequency and the amplitude of the output voltage.

Figure 61: Sine wave generator TTi TG550

Studiomaster MOSFET 1000 Amplifier used to amplify the sine wave generator.

Figure 62: Studiomaster MOSFET 1000 audio amplifier.

Tektronix TDP1500 A fast-sampling differential voltage probe used for measuring the voltage drop over the 1Ω-resistor.

Figure 63: Tektronix TDP1500 differential voltage probe.

Tektronix MSO 2014B The mixed signal oscilloscope allowing visualization of voltage and current properties on its display.

Figure 64: Tektronix MSO 2014B oscilloscope.

Passive voltage probe Probe to measure the voltage drop over the CM-filter.

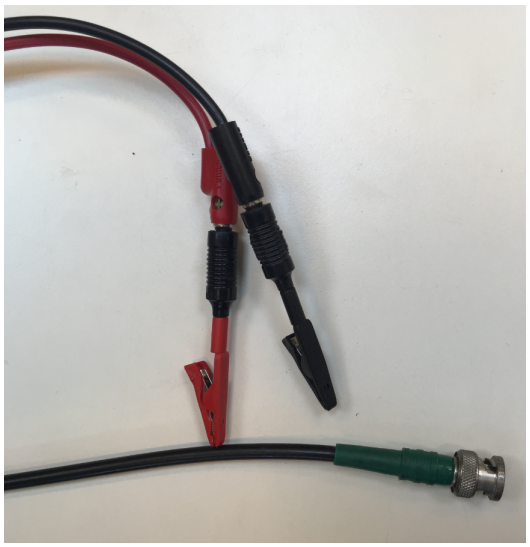

Figure 65: Passive voltage probe

Resistor A 1Ω-resistor used to measure the current.

Figure 66: Resistor.

Common mode filters CM-filters from the EMD type B, HVAC, air compressor and OnBC were measured. Below is a picture of the HVAC CM-filter as an example.

Figure 67: HVAC common mode filter.

Connectors Additional cables were required for the measurement setup. As an example banana plugs were used.

Measurement calculations

To find the differential mode inductance for a CM-filter the following calculations were executed. Voltage, current and phase shift time were measured. The measured frequencies was 2000Hz, 4000Hz, 8000Hz, 10000Hz, 20000Hz, 40000Hz, 60000Hz.

$$U = Z \cdot I \iff Z = \frac{U}{I},\ Z = R + j \cdot \omega \cdot L_{dm}\ j \cdot \omega \cdot L \text{ is}$$

$$\omega \cdot L_{dm} = Z \cdot sin\varphi, \text{ where}$$

φ is the phase shift angle in radians calculated according to

$$\varphi = (\delta t \cdot \frac{1}{T_{sw}}) \cdot 360, \text{ where } \delta t \text{ is the measured phase shift time.}$$

This gives with $\omega = 2 \cdot \pi \cdot f_{sw}$

$$L_{dm} = \frac{Z \cdot sin\varphi}{2 \cdot \pi \cdot f_{sw}}.$$

7.1.2 Measurements result

A mean value for the frequency dependent inductance is calculated see table 15.

CM-filter	DM-inductance
$Aircompressor$	Volvo value
EMD_{typeB}	Volvo value
$HVAC$	Volvo value
$OnBC$	Volvo value

Table 15: Measured differential mode inductances.

7.1.3 Discussion

The purpose of the measurement was to attain CM-filters leakage inductance as the manufacturer were unable to give us these values at the time. However, in the end of this thesis the manufacturer gave us these parameters. Also it was found that the resistor is not purely resistive but also has an inductive part $1.2\mu H$. This has due to time not been further investigated. Values from the manufacturers can be seen in the table 16.

CM-filter	DM-inductance
$Aircompressor$	Volvo value
EMD_{typeB}	Volvo value
$HVAC$	Volvo value
$OnBC$	Volvo value

Table 16: Differential mode inductances from the manufacturers.

According to the secret Volvo values there is a great difference on the measurement and the manufacturers value on the EMD CM-filter. Due to the fact the other measurements seem more likely it is probable that some sort of fault has occurred when measuring the EMD CM-filter. It is probable that differential probe have not been properly setup with the oscilloscope. As a result the measurements of the currents are probably not correct in this case. Furthermore, the audio amplifier had a limit as to how high the voltage and

current could be amplified. For some frequencies on some filters it was not possible to reach a point where the current and voltage signals distorted. If a higher current and higher voltage was allowed then perhaps even more correct values could be attained. For instance in the case of the EMD CM-filter. Presumably the EMD CM-filter is designed for higher current than the other CM-filters due to the higher rated power of the EMD and EM. It is probable that further measurements of the EMD CM-filter will result in a more correct value.

7.2 Bus measurement

7.2.1 Measurement setup

To compare the LTspice simulations with reality, measurements are required from a real TVS. Breakout boxes installed in the bus were used to measure the voltage and current as close to the subsystem's input filters in the TVS as possible, see figure 68. The software DEWEsoft was used to record the measurements. The EMD, DCDC, HVAC and air compressor are active one at a time individually to be able evaluate the different subsystem's current ripple. Subsystem's electrical machine speeds were recorded via CAN-signals. In addition, voltage and current are measured on the other subsystems to evaluate how the other subsystems are affected by the active subsystem's current ripple. As a consequence DC current consumed by the HVAC, the air compressor and the DCDC are measured when the bus is at a standstill. The bus is accelerating and decelerating to measure the current ripple from the EMD.
However the cable to the measurement set up to the DCDC was not properly plugged in and as a consequence no current from the other subsystems current ripple in to the DCDC could be measured.

However additional measurements were included with the EMD and the DCDC active at the same time. Therefore the EMD current ripple in to the DCDC could be evaluated because the EMD has a greater rated power. As the DCDC current ripple has a minor influence on the greater current ripple of the EMD.

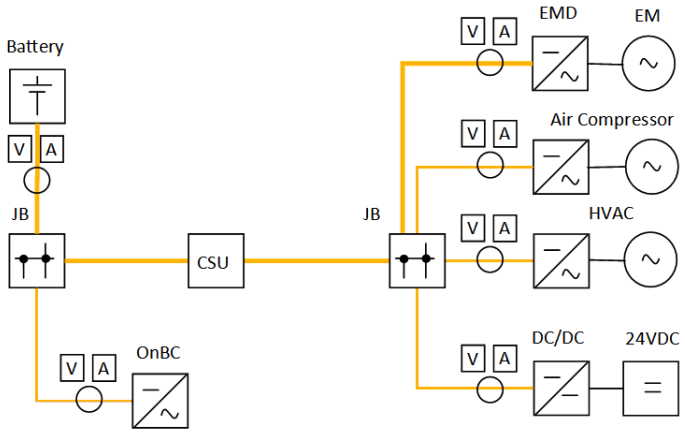

Figure 68: Scheme of the TVS measuring set up on the electric hybrid

7.2.2 Measurement results

Fast Fourier Transforms (FFT) are included to show each subsystems current ripple frequency.

Only EMD and DCDC active

3D-plots were used to see the worst case for the current ripple. The bus is accelerated uphill with full throttle. The DCDC is loaded at maximum load and the combustion engine is not active. The time around 20.6 seconds corresponds to $\frac{\omega_{basespeedEM}}{2}$ according to measurements made by Volvo. As seen in figure 69 and in table 17 two peaks are prominent. At the 0Hz the mean current can be seen.

Frequency[Hz]	Time[s]	Current RMS[A]
$2(f_{sw3})_{EMD_{typeC}}$	20.60	14.56
$2(f_{sw3})_{EMD_{typeC}}$	19.32	16.15

Table 17: Table showing FFT peak values of the 3D-plot of the EMD current ripple.

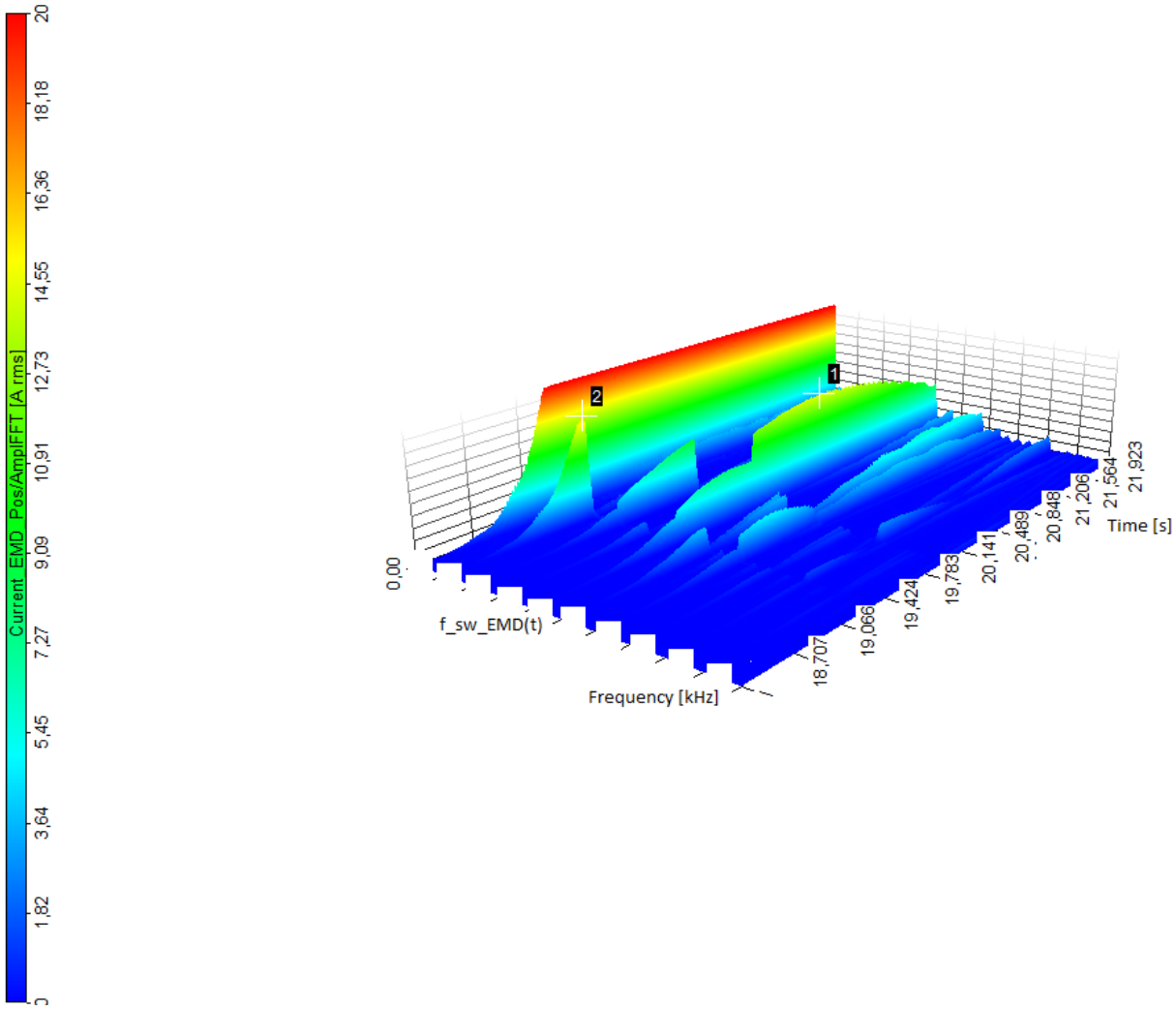

Figure 69: FFT of the EMD current ripple during acceleration of the EM with EMD and DCDC active. Frequency, time and current plotted.

As seen in figure 70 and in table 18 one peak can be seen. However, this is very small compared to the peak measured at the EMD.

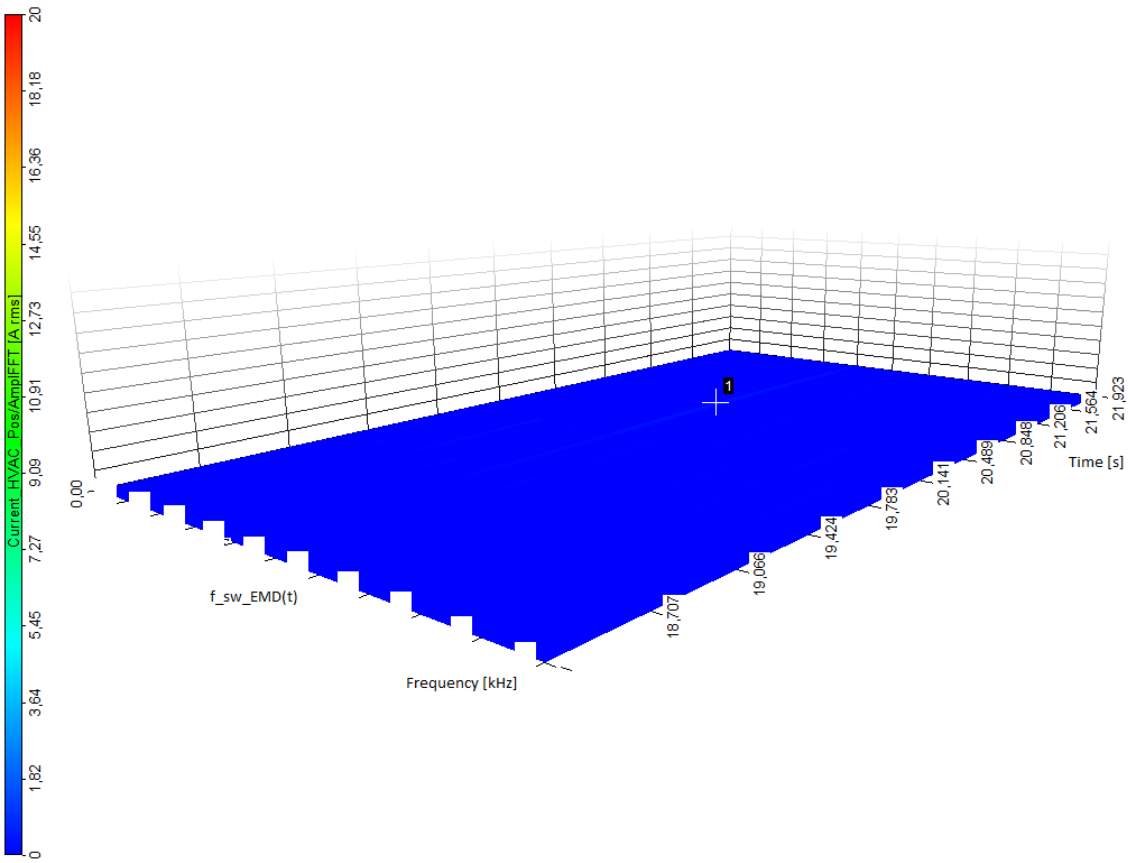

Figure 70: FFT of the HVAC current ripple during acceleration of the EM with EMD and DCDC active. Frequency, time and current plotted.

Frequency[Hz]	Time[s]	Current RMS[A]
$2(f_{sw3})_{EMD_{typeC}}$	20.65	0.44

Table 18: Table showing FFT peak values of the 3D-plot of the HVAC current ripple.

As seen in figure 71 and in table 19 the most prominent peak is at around $2f_{swEMD}$.

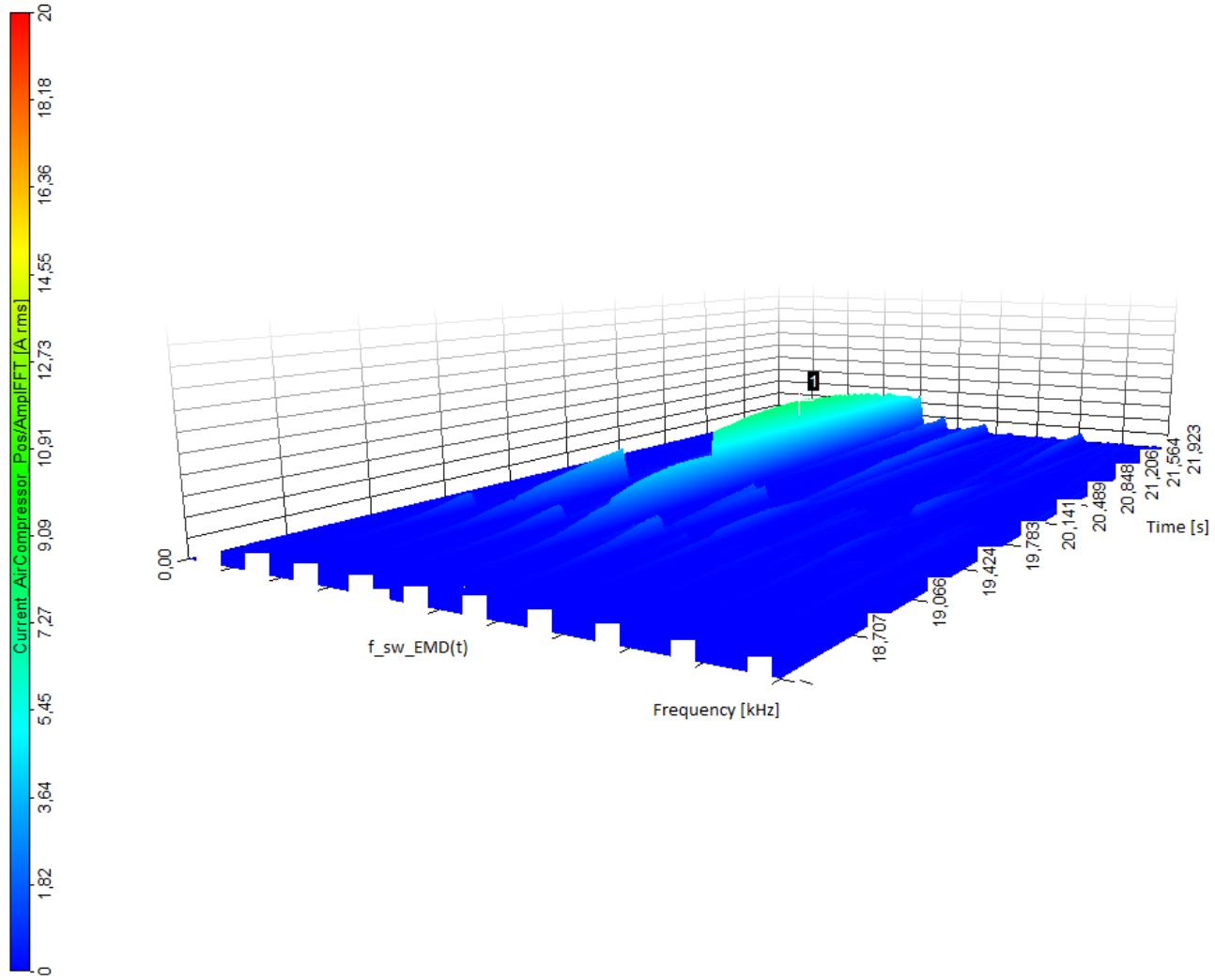

Figure 71: FFT of the air compressor current ripple during acceleration of the EM with EMD and DCDC active. Frequency, time and current plotted.

Frequency[Hz]	Time[s]	Current RMS[A]
$2(f_{sw3})_{EMD_{typeC}}$	20.65	8.00

Table 19: Table showing FFT peak values of the 3D-plot of the air compressor current ripple.

Frequency[Hz]	Time[s]	Current RMS[A]
$2(f_{sw3})_{EMD_{typeC}}$	20.65	9.58

Table 20: Table showing FFT peak values of the 3D-plot of the DCDC current ripple.

As seen in figure 72 and in table 20 the most prominent peak is also at around $2f_{swEMD}$.

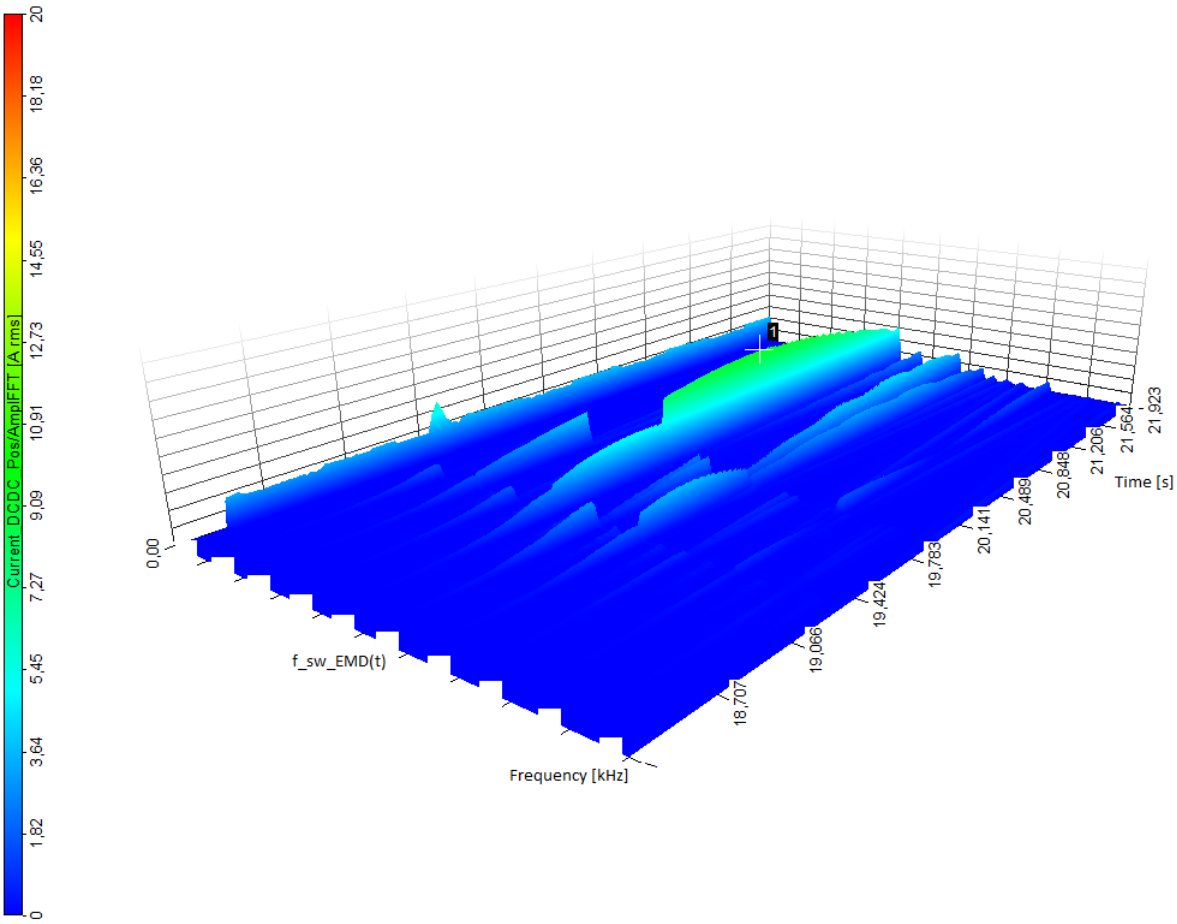

Figure 72: FFT of the DCDC current ripple during acceleration of the EM with EMD and DCDC active. Frequency, time and current plotted.

As seen in figure 73 and in table 21 the most prominent peak is also at around $2f_{swEMD}$.

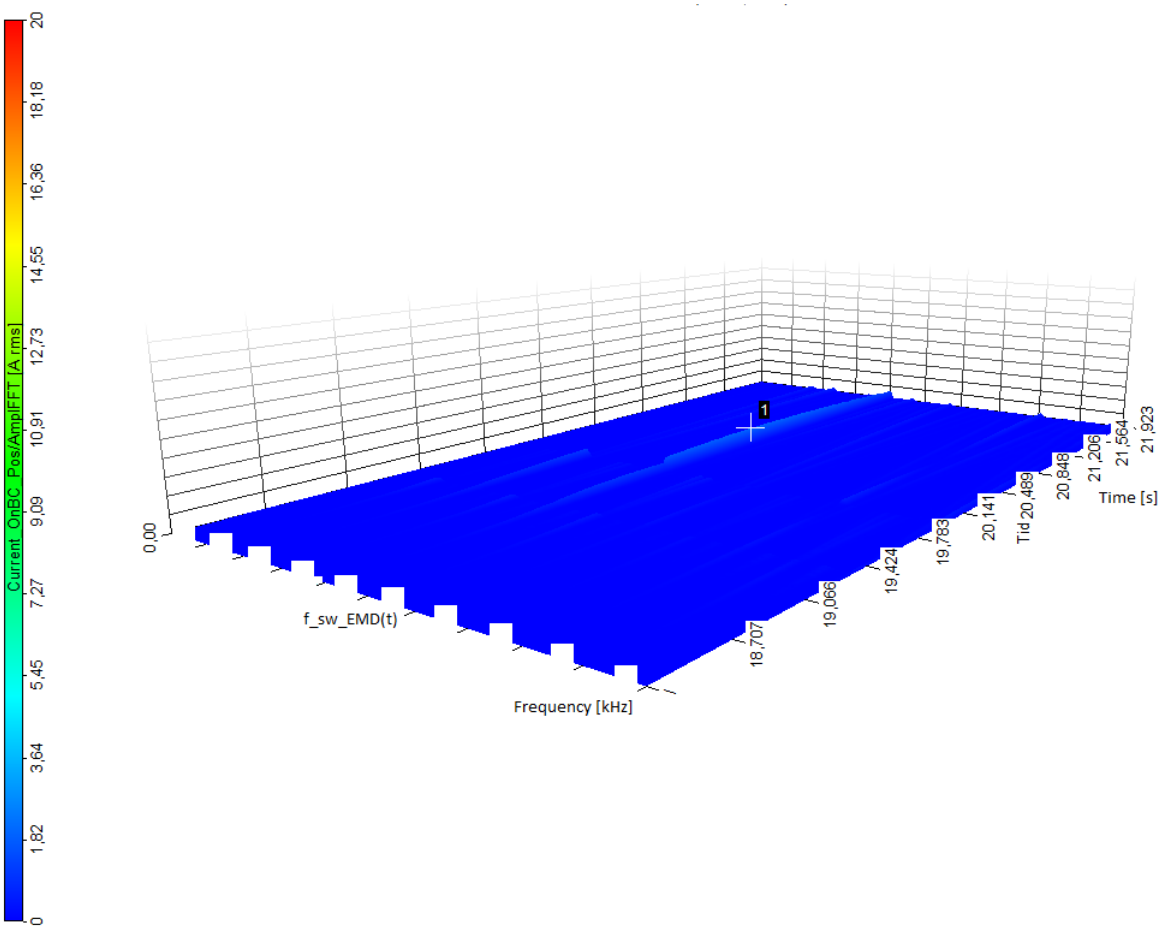

Figure 73: FFT of the OnBC current ripple during acceleration of the EM with EMD and DCDC active. Frequency, time and current plotted.

Frequency[Hz]	Time[s]	Current RMS[A]
$2(f_{sw3})_{EMD_{typeC}}$	20.60	1.99

Table 21: Table showing FFT peak values of the 3D-plot of the OnBC current ripple.

The zoomed in current ripple of the EMD as seen in figure 74 indicates that the waveform of the current ripple does not appear to have a sinusoidal shape. The current ripple of the remaining subsystems appears to have similar waveform shape though with varying amplitude.

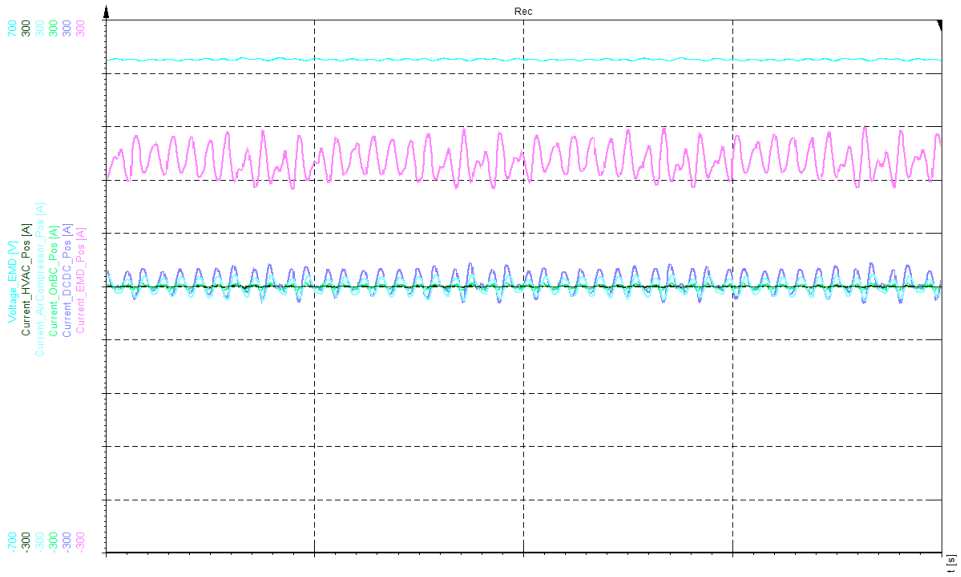

Figure 74: Current ripple during acceleration with EMD and DCDC active zoomed in at the time where the FFT showed the peak values of the current ripple RMS. The speed of the EM is here around $\frac{\omega_{basespeedEM}}{2}$.

FFT over the ripple currents distributed in the TVS while the EMD and DCDC are active can be seen in figure 75 and figure 76.

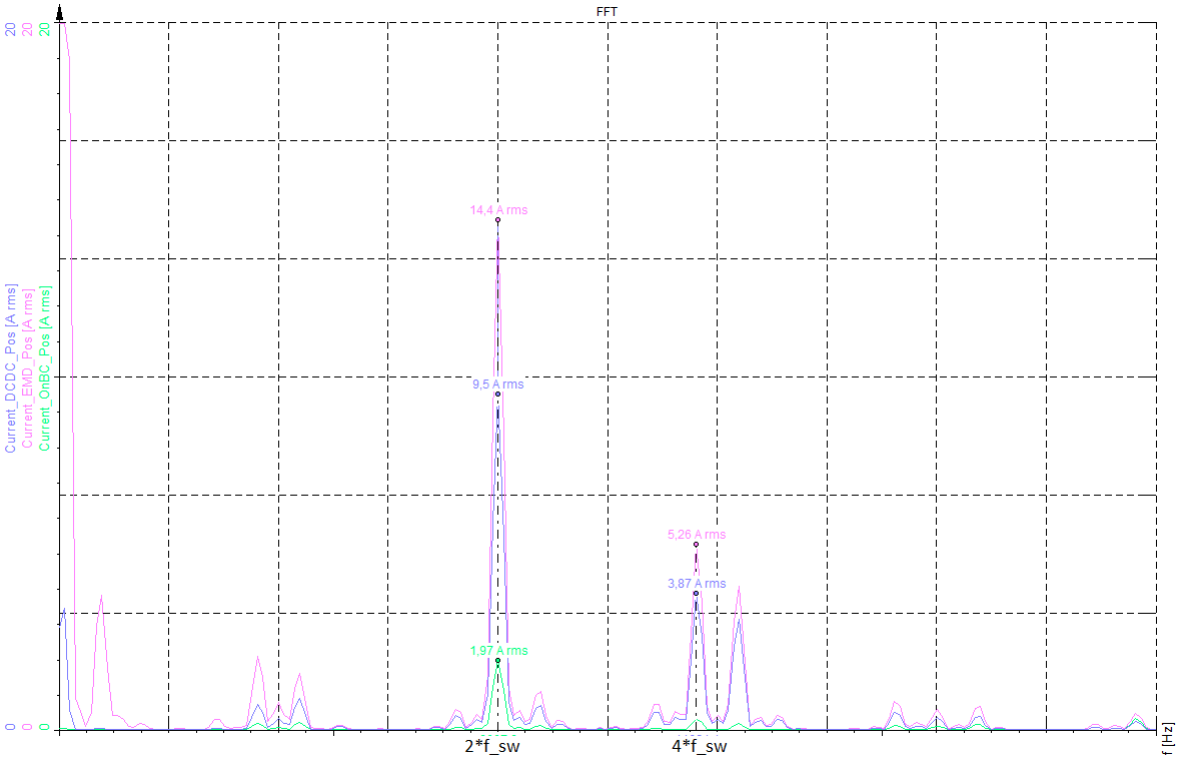

Figure 75: FFT of the subsystems current ripple with EMD and DCDC active. The speed of the EM is here around $\frac{\omega_{basespeedEM}}{2}$. Frequency and current plotted.

Figure 76: FFT of the subsystems current ripple with EMD and DCDC active. The speed of the EM is here around $\frac{\omega_{basespeedEM}}{2}$. Frequency and current plotted.

Only HVAC active

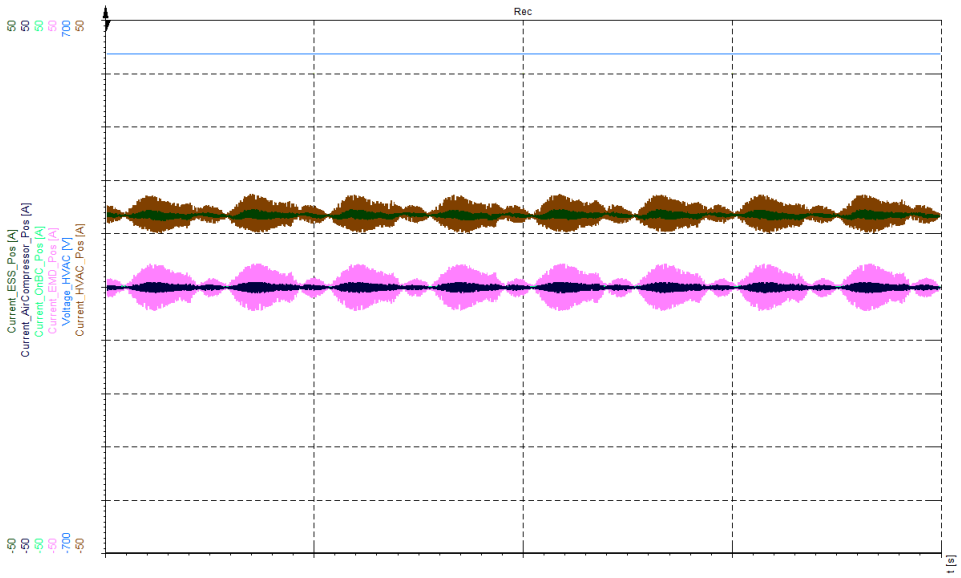

Figure 77: Current ripple with HVAC active.

In figure 77 the shape of the current ripple of the HVAC is due to the compressor's mechanical behaviour as seen in plots from the sub-supplier. In figure 78 the shape of the current ripple of the HVAC is zoomed in. The max value for the ripple peak to peak is around for the HVAC is 7A. However the EMD current ripple is greater at around 9A. This can be seen more evident in figure 79 and figure 80. The EMD is not active at the time though it has a greater current ripple at around $(f_{sw})_{HVAC}$ than the HVAC.

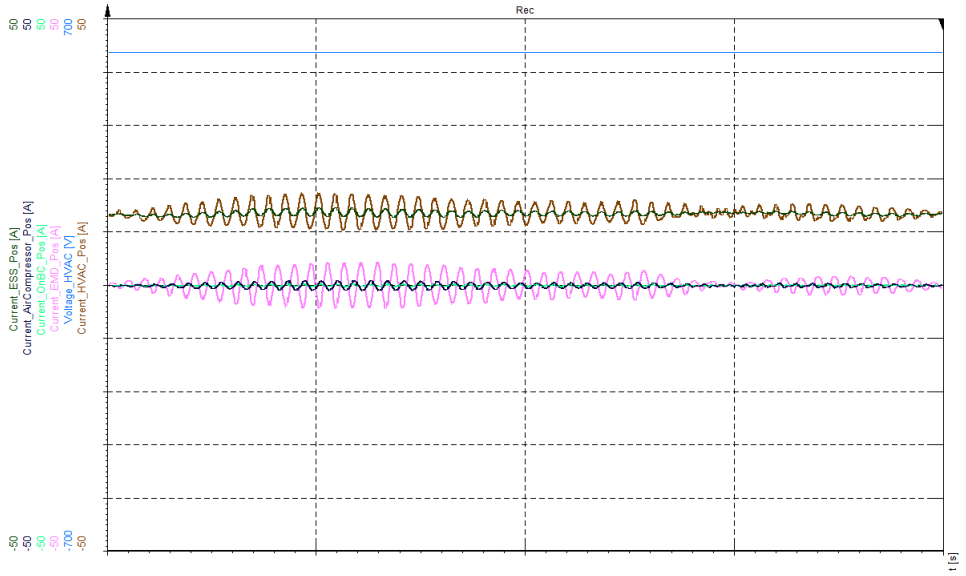

Figure 78: Current ripple zoomed in with HVAC active.

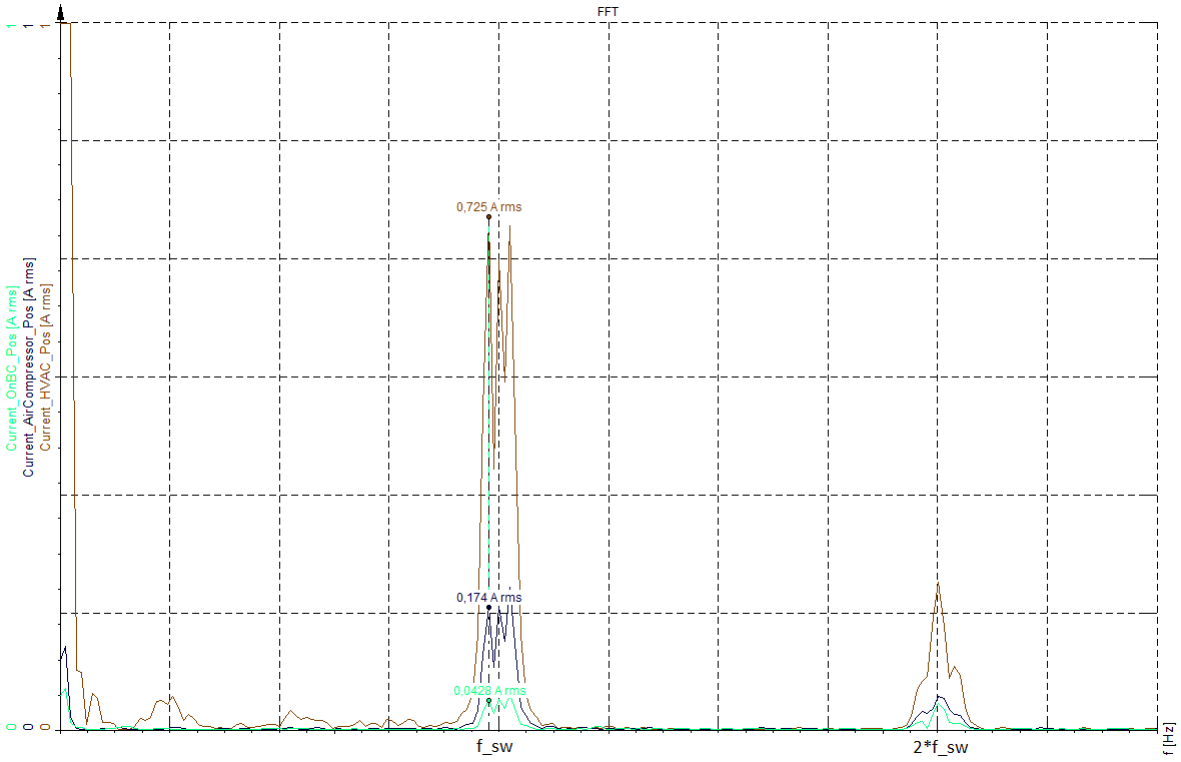

Figure 79: FFT of the subsystems current ripple with HVAC active. Frequency and current plotted.

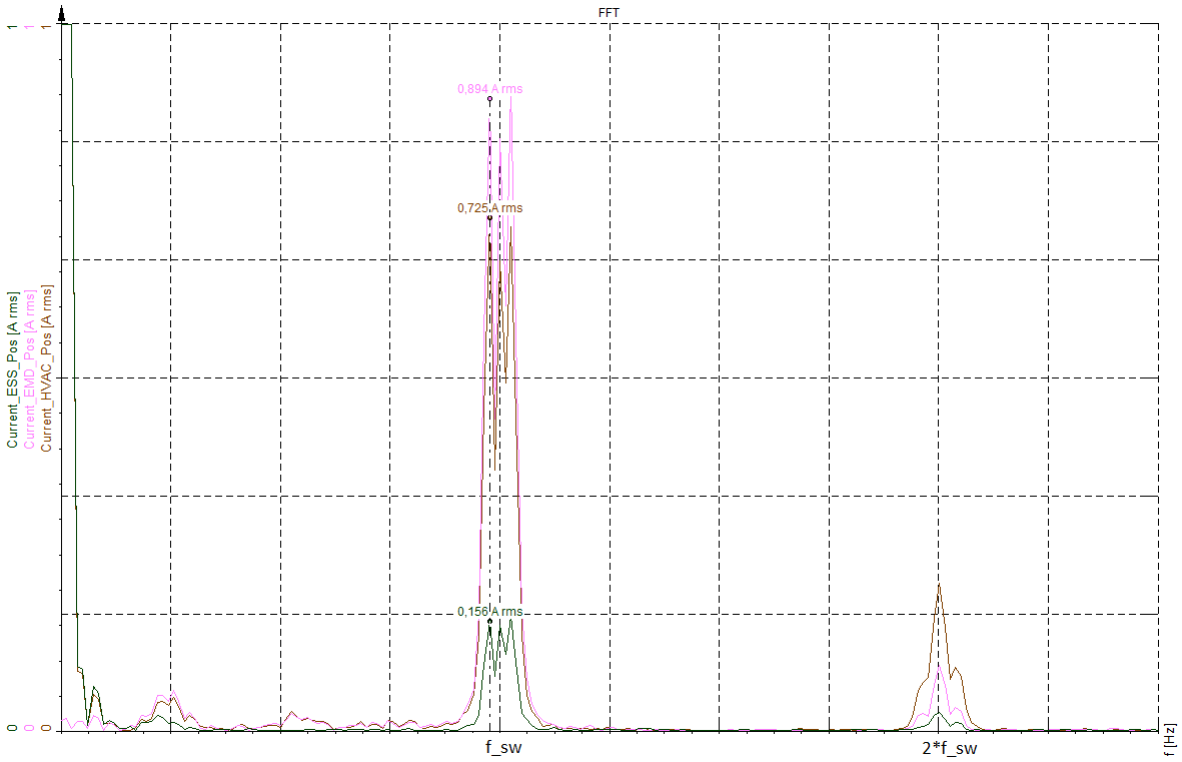

Figure 80: FFT of the subsystems current ripple with HVAC active. Frequency and current plotted.

Only air compressor active

In figure 81 the shape of the current ripple of the air compressor is zoomed in. The EMD current ripple appears to reverse phased compared to the air compressor current ripple. As with the HVAC the EMD current ripple is greater than the air compressor current ripple. figure 82 andfigure 83 shows this more clearly. Worth mentioning is that the EMD current ripple at around $(f_{sw})_{aircomp}$ is somehow of higher magnitude though it is inactive.

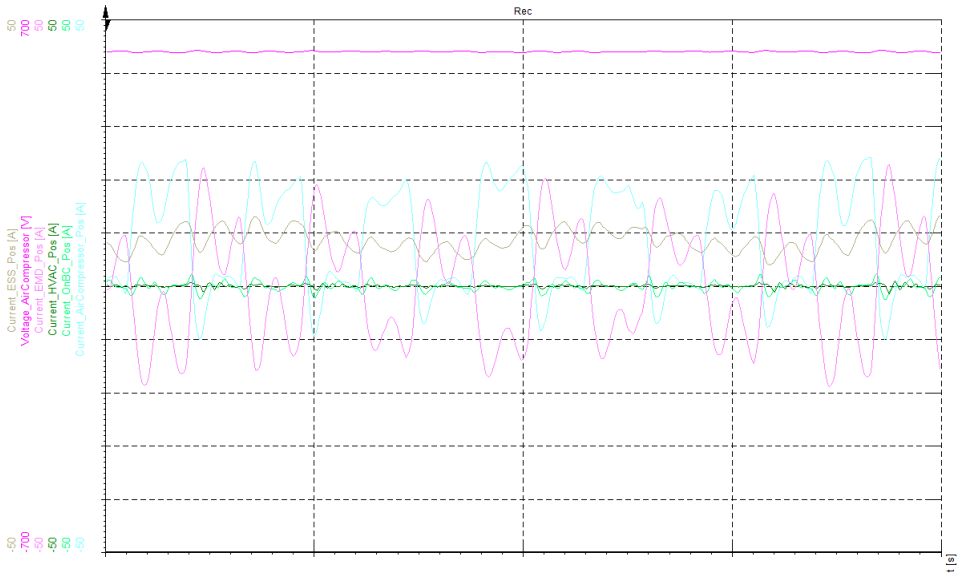

Figure 81: Current ripple zoomed in with air compressor active.

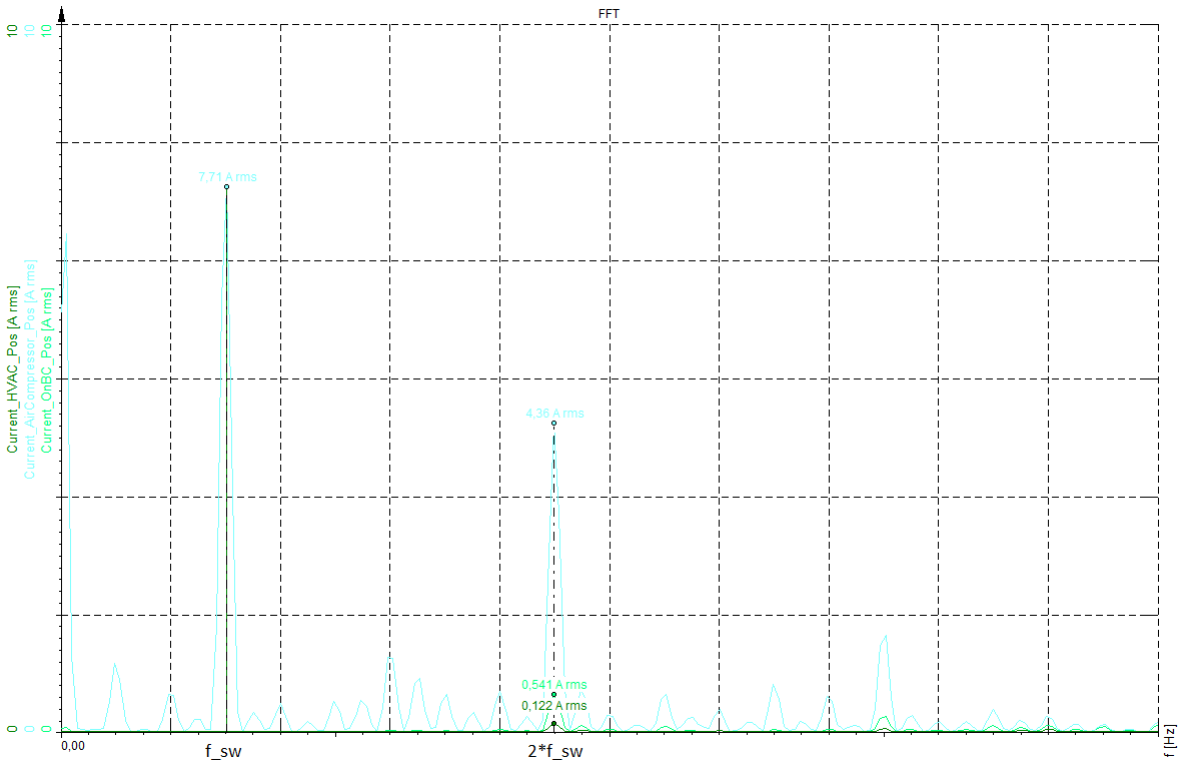

Figure 82: FFT of the subsystems current ripple with air compressor active. Frequency and current plotted.

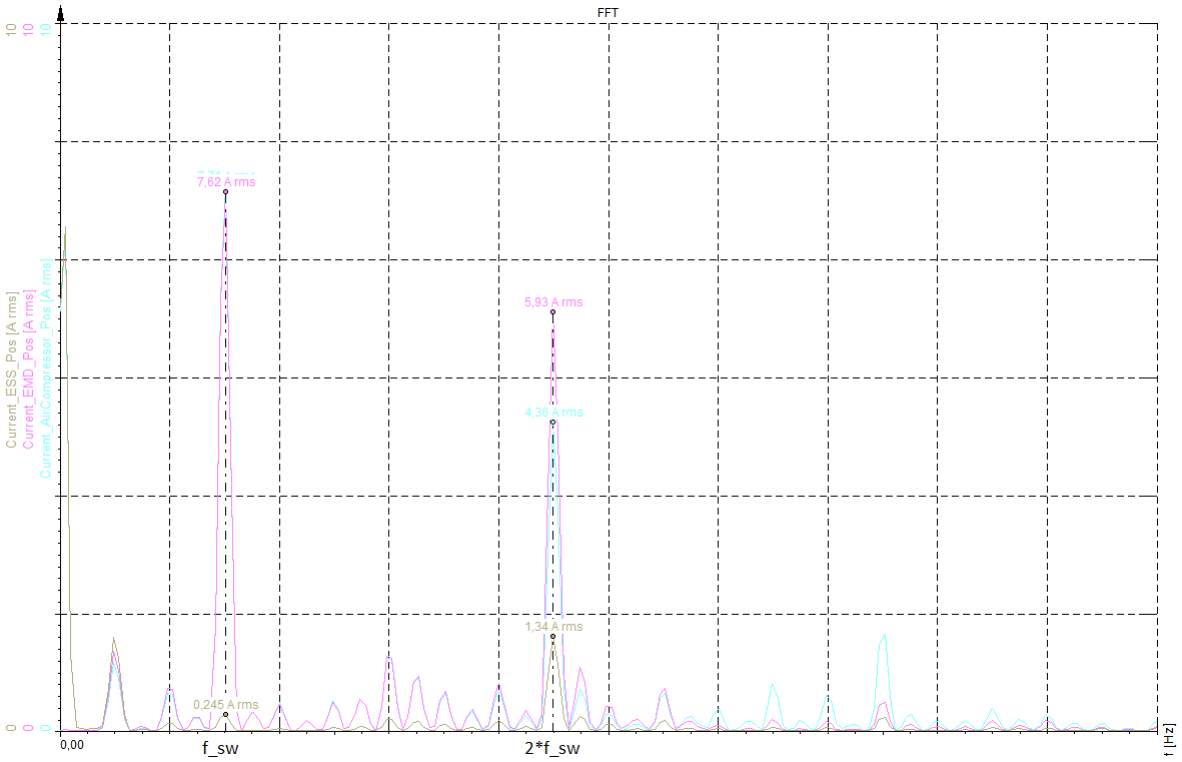

Figure 83: FFT of the subsystems current ripple with air compressor active. Frequency and current plotted.

Only DCDC active

In figure 84 the shape of the current ripple of the DCDC is zoomed in. The EMD current ripple appears to reversed phased compared to the DCDC current ripple. As with the HVAC the inactive EMD has a higher current ripple than the DCDC current ripple at $2(f_{sw})_{DCDC}$, see figure 85 andfigure 86.

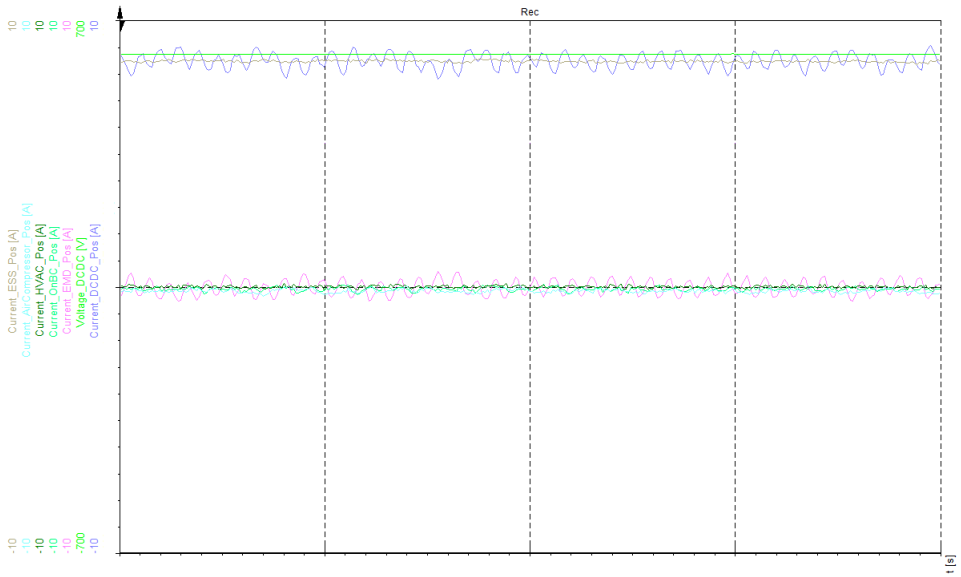

Figure 84: Current ripple zoomed in with DCDC active. The 24V DC-system is loaded with around 164A.

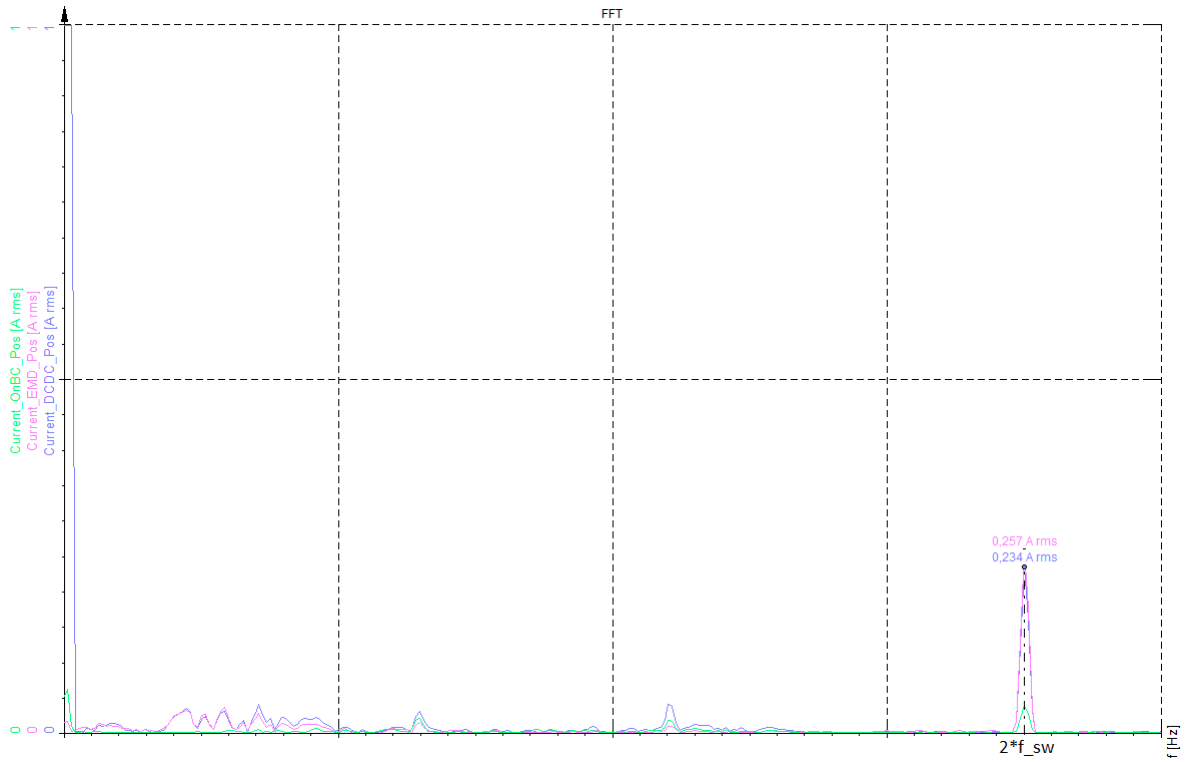

Figure 85: FFT of the subsystems current ripple with DCDC active. The 24V DC-system is loaded with around 164A.

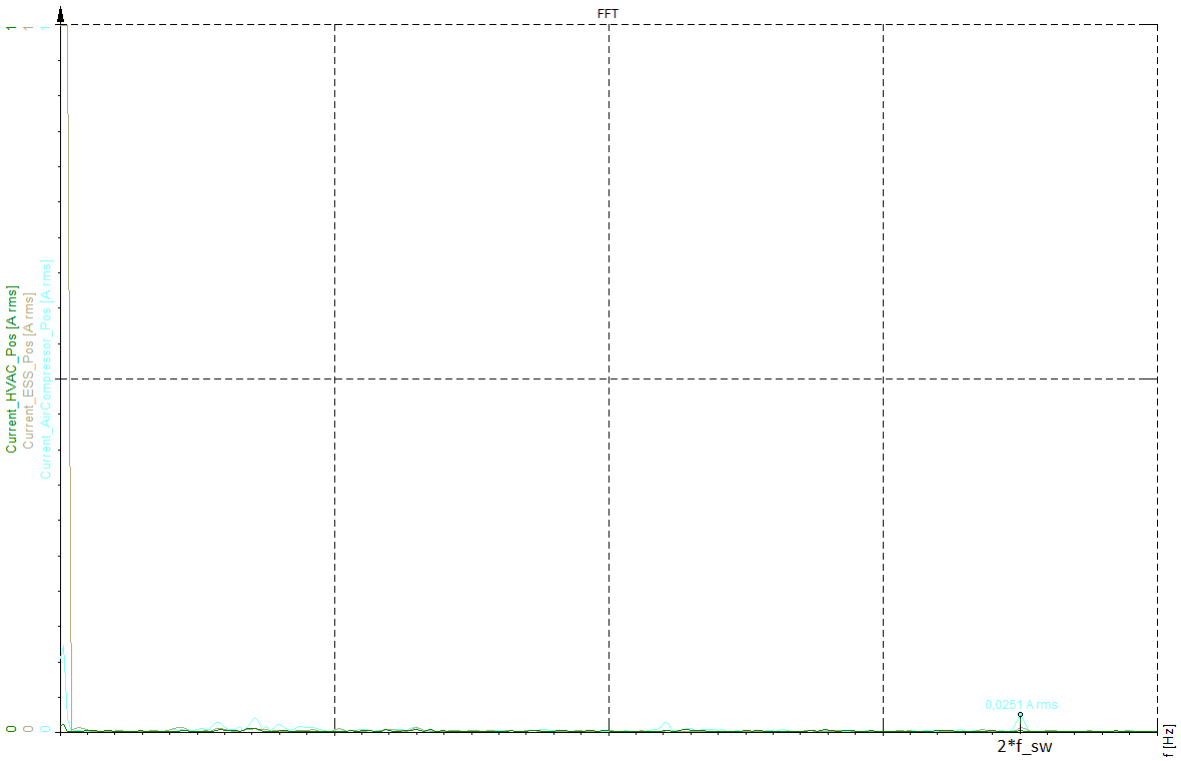

Figure 86: FFT of the subsystems current ripple with DCDC active. The 24V DC-system is loaded with around 164A.

7.2.3 Discussion

EMD and DCDC active

The effects of the DCDC current ripple on the EMD current ripple can be disregarded for this analysis as the EMD has a greater rated power (180kW max) than the DCDC (7.5kW max). Furthermore, as seen in table 1 and table 5 the converters have a great difference in switching frequency.
As previously mentioned in *section 4.2.2 - Worst case ripple* the worst case of the current ripple is at half the base speed. As presumed in *section 3.3.11 - Presumed system dynamics* the EMD is producing the greatest current ripple when active. However, to evaluate at what time and as a consequence at what EM speed the worst case point for the current ripple appears the other subsystems needed evaluation too. As seen in 3D-plots in figure 69, figure 70, figure 71, figure 72 and figure 73 the worst current ripple from the EMD occurs at $2(f_{sw_3})_{EMD_{typeC}}$ at the time around 20.60-20.65 seconds. This time interval corresponds, according to Volvo measurements, to the EM speed of around $\frac{\omega_{basespeedEM}}{2}$. The first peak seen in figure 69 is higher than the second peak due to a lower switching frequency at the first peak. However the first peak does not effect the other subsystems as seen in figure 70, figure 71, figure 72 and figure 73. Therefore the effects of the second peak is worse on the other subsystems.

When comparing the simulated worst case with cable values given by Volvo as seen in figure 44 and table 7 with the measurements as seen in figure 74 there is a difference in the current ripple. This is more evident when comparing the FFT analysis of the simulated cases as seen in figure 45 and table 7 compared to the measurement as seen in figure 75 and figure 76 summarized in table 22. There is a difference of $\frac{10.3}{14.4}$ resulting in a percent difference of around 28% less magnitude of the current ripple according to the FFT at $2(f_{sw_3})_{EMD_{typeC}}$.

Likewise when comparing the simulated cases with experimental parameters set for the cables there is also a great difference in the magnitude of the current ripple as seen in figure 52 compared to figure 74. This is more evident when comparing the FFT analysis of the simulated cases as seen in figure 53 and table 11 compared to the measurement as seen in figure 75 and figure 76 summarized in table 22. There is a difference of $\frac{20.3}{14.4}$ resulting in a percent difference of around 41% larger magnitude of the current ripple according to the FFT at $2(f_{sw_3})_{EMD_{typeC}}$.

Parameters	FFT-current $2(f_{sw_3})_{EMD_{typeC}}$	Measured current [A]	Difference [%]
Volvo's	10.3	14.4	$\frac{10.3}{14.4} \Longrightarrow 28\%$
Exp.	20.3	14.4	$\frac{20.3}{14.4} \Longrightarrow 41\%$

Table 22: The difference in current ripple when comparing the simulations with cable values given by Volvo and the experimental values to the measured values. The difference in magnitude is shown in percent in the last column. Here the amplitude with Volvo parameters is 28% smaller than the measured value. For the experimental parameters the amplitude is 41% larger than the measured amplitude.

HVAC active

As seen in figure 77 the HVAC has a particular current ripple. This is because the HVAC is an air compressor and therefore it has a fish-shaped current ripple. This can be seen in plots from the sub-supplier. The simulations as seen in *chapter 6 - Simulation* are executed with the max peak to peak value for the HVAC current ripple as seen in figure 77.

Comparisons between simulations and measurements show a difference, see figure 46 and figure 54 compared to figure 78. For clarification of values see the tables 8 and 12. The table values can be compared to the FFT plots in figure 79 and figure 80 which shows the the obvious difference. A summery of the differences can be seen in table 23.

Parameters	FFT-current $@(f_{sw})_{HVAC}$	Measured current [A]	Difference [%]
Volvo's	1.1	0.725	$\frac{1.1}{0.725} \Longrightarrow 52\%$
Exp.	0.487	0.725	$\frac{0.487}{0.725} \Longrightarrow 33\%$

Table 23: The difference in current ripple when comparing the simulations with cable values given by Volvo and the experimental values to the measured values. The difference in magnitude is shown in percent in the last column. Here the amplitude with Volvo parameters is 52% larger than the measured value. For the experimental parameters the amplitude is 33% smaller than the measured amplitude.

Air compressor active

As seen in figure 81 and from the simulations seen in figure 48 and in figure 56 the air compressor current ripple and the EMD current ripple is reversed phase. It is probable that this is due to the fact that the current ripple at this frequency moves from the air compressor to the EMD. However the DC current is taken from the battery.

When comparing the simulated cases with the measurements as seen in figure 48, figure 56 and figure 81 there is a difference.

This is more evident when comparing the FFT analysis simulations with measurements as seen in figure 49, table 9,figure 57, table 13, figure 82 and figure 83. See table 24.

Parameters	FFT-current $(f_{sw})_{aircomp}$	Measured current [A]	Difference [%]
Volvo's	3.2	7.71	$\frac{3.2}{7.71} \Longrightarrow 70\%$
Exp.	2.5	7.71	$\frac{2.5}{7.71} \Longrightarrow 68\%$

Table 24: The difference in current ripple when comparing the simulations with cable values given by Volvo and the experimental values to the measured values. The difference in magnitude is shown in percent in the last column. The amplitude with Volvo parameters is 70% smaller than the measured value. For the experimental parameters the amplitude is 68% smaller than the measured amplitude.

DCDC active

As seen in figure 84 and from the simulations seen in figure 50 and in figure 58 the DCDC current ripple and the EMD current ripple is are not in phase. It is probable that this is due to the fact that one subsystem draws current from the other.

Differences are also present in the comparison between the simulation and the measurements. This can be seen in figure 50, figure 58 compared to figure 84. Here it is also more evident in the FFT. See simulated values in table 10 and table 14 compared to the measured values in figure 85 and figure 86. A full overview is given in table 25.

Parameters	FFT-current $2(f_{sw})_{DCDC}$	Measured current [A]	Difference [%]
Volvo's	0.3	0.234	$\frac{0.3}{0.234} \Longrightarrow 28\%$
Exp.	0.06	0.234	$\frac{0.06}{0.234} \Longrightarrow 74\%$

Table 25: The difference in current ripple when comparing the simulations with cable values given by Volvo and the experimental values to the measured values. The difference in magnitude is shown in percent in the last column. The amplitude with Volvo parameters is 28% larger than the measured value. For the experimental parameters the amplitude is 74% smaller than the measured amplitude.

Model discussion

In table 27 the faulty margin of the simulations compared to the measurements can be seen. Both cases appears to have similar magnitude of the faulty margin. However, none of the cases are accurate enough to be used in practise. The cable values given by Volvo and the values taken as a rule of thumb differ greatly. As a result it is probable that the cable values given by Volvo are incorrect. Further on, cable inductance changes depending on where and how you install them according to [3]. Therefore, it would be recommended to re-evaluate the cable inductance values given by Volvo.

Furthermore, the model for the battery used during the simulations is simple as a inductance and an resistance in series. A more sophisticated model of the battery might result in a more correct simulation. Finally, the input filter of the DCDC has an unknown leakage inductance from a common mode filter. With this value the simulation might have been more accurate.

	Volvo parameters	Experimental parameters
$2x4mm^2 cable$	Volvo value	$1.35E-6$H
$50mm^2 cable$	Volvo value	$1.0E-6$H

Table 26: Cable parameter values given by Volvo and experimental cable parameter values as seen in *section 6.2 - Simulation cases with experimental parameters* [10]. All values are given per meter. The fault margin with with the different parameter values can be seen in table 27 below.

	Volvo parameters	Experimental parameters
EMD and DCDC	28% smaller	41% larger
HVAC	52% larger	33% smaller
Aircompressor	70% smaller	68% smaller
DCDC	28% larger	74% smaller

Table 27: Fault margin of the simulated values (in percent) compared to the measured values. The cable parameter values per meter can be seen in table 26 above.

In summary the simulation model of the TVS is very sensitive to small alternations. Factors that have a major impact on the current ripple simulation are the following:

- **Duty cycle** a small alternation of the duty cycle will can have a great impact of the current ripple. Furthermore, it has been difficult to get an exact value of the actual duty cycle on a converter in reality.
- **Input filters parameters** DC-link capacitance and differential mode inductance on the subsystems input filters have a great impact of the current ripple. Tolerance differences for DC-link capacitance is therefore important to account for.
- **Cable dynamic behaviour** The impedance of the cable depending on how and where is installed in the bus. The ambition level of this thesis did not account for this.
- **Battery model** Due to the ambition level of this master thesis a simple battery model was chosen with an inductor and a resistor in series with a constant voltage source. However this a more sophisticated battery model could give more correct simulation results.

8 Conclusion

8.1 Conclusion

From the the comparison of the simulated and measured test cases it can be seen that no simulation had exactly the same behaviour as the measured data. The model does obviously not reach the intended accuracy. It is difficult to say exactly why but the most probable cause is unknown parameter values in the bus that are not in the model.

As a modification the cable values were changed but the new cable values lead to a significant improvement of accuracy. As already mentioned the cable properties are a complex matter and the manufacturer has, in this case, verified the values simulated in the cases where Volvo parameters were used. Unknown parameters should be evaluated. However also the cables ought to be evaluated even though they are verified by the manufacturer. As cable properties varies with placement, lengths and also interference with other cables and electro-magnetic components that acts as conductors [3].

This thesis is the first step towards building a useful design tool for the development of new electric or hybrid buses at Volvo. The circuits of two buses are completely finished with subcircuits in a library of the simulation environment LTspice. Verifications of the electrical behaviour are made through test data from one of the real buses. The model for this bus, the electric hybrid, is therefore more tuned to be more realistic as there actually was data to compare with. As could be seen in *chapter 7 - Experimental verification and model discussion* the model is not 100 percent consistent with reality.

The thesis work has been located at Volvo Group Trucks and Technology at Lundby in Gothenburg but both of us have been working out of office most of the time. It was vital for us to be in Gothenburg during the start of the project to meet key people for the project, keep track of important places and gather important information and software to our project computers. It was also vital for us to be in Gothenburg for doing tests on the real buses and to attend certain training sessions to have access to the workshop and to be able to do measurements. It has worked well and most meetings have been done via Skype Business. The cooperation with Volvo employees and especially with our supervisor has worked very well. A lot of time has been put down in finding parameter values for the systems, both in reality and on telephone. It has been the most time consuming task during the whole project due to our inexperience of realistic parameter values and also

employees or subcontractors not knowing specific details. As a solution to this measurements of single passive components have been carried out with mixed results even though no time was planned for that in the thesis (see *chapter 7*). The reason why most work has been put down on the electric hybrid when the original focus was on the electric (since its has a larger electric system) is that tests on the electric hybrid were realized in the end of November, beginning of December whereas tests on the electric has not yet been realized. Tests also required more time than planned because we had no or little experience of this from before and thus needed help with them. We had great help to perform the tests from a test engineer who learned how the testing (and the software needed) worked very quickly. We also had some expertise help from a software engineer manipulating the bus to behave in the ways we wished. To improve the outcome of this thesis it would have been better if measured data had been available to us earlier. Then we would have had more time to analyse simulations and measured data, evaluate parameter values in the models, improve the models and further analyse their behaviour. With more time with the test data more different simulations could have been done to achieve greater understanding of the models behaviour.

8.2 Proposed solution

8.2.1 Increased capacitance

By increasing the DC-link capacitor closest to the transistor bridge the ripple can be greatly decreased. For instance, if the DC-link capacitor in the EMD input filter would be doubled the ripple would decrease. However, the amount of current ripple each capacitor would have to endure needs to be investigated to fully understand how the current ripple affects the capacitor lifetime expectancy. Further on, the increased cost for an increase of the capacitor would then result in a trade off for decreased capacitor lifetime expectancy and the capacitor size.

8.2.2 Increased switching frequency

By increasing the switching frequency the ripple can be decreased. However, an increase of switching frequency would result in greater switching losses. As a consequence of the increased switch losses additional cooling might be introduced to the subsystem. Therefore an increased switching frequency is a trade-off between decreased current ripple and increased switch losses. However, an increased switching frequency increases the amount of charge and discharge cycles. This might be worth consideration too.

The best solution would therefore be to combine an increased switching frequency with an increase of the DC-link capacitor.

8.3 Recommendations for future work

8.3.1 Parameter investigation and validating measurements

The scope of this thesis was to investigate the behaviour of the TVS DC-side with a simplification of the AC-side. A rough estimate model of the real systems has been made and with parameters given or measured. Simplifications have been made in some filters where smaller passive components like capacitors to ground etc. have been neglected. For a better understanding of the whole system and a more realistic result all parameters should be thoroughly investigated internally at Volvo and with subcontractors.

8.3.2 Additional bus measurements

To achieve a robust model and component library more tests needs to be done on different systems to ensure that the model is customizable to different systems. This is recommended before trying to design a not yet existing bus in the model and believing that the model is 100 percent consistent with reality. The goal is to have a model that does not need to be custom for each system apart from the circuitry and setting parameter values.

8.3.3 Extended library

To accomplish an extended simulation environment there is also a need of more subsystem components in the library to be able to build models of future projects.

References

Litterature

[1] Alaküla, Mats; Johansson, Jonas; Lindstedt, Gunnar; Simonsson, Bengt. (2010). Grundläggande Elektroteknik. Lund: KFS i Lund AB.

[2] Alaküla, Mats; Karlsson, Per. (2015 ver 1). Power Electronics. Lund: Department of Industrial Electrical Engineering and Automation.

[3] Alexandersson, Sabine. (2008). Automotive Electromagnetic Compatibility - Prediction and Analysis of Parasitic Components in Conductor Layouts. Lund: Department of Industrial Electrical Engineering and Automation.

Webpages

[4] Gillis, Justin (28 November 2015). "Short Answers to Hard Questions About Climate Change". The New York Times. http://www.nytimes.com/interactive/2015/11/28/science/what-is-climate-change.html, (Retrieved 2016-11-03)

[5] European Commission.(2016). Horizon 2020 Transport. https://ec.europa.eu/programmes/horizon2020/en/area/transport,(Retrieved 2016-11-03)

[6] Volvo Buses. (2016). News, http://www.volvobuses.se/sv-se/news/2016/oct/volvo-och-abb-inviger-laddstation-for-elbussar.html, (Retrieved 2016-11-24).

[7] IEA LTH. (2016). Kraftelektronik, http://www.iea.lth.se/kel/Lectures16/, (Retrieved 2016-11-21).

[8] IEA LTH. (2016). Elmaskinskonstruktion, http://www.iea.lth.se/eief10/old_exams/TentaEIEF10-20130115.pdf, (Retrieved 2016-11-18).

[9] Wikipedia. (2016). Lorentz Force, https://en.wikipedia.org/wiki/Lorentz_force, (Retrieved 2016-12-12).

[10] EEWeb. (2016). Toolbox, https://www.eeweb.com/toolbox/wire-inductance/, (Retrieved 2016-12-22).

[11] Wikipedia. (2016). Voltage source, https://en.wikipedia.org/wiki/Voltage_source, (Retrieved 2016-12-23).

Software

[12] Linear Technology Corporation, (2016). Design Support. http://www.linear.com/designtools/software/, (Retrieved 2016-12-13)

List of Figures

List of Tables

List of abbreviations

AC - Alternating Current
CM-filter - Common Mode filter
CM-choke - Common Mode choke
DC - Direct Current
DCDC - Direct current converter from the 600V system to the 24V system
EM - Electric Machine
EMD - Electric Machine Driver
FFT - Fast Fourier Transform
ESS - Energy Storage System
HPC - High Power Charger
HVAC - Heat ventilation and air conditioning
ICE - Internal Combustion Engine
IM - Induction Machine
LPC - Low Power Charger
MDS - Motor Drive System
PEC - Power Electronic Converter
PMSM - Permanent Magnetized Synchronous Machine
TVS - Traction Voltage System

A Matlab script for calculating motor simulation values

Table of Contents

Fictional motor parameter values

```
Pmax=52E3;                  % Maximum power
Udc=600;                    % DC-link voltage
R=0.3;                      % Motor's inner resistance
L=0.5E-3;                   % Motor's inner inductance
Psi=0.8;                    % Motor's flux
dutycycle=0.5;              % Duty cycle of the inverter
```

What are the maximum current and voltage vector values depending on the motor characteristics?

```
Umax=Udc/sqrt(2);           % Depending on symmetrized three-
phase modulation
Iph_rms=Pmax/(Umax*sqrt(3));    % Three-phase power equation
Imax=Iph_rms*sqrt(3);
```

Maximum back-emf vector value depending on the voltage vector and the duty cycle

```
Ealfabeta=Umax*dutycycle;
Eabc_top=Ealfabeta*sqrt(2/3);   % Conversion from alfa-beta-plane to
 abc-plane
```

The motors mechanical frequency dependent on the size of the back-emf and the motor characteristics

```
omega_mech=Ealfabeta/Psi;
Freq_mech=omega_mech/(2*pi);
```

With the help of the voltage equation U = R*i + j*w*L*i +j*w*Psi one can calculate the required u for the load applied

```
Ualfabeta=R*Imax*i+i*omega_mech*Imax*L*i+Ealfabeta*i;
Uabc_top=abs(Ualfabeta)*sqrt(2/3);   % Convertion to top value in abc-
plane

Phi=abs(atan(real(Ualfabeta)/imag(Ualfabeta)))*(360/(2*pi)); % Angle
 between E and U in abc
```

Results

```
Uabc_top  %in [V]
Eabc_top  %in [V]
Freq_mech %in [Hz]
Phi       %in [degrees]
```

```
Uabc_top =

  203.6599


Eabc_top =

  173.2051


Freq_mech =

   42.2023


Phi =

    3.7354
```

Published with MATLAB® R2015b

B Load simplification model in LTspice

However to confirm this theory for a 4Q three-phase converter with an electric motor a LTspice model was built, see figure 87. The model consist of a simple 4Q three-phase converter bridge with six switches acting as transistors. Further on there is a simple DC-voltage source supplied straight to the transistor bridge. The voltage source is to represent the $600V$ battery without any parasitic involvement from cables, input filters or any other components from the actual TVS. With this simple voltage source applied direct to the transistor bridge an accurate evaluation of how the current ripple behaves before the subsystems input filter was attained. In reality the voltage source represents the voltage after the input filter but before the transistor bridge. Furthermore, the electric machine is represented with a three-phase RLE-load with parameters taken from electric machine construction, [8]. Calculations for the simulation can be seen in chapter 6.2.

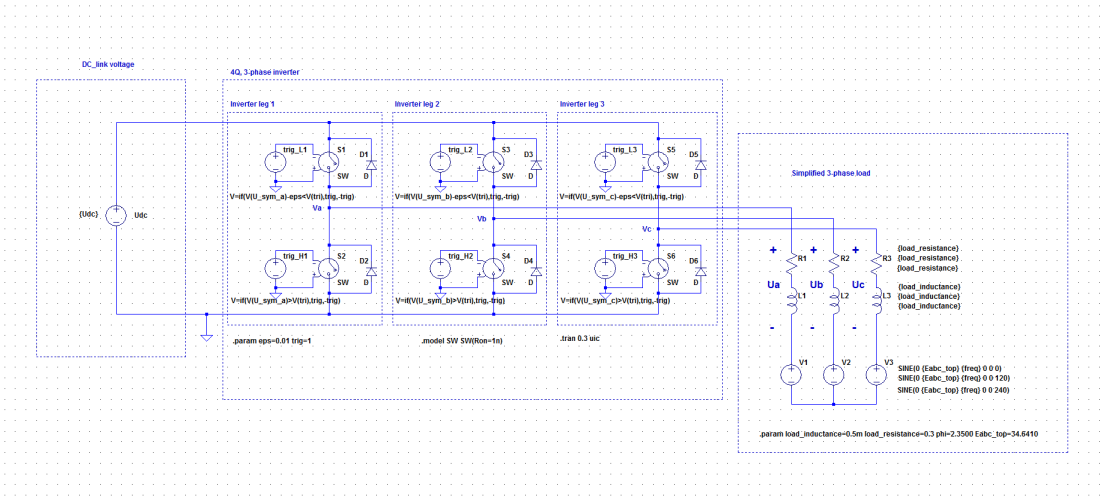

Figure 87: LTspice model of the DC-side, a 4Q-three-phase converter and a three-phase AC-motor load. No input filters included.

C Software evaluation

Prerequisites:

- Perform steady and dynamic simulations.
- Incorporation of complete electrical system for overall testing.

PSIM:

- Originally developed for simulating power electronic converters and electrical machine drives.
- Newer version includes magnetics and thermal model for better accuracy.
- Includes module boxes that can be stored in library for the user to build a hybrid model however there is no capability of simulating the entire system of an automobile.
- Provides options for plug-and-play.
- Design can be focused to operate the ICE at an optimum region.

Simplorer:

- Comprehensive predefined library including batteries, fuel cells, alternators, engine models, power electronics and controllers.
- Best in class for EM field solvers with precise physics based modeling.
- Can be linked with FEM based simulation package, Maxwell for better accuracy of electronics and machine design.
- Effective approach for EMC/EMI for tracing the source to victim.
- Dynamic simulations can be performed under different drive cycles.
- Vehicle response for difference road grades can be performed to computing overall system efficiency.

Virtual Test Bed:

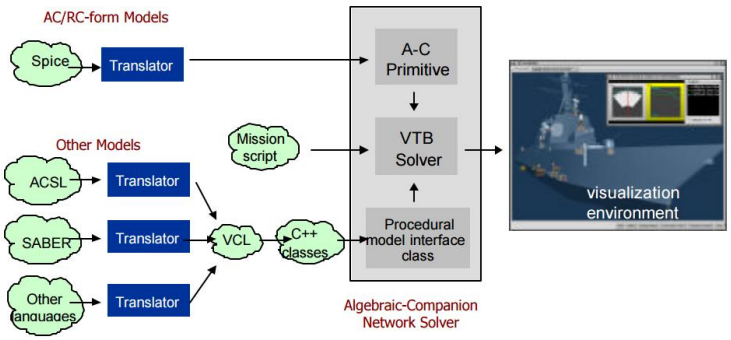

- Integration into one simulation environment created in a variety of programming languages.
- Need other expensive software to make the interaction work in 3D.

V-ELPH:

- Modeling based on MATLAB/SIMULINK which becomes complex on huge systems.

Modelica:

- Includes predefined library modules for simulation and analysis of hybrid system.
- Based on mathematical derivation of dynamic variables.
- Need previous knowledge and experience on software to work on.

Synopsis Saber:

- Proliferation of electrical and mechanical in hybrid vehicles for design of robust system.
- Analyze complex power electronics circuit for its integrity and EMC.
- Incorporated mechanical, electrical, thermal and magnetics.
- Includes FEA analysis for rotating machine
- Incorporates most of the features of simplorer and PSIM.
- Co-simulation of saber and ADVISOR for better control strategy.

Autonomie:

- Validation done with Toyota Prius.
- Simulation strategy unknown.

Conclusion:

- Points are completely based on papers and from the websites.
- Saber has features of both PSIM and simplorer and turns out to be top among the ones that I have listed.

Questions:

Any other software's that have better advantages?

Do you think it requires more investigation?

Feedback:

D Manual

Volvo Group Trucks Technology

TVS Current Ripple Manual
to the simulation tool

Christian Lugnberg and David Wenander
Version 1
December 2016

Abstract

The simulation model was built during a master thesis where studies of the traction voltage systems' (TVS) of Volvos' electric and electric hybrid buses were made. Focus was the DC-side of the TVS and therefore a simplification of the AC-side and its loads were made. The purpose was to build a generic simulation model of the TVS to analyze the current ripple. During the thesis a component library was established so that different TVS and subsystems can be built. The aim for the thesis was to build a simulation model with an error margin between 10-20%. This is a manual of how to use the simulation model. If you are unfamiliar with LTspice there is also a thorough help guide built in to LTspice found under "Help" and "Help Topics". Google is your friend ☺

Table of Contents

Default model

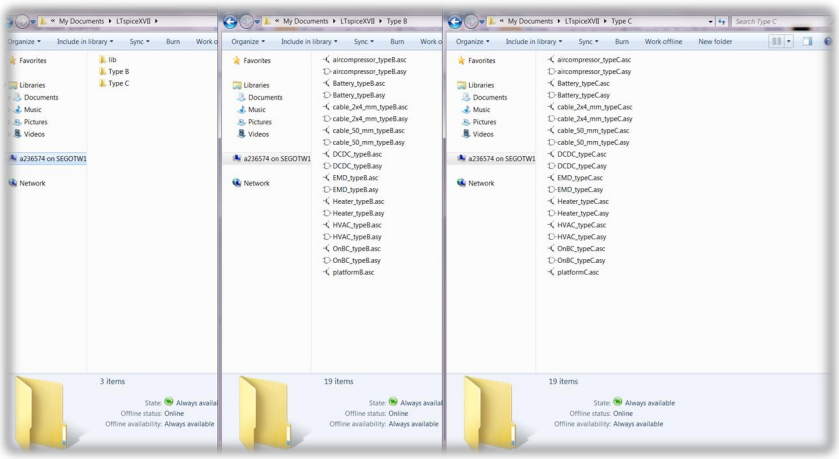

Figure 1. The folder structure of the two systems in the simulation model.

The simulation tool is originally consistent of two different systems, platform B and platform C. The simulation tool can be extended, more about how to do that in chapter “Making changes in the TVS”. There will be presented two levels of usage in this guide, one where parameters are manipulated in the already existing systems and one where existing systems are extended or new systems are built. The original systems are separated in two different folders representing one system each. The folders contain their subsystem files that sometimes are exact copies of subsystem files in another system but with different names, depending on which platform they belong to. This is to separate the files used in each system to not be affected by changes made in one system where it is not wanted in the other system. The same subsystem circuit can thus be used in both models but with different parameter settings as long as the files are placed in different folders and have different names.

Platform B

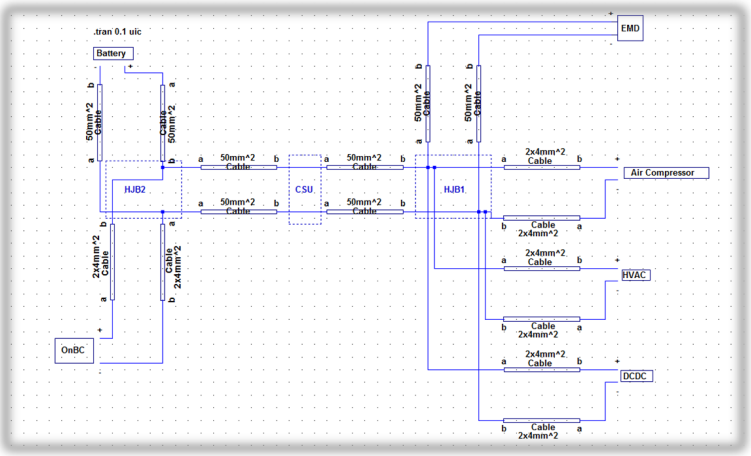

Figure 2. A system circuit of platform B in LTspice.

Platform B is represented of:

- ESS – Energy storage system (called battery in the circuit)
- EMD – Electric motor drive
- Air compressor
- HVAC – Heat ventilation and air conditioning
- DCDC
- 2x4mm^2-cables
- 50mm^2-cables

Platform C

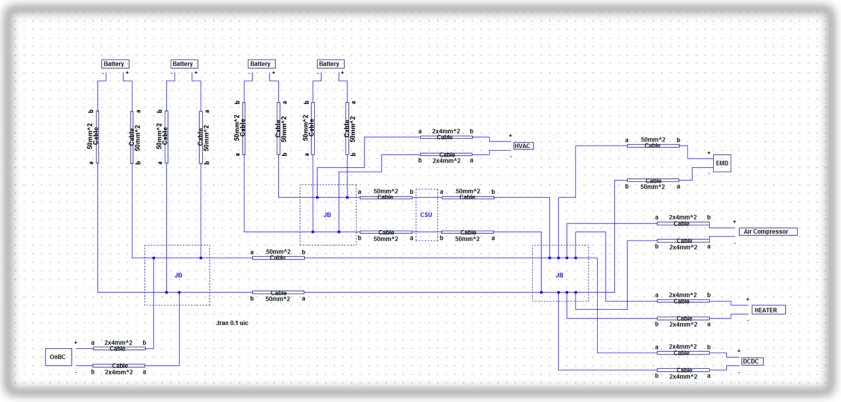

Figure 3. A system circuit of platform B in LTspice.

Platform C is represented of:

- ESS – Energy storage system (called battery in the circuit)
- EMD – Electric motor drive
- Air compressor
- Heater
- HVAC – Heat ventilation and air conditioning
- DCDC
- 2x4mm^2-cables
- 50mm^2-cables

File changes are global

When opening a system file, named for example “platformB.asc”, one can see the whole system consisting of the different subsystems mentioned on page 5 and 6, for example HVAC. Now the HVAC is a subsystem in both platform B and C and has the same circuit design and parameter values in both applications. To make it possible to click on and make changes in the HVAC of one system without changing the characteristics of the HVAC for the other system, separate folders are used for keeping the subsystem files separate. So when clicking a subsystem like the HVAC an instance of it opens as a circuit and one can look at and, or change its specified parameter values. Be aware that saving after a change will globally change the characteristics of the HVAC in the file HVAC_typeB.asc for example. This means that all changes made and saved to an instance of a schematics file (.asc) are saved globally to its schematics file. So where this subsystem (HVAC_typeB) is used in other applications, like another simulation model, within the same folder it will have the new changes and thus also a new behavior.

LT-Spice Setup

To be able to measure properties within the subsystems a certain setting must be setup in LT-Spice. To enable this go under “Tools” then “Control Panel” and under “Save Defaults” cross the boxes “Save Subcircuit Node Voltages[*] ” and “Save Subcircuit Device Currents[*]”

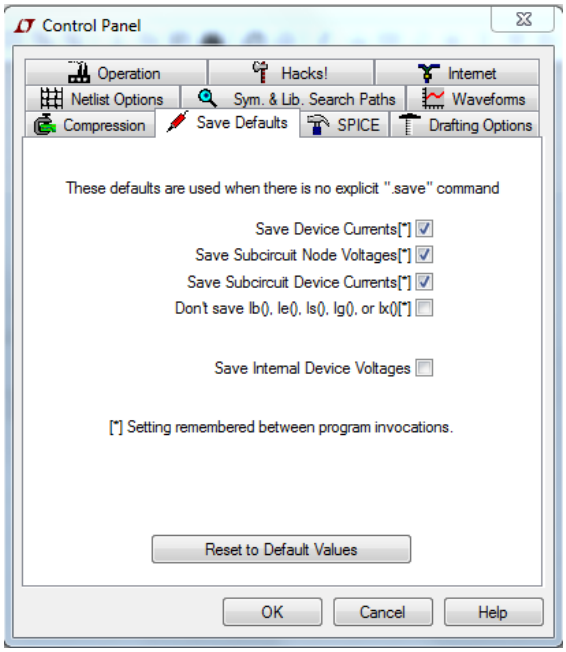

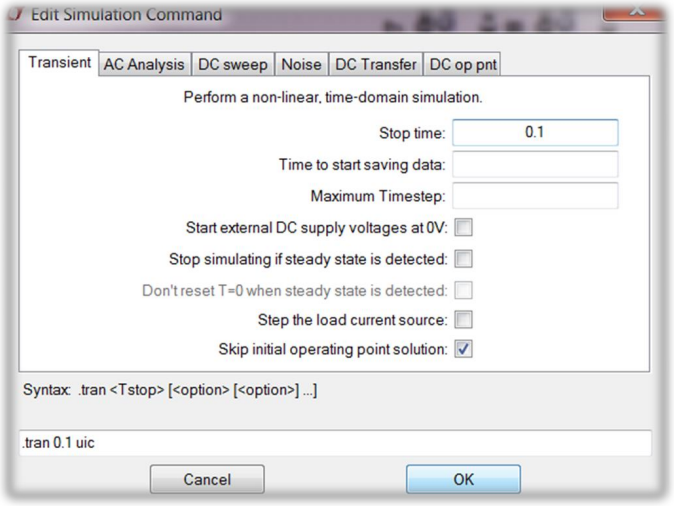

Figure 4. Edit Simulation Command settings.

Simulation settings can be defined in “Edit Simulation Cmd” under “Simulate” in the drop down menu. In this thesis transient analysis during 0.1s was used to run the simulations.

Setting simulation parameter values

Loads

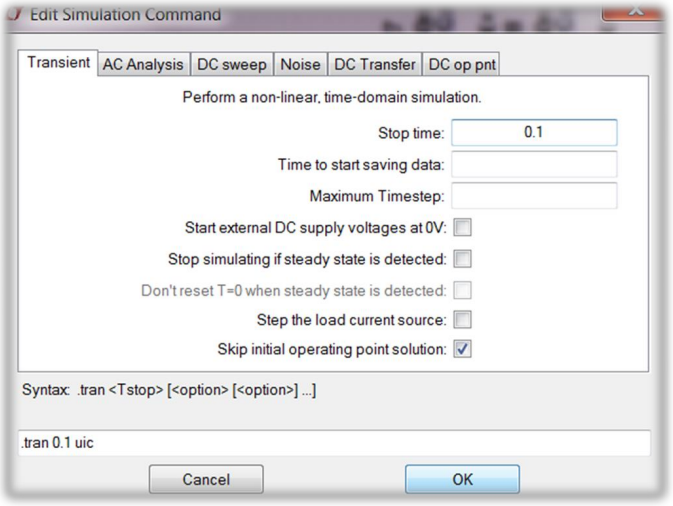

Figure 5.

ESS level

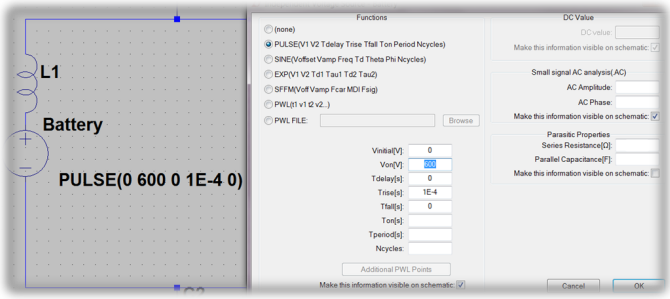

Figure 6. A voltage source named "Battery". How to edit the DC-link voltage in a battery.

The level of the DC-link voltage is set by right-clicking the voltage source in an instance of a battery. By default the voltage is ramped up to 600V during 0.1ms but all this can be changed to own preferred values.

Cables

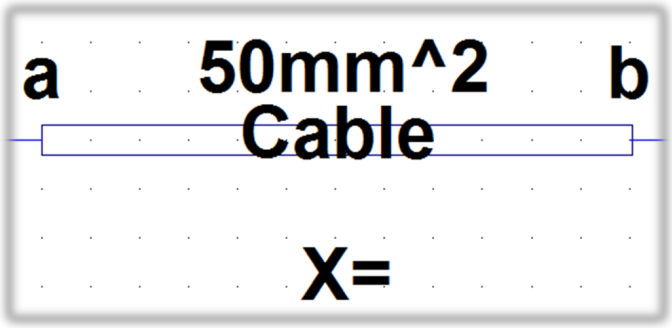

Figure 7. A cable in a LTspice-schematic. X is the parameter that determines the cable's length.

To set a cable's length one change the parameter value of X to desired length in millimeters and the subsystem automatically calculates the new properties of the cable.

EMD type B

The EMD can be simulated up to base speed. Data required taken from the thesis report.

Converter type	DC/AC 4-quadrant 3-phase
Switching Frequency	f_{sw}
Converter load type	PMSM
Converter load power	180kW max, 72kW nominal
Electric Machine base speed	$\omega_{basespeed}$

To simulate the load for a subsystem a current pulse generator is used. This current pulse generator has three input parameter to simulate the Load.

During simulation there are three input parameters for a to simulate the load for a subsystem.

- **I2[A]:**The first input parameter is the height of the current pulse. This is calculated by $\frac{Load\ Power}{\text{Battery Voltage}} = \text{Current height}$. In figure x it is derived as the Load nominal power at 150kW divided by the battery voltage at 600V resulting in a current pulse at 250A.
- **Ton[s]:** The second input parameter is the duration of the current pulse. This is dependent of the duty cycle, $\frac{Duty\ Cycle}{\text{Perceived switching frequency}} = \text{pulse duration}$, e.g. 50% duty cycle = 0.5. In the case for the EMD the duty cycle is proportional to the speed of the machine up to base speed.
- **Tperiod[s]:** The third input parameter is the period time for the current pulses. This is dependent of the switching frequency of the converter. However, the actual and perceived switching frequency is dependent on the type of modulation executed by the converter. The EMD has a Symmetrized voltage modulation and as a result the perceived switching frequency is the switching frequency times two. As a consequence the third input period time results in $\frac{1}{\text{Perceived switching frequency}} = \text{Period Time}$.

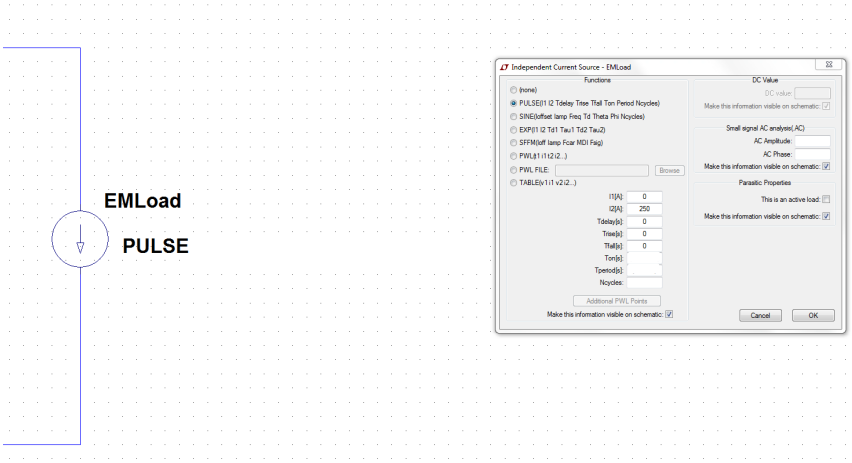

EMD type C

Converter type	DC/AC 4-quadrant 3-phase
Switching Frequency	f_{sw}
Converter load type	PMSM
Converter load power	185kW max, 105kW nominal
Electric Machine base speed	$\omega_{basespeed}$

Same parameter input procedure as for EMD type B.

HVAC

Converter type	DC/AC 4-quadrant 3-phase
Switching Frequency	f_{sw}
Converter load type	IM
Converter load power	11kW max
Electric Machine base speed	$\omega_{basespeed}$
Lowest voltage applied to reach base speed	560V

- **I2[A]:**The first input parameter is the height of the current pulse. This is calculated by $\frac{Load\ Power}{\text{Battery Voltage}} = \text{Current height}$. In figure x it is derived as the Load max power at 11kW divided by the battery voltage at 600V resulting in a current pulse at 18.3A.
- **Ton[s]:** The second input parameter is the duration of the current pulse. This is dependent of the duty cycle, $\frac{Duty\ Cycle}{\text{Perceived switching frequency}} = \text{pulse duration}$, e.g. 50% duty cycle = 0.5. However, the duty cycle of the HVAC is dependent of the lowest applied voltage to reach base speed, $\frac{Lowest\ voltage\ applied\ to\ reach\ base\ speed}{\text{Battery voltage}} = Duty\ Cycle$. In figure x the duty cycle is derived as lowest voltage applied to reach base speed at 560V divided by the Battery Voltage at 600V resulting in a duty cycle of 0.93.
- **Tperiod[s]:** The third input parameter is the period time for the current pulses. This is dependent of the switching frequency of the converter. However, the actual and perceived switching frequency is dependent on the type of modulation executed by the converter. The HVAC has a bus-clamped voltage modulation and as a result the perceived switching frequency is the same as the switching frequency. As a consequence the third input period time result in $\frac{1}{\text{Perceived Switching frequency}} = \text{Period Time}$.

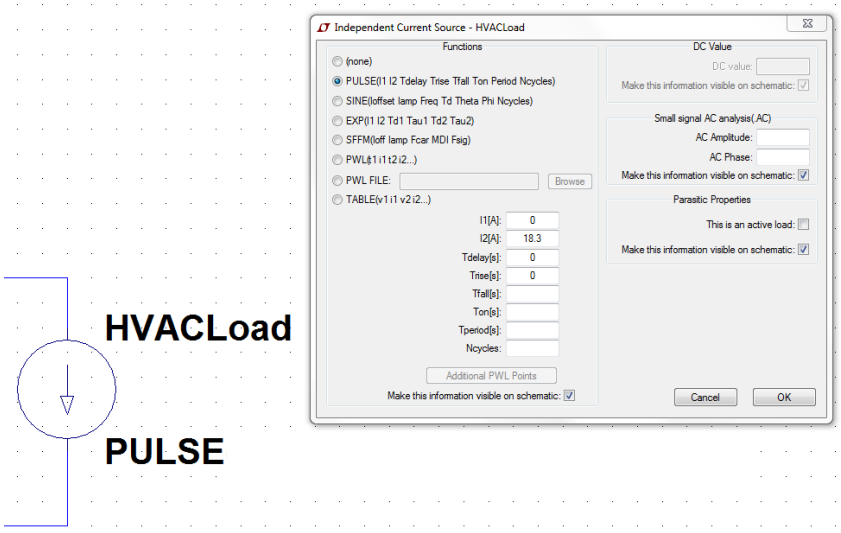

Air Compressor

Converter type	DC/AC 4-quadrant 3-phase
Switching Frequency	f_{sw}
Converter load type	PMSM
Converter load power	7.5kW max
Electric Machine base speed	$\omega_{basespeed}$
Lowest voltage applied to reach base speed	500V

Same parameter input procedure as for the HVAC.

DCDC

Converter type	DC/DC 4-quadrant 1-phase
Switching Frequency	f_{sw}
Converter load type	24V DC-system
Converter load power	7.5kW max
Lowest voltage applied for full performance	500V

- **I2[A]:**The first input parameter is the height of the current pulse. Furthermore the current height is dependent on how loaded the 24V DC-system is loaded. Therefore, the current height is set by $\frac{Applied\ Load\ Power}{\text{Battery 600Voltage}} = \text{Current height}$. In figure x it is derived as the Load max power at 7,5kW divided by the battery voltage at 600V resulting in a current pulse at 12.5A.
- **Ton[s]:** The second input parameter is the duration of the current pulse. This is dependent of the duty cycle, $\frac{Duty\ Cycle}{\text{Perceived switching frequency}} = \text{pulse duration}$, e.g. 50% duty cycle = 0.5. However, the duty cycle of the DCDC is dependent of the lowest applied to reach full performance, $\frac{Lowest\ voltage\ applied\ to\ reach\ full\ performance}{\text{Battery voltage}} = Duty\ Cycle$. In figure x the duty cycle is derived as lowest voltage applied to reach base speed at 500V divided by the Battery Voltage at 600V resulting in a duty cycle of 0.83.
- **Tperiod[s]:** The third input parameter is the period time for the current pulses. This is dependent of the switching frequency of the converter. However, the actual and perceived switching frequency is dependent on the type of modulation executed by the converter. The DCDC has a Symmetrized voltage modulation and as a result the perceived switching frequency is the switching frequency times two. As a consequence the third input period time results in $\frac{1}{\text{Perceived switching frequency}} = \text{Period Time}$.

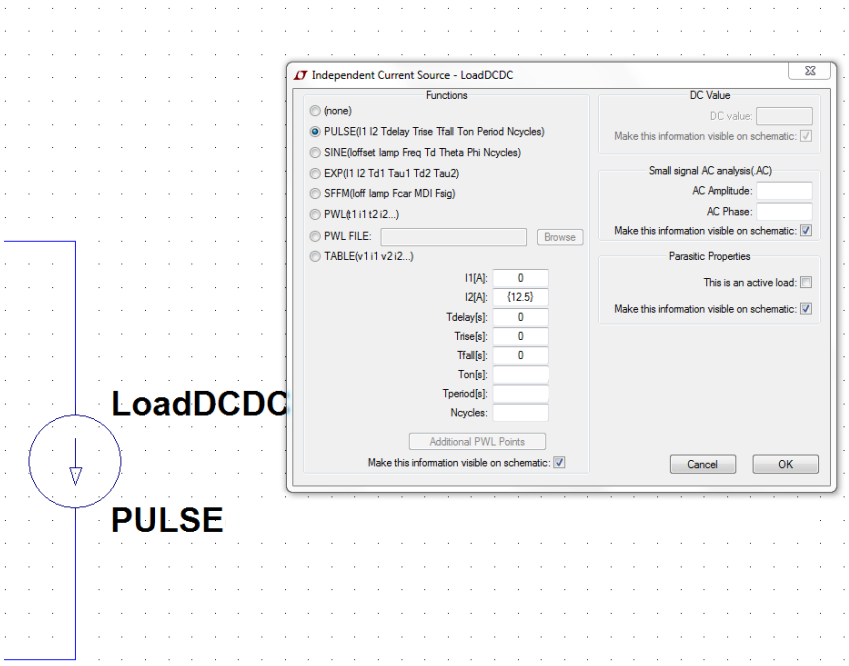
LoadDCDC
PULSE
Independent Current Source - LoadDCDC
Functions
(none)
PULSE(I1 I2 Tdelay Trise Tfall Ton Period Ncycles)
SINE(Ioffset Iamp Freq Td Theta Phi Ncycles)
EXP(I1 I2 Td1 Tau1 Td2 Tau2)
SFFM(Ioff Iamp Fcar MDI Fsig)
PWL(t1 i1 t2 i2...)
PWL FILE:
Browse
TABLE(v1 i1 v2 i2...)
I1[A]: 0
I2[A]: {12.5}
Tdelay[s]: 0
Trise[s]: 0
Tfall[s]: 0
Ton[s]:
Tperiod[s]:
Ncycles:
Additional PWL Points
Make this information visible on schematic:
DC Value
DC value:
Make this information visible on schematic:
Small signal AC analysis(.AC)
AC Amplitude:
AC Phase:
Make this information visible on schematic:
Parasitic Properties
This is an active load:
Make this information visible on schematic:
Cancel
OK

Results

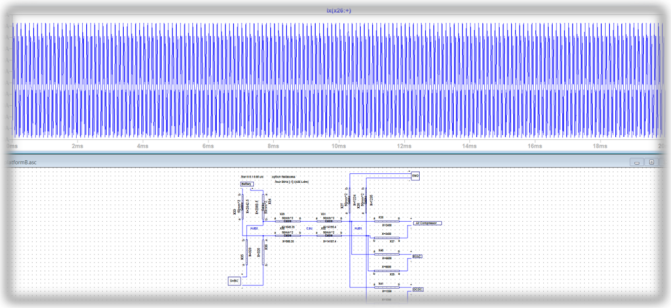

Figure 8. A current measurement on one of the cables after a simulation.

After a simulation is run one can easily analyze the results in the waveform viewer that appears as a simulation starts.

Making changes in the TVS

To make simulations of temporary changes there is no need to save schematics in between changing and simulating, this way one can run many simulations without overwriting any of the original schematics as long as one does not save them before quitting.

To create a new system or a rearrange an already existing system it is recommended to create a new system's folder. Paste all the already existing schematic and symbol files that you want to use there and rename them to the new system's specific name so that LTspice will not be confused.


VOLVO